
Electronic Thesis and Dissertation Repository

9-17-2018 3:30 PM

Probing Trapped Extracellular Vesicles by Surface-Enhanced Raman Spectroscopy


Lauren Kaufman
The University of Western Ontario

Supervisor
Lagugné-Labarthe, François
The University of Western Ontario

Graduate Program in Chemistry

A thesis submitted in partial fulfillment of the requirements for the degree in Master of Science
© Lauren Kaufman 2018

Follow this and additional works at: <https://ir.lib.uwo.ca/etd>

 Part of the [Analytical Chemistry Commons](#), [Other Chemistry Commons](#), and the [Physical Chemistry Commons](#)

Recommended Citation

Kaufman, Lauren, "Probing Trapped Extracellular Vesicles by Surface-Enhanced Raman Spectroscopy" (2018). *Electronic Thesis and Dissertation Repository*. 5711.
<https://ir.lib.uwo.ca/etd/5711>

This Dissertation/Thesis is brought to you for free and open access by Scholarship@Western. It has been accepted for inclusion in Electronic Thesis and Dissertation Repository by an authorized administrator of Scholarship@Western. For more information, please contact wlsadmin@uwo.ca.

Abstract

Extracellular vesicles (EVs) are released by nearly all cell types within the human body and have been found to play important biological roles including cell-to-cell communication, apoptosis and tissue repair. Lacking cellular machinery, these nano-sized vesicles carry functional proteins and nucleic acids from their parent cells, providing insight into biomarkers present in healthy, cancerous and diseased cells. EVs may be isolated from biofluids such as from blood or urine. Their detection and characterization holds extreme potential in developing less invasive disease detection and treatment methods.

In this work, we propose use of lithographic techniques to fabricate platforms to allow for molecular-level characterization by surface-enhanced Raman spectra (SERS). Two methods of lithography are proposed to probe spectral signatures of individual EVs without use of labelling agents. SERS spectra are acquired for EVs released from two cell lines, allowing for determination of the diversity existent within a cell line, and amongst different cell lines.

Keywords

4-mercaptophenyl boronic acid (4-MPBA), biosensing, electron beam lithography (EBL), exosome, extracellular vesicle (EV), localized surface plasmon resonance (LSPR), nanosphere lithography (NSL), Raman spectroscopy, surface enhanced Raman spectroscopy (SERS).

Dedication

In blessed memory of my late father, Elliot Kaufman.

Your love for optics seems to have passed on.

Co-Authorship Statement

This thesis contains materials from a submitted paper. Dr. François Lagagné-Labarthe is the corresponding author of the paper and was responsible for supervision of Lauren Kaufman throughout her studies.

The submitted paper is presented throughout Chapters 3 and 4. Lauren Kaufman was responsible for experimental work and writing of the manuscript. Some experimental work, namely cell culture of prostate cancer cells was performed through collaboration with Lawson Research Institute with assistance and guidance from Andrew Poon, Dr. Thamara Dayarathna and Dr. Hon S. Leong. Cell culture of mesenchymal stem cell lines was performed through collaboration with Schulich School of Medicine and Dentistry with Dr. David A Hess and Tyler T Cooper. Tyler Cooper was responsible for isolation of biological materials from the mesenchymal stem cell line studied throughout this thesis.

Acknowledgments

Firstly, I would like to acknowledge my supervisor, Dr. François Lagurné-Labarhet for his guidance, mentorship and support throughout my time at Western University.

François allowed me to formulate a project catered to my own research interests, allowing me to gain hands-on skills and knowledge in areas I was interested in exploring in chemistry and biology. Thank you for your flexibility and guidance.

I would like to acknowledge the FLL group. Throughout the past two years, I have largely enjoyed our adventures both inside and outside of the lab. Dr. Gregory Wallace, I am thankful for the many hours you spent training me, helping me understand concepts, reviewing my work, and providing feedback. Danielle McRae, thank you for the many conversations we have shared over cups of tea, I will surely cherish them. Alex Therien, thank you for the many discussions we have shared and for your friendship. Maria Olivia Aviles, your positivity and smile always brightened our days! Finally, Sydney Legge, I am so thankful for our friendship and hope you enjoy your next chapter as a MSc. student. I know you will all accomplish great things.

To those who have played a significant role in my research, Dr. Todd Simpson and Dr. Tim Goldhawk of Western Nanofabrication facility. Thank you for your guidance and the many fruitful discussions we have shared about both science and life. To Dr. Hon S. Leong, thank you for welcoming me into your lab and for supporting me throughout my academic endeavors.

To my fiancé, Chaim Katz. Your unconditional support throughout this chapter of my life allowed me to push forward when times were tough, to always remember my worth and

to never give up. Your curious mind kept me pursuing research questions and actively seeking knowledge. Thank you for continually supporting me, while simultaneously challenging me to grow into a better researcher and version of myself.

To the Kaufman/Rasminsky side of my family. Firstly, to my brother Daniel Robert Kaufman. Thank you for paving the way for me upon completing your MSc. in Physiology. You opened my eyes to the research world and instilled within me a curiosity to pursue the sciences from a young age. I have always looked up to you for your work ethic and kind heart. To my mother, our conversations and weekend hangouts kept me sane. You truly are the embodiment of unconditional love and support, and I am thankful for everything you have done for me and taught me.

To the Katz/Davids/Rogers side of my family. Thank you for your continuous support, friendship and mentorship. Friday night Shabbat dinners, Passover Seders, fun science experiments, and family trips reminded me that the most important and precious things in life are intangible. Thank you for keeping me motivated and happy during times of stress.

Table of Contents

Abstract	i
Keywords	i
Dedication	ii
Co-Authorship Statement.....	iii
Acknowledgments.....	iv
List of Tables	x
List of Figures (where applicable)	xi
List of Abbreviations, Symbols and Nomenclature	xiv
Chapter 1	1
1 General Introduction	1
1.1 Overview.....	1
1.1.1 Applications of SERS in Biology	4
1.2 Biological SERS Detection Methodologies.....	4
1.2.1 Indirect Detection methods	4
1.2.2 Direct Detection Methods	6
1.2.3 Scope of Thesis	7
1.3 References.....	8
Chapter 2.....	12
2 Extracellular Vesicles (EVs).....	12
2.1 History of EVs	12
2.1.1 Classification and Composition of EVs.....	13
2.1.2 Methods of Isolating EVs	15
2.1.3 EVs as Human Liquid Biopsies	17
2.1.4 Spectroscopic Studies of EVs	18

2.2	Principles of Surface-Enhanced Spectroscopies	19
2.2.1	Plasmon Resonances in Metal	19
2.2.2	Surface Plasmon Polaritons (SPP)	19
2.2.3	Localized Surface Plasmon Resonance	20
2.2.4	Raman Spectroscopy.....	21
2.3	Surface-Enhanced Raman Spectroscopy (SERS)	23
2.3.1	Electromagnetic Mechanism of SERS.....	23
2.3.2	Chemical Enhancement Mechanism of SERS.....	25
2.4	Preparation of Plasmonic Platforms by Nanosphere Lithography.....	25
2.4.1	Preparation of Plasmonic Platforms by Electron Beam Lithography.....	27
2.4.2	Characterization of Plasmonic Platforms.....	29
2.5	Summary	30
2.6	References.....	31
Chapter 3.....		35
3	Fabrication and Characterization of Plasmonic Platforms.....	35
3.1	Introduction.....	35
3.2	Experimental.....	37
3.2.1	Materials for Nanosphere Lithography.....	37
3.2.2	Materials for Electron Beam Lithography	38
3.2.3	Raman and Surface-Enhanced Raman Spectroscopy	39
3.2.4	Fluorescence Imaging	40
3.2.5	Functionalization of Nanohole Arrays.....	40
3.3	Results and Discussion	40
3.3.1	Characterization of Platforms Prepared by Nanosphere Lithography	40
3.3.2	Preparation of Plasmonic Platforms by Electron Beam Lithography.....	43
3.3.3	Plasmonic Properties of Metallic Nanohole Arrays.....	48

3.3.4	Trapping Capabilities of Nanohole Arrays	51
3.4	Conclusions.....	55
3.5	References.....	56
Chapter 4.....		59
4	Surface-Enhanced Raman Spectroscopy of Extracellular Vesicles	59
4.1	Introduction.....	59
4.2	Experimental.....	63
4.2.1	Cell Culturing of Pancreatic Mesenchymal Stem Cell Line.....	63
4.2.2	Isolation of EVs from Mesenchymal Cell Line	63
4.2.3	Cell Culturing of Human Prostate Cancer Cell Line (PC3).....	64
4.2.4	Isolation of EVs from Human Prostate Cancer Cell Line (PC3).....	65
4.2.5	EV Preservation for SEM Imaging	65
4.2.6	Substrate Fabrication and Trapping of EVs within Nanohole Arrays	65
4.2.7	Spectroscopic Characterization.....	66
4.3	Results and Discussion	66
4.3.1	Characteristics of EVs.....	66
4.3.2	SERS of EVs (PC3)	69
4.3.3	Trapping and Spectral Probing of EVs in NHAs.....	74
4.3.4	Extracellular Vesicle Differentiation and Similarity	81
4.4	Conclusion	83
4.5	References.....	84
Chapter 5.....		88
5	Conclusions and Outlook.....	88
5.1	Conclusions.....	88
5.2	Outlook	91
5.3	References.....	93

Appendix A - Copyright	94
Curriculum Vitae	96

List of Tables

Table 1 - Classification of EVs	14
Table 2 - Optimal electron beam dosage for fabrication of nanostructures of desired sizes ..	47
Table 3 - SERS peak assignment for PC3 EV	71
Table 4 - SERS peak assignment for mesenchymal EVs	79
Table 5 - Peak assignment for peaks shared amongst PC3 and mesenchymal EVs	83

List of Figures (where applicable)

Figure 2.1 - Number of publications retrieved from webofknowledge.com mentioning ‘extracellular vesicle’ as of June 20, 2018.....	13
Figure 2.2 - (a) Schematic of the charge distribution and local electric field associated with surface plasmons; (b) The strength of the SP decays exponentially with increasing distance from the metal and dielectric	20
Figure 2.3 – Localized surface plasmon resonance of a metallic nanoparticle	21
Figure 2.4 - Illustration of the various elastic and inelastic scattering paths an emitted photon may undergo following interaction with a molecule of interest	22
Figure 2.5 – SERS (red) and Raman (blue) spectra of malachite green	24
Figure 2.6 – Schematic of NSL fabrication, with top and side views	26
Figure 2.7 - SEM images of nanostructures prepared by NSL; A, B) Top view of nanostructures following lift-off; C) Boundary between a bilayered area and monolayered area following lift-off of nanospheres.....	27
Figure 2.8 - Schematic illustration of electron beam lithography process performed on a positive and negative resist. ⁶⁶	28
Figure 2.9 – Schematic of absorption spectra setup enabling the measurement of plasmon resonances of the nanostructured surfaces over a surface limited to a few tens of microns...	29
Figure 3.1 – Photographs of the O-ring method of NSL (A) prior to drying and (B) after 12 hours of drying time, prepared with 1 μm diameter polystyrene spheres.....	41
Figure 3.2 – Characterization of NSL nanostructures fabricated using 1-micron spheres by (A) SEM (B) absorption spectra.	42
Figure 3.3 - (A) NHA fabricated with a positive resist for assessment of trapping abilities of NHAs; (B) Close-up of positive resist-fabricated 0.9 μm diameter circular nanowells; (C) NHA fabricated with negative resist, coated with 30 nm of gold prior to lift-off of	

nanopillars; The different colors of the individual patches indicate distinct plasmon frequencies (D) Close-up of negative resist-fabricated 0.9 μm diameter circular nanopillars; (E) NHA fabricated with negative resist, coated with 30 nm of gold following lift-off of nanopillars, revealing nanowells; (F) Close-up of negative resist-fabricated 0.9 μm diameter circular nanowells. 44

Figure 3.4 - SEM nanopillars and nanowells. (A) 200 nm circular nanopillars; (B) 900 nm circular nanopillars; (C) 900 nm square nanopillars; (D) 300 nm circular nanowell; (E) 700 nm circular nanowells; (F) 600 nm square nanowells. 46

Figure 3.5 – Lift-off of nanopillars. (A) Intact nanopillar followed by (B) lift-off revealing residual resist in nanowells, which is removed fully in (C), showing exposed glass nanowells. 48

Figure 3.6 – Absorption for horizontally polarized light through (A) square and (B) circular nanowells of varying size..... 49

Figure 3.7 - Mapping of 4-MPBA on a nanohole array surface with f. (A) SEM image of 0.9 μm diameter circular nanohole; (B) SERS map of corresponding nanohole; (C) SERS spectra of pixels indicated in (B); (D) SEM image of 0.9 μm diameter square nanohole; (E) SERS map of corresponding nanohole; (F) SERS spectra of pixels 3 and 4 selected in (E). 50

Figure 3.8 - Polystyrene spheres trapped within PMMA nanohole arrays. (A) Nanohole array of 0.3 μm circles with 0.2 μm polystyrene beads (B) nanohole array of 0.4 μm squares with 0.2 μm polystyrene beads (C) 1.0 μm fluorescent polystyrene beads trapped in 1 μm circular wells. (D) 1.0 μm fluorescent polystyrene beads trapped in 0.9 μm square wells. 52

Figure 3.9 - Sensing of polystyrene spheres through a nanohole array. The sample was mounted face-up, facing away from the laser beam source. (A) Areas of interest for SERS spectral acquisition. Area 1 highlights a trapped polystyrene sphere 1 μm in diameter trapped within a nanowell, whereas area 2 corresponds to a background area with no trapped material. Corresponding spectra to (A) are displayed in (B), where area 1 displays a peak characteristic of polystyrene and area 2 lacks this spectral peak..... 54

Figure 4.1 – Images of a healthy PC3 cell line used for EV isolation and characterization (A) Optical image of a growing cell culture, with its corresponding fluorescence image (B); (C) SEM of a healthy PC3 cell, displaying sharp edges and protrusions.....	67
Figure 4.2 – Images of isolated EVs. (A) Fluorescent image of isolated EVs (B) preserved EVs on a silicon wafer.	68
Figure 4.3 (a) NSL substrate containing dried EVs, of which a (b) SERS spectra was obtained of an EV (red) and of the background (blue).	69
Figure 4.4 – SERS spectra obtained from PC3 derived EVs on a NSL substrate prepared by the O-ring method.	72
Figure 4.5 – Representative background spectra from PC3 cell line.....	73
Figure 4.6 – SERS of EVs from a mesenchymal stem cell line on a NSL platform.	74
Figure 4.7 – SEM images of EVs trapped within (A) a square nanowell of 0.8 μm diameter; (B) a 1 μm diameter circular nanowell (C) a 0.5 μm square nanowell; (D) optical image of a 1 μm diameter square nanowells.....	75
Figure 4.8 - Background Raman spectra of cell culture media for mesenchymal stem cell line.	77
Figure 4.9 - SERS of EVs trapped in a nanohole array within (1) 0.7 μm diameter circular well; (2) 0.9 μm diameter square well; (3) 0.8 μm diameter square. Spectra are shifted for clarity.	78
Figure 4.10 - Comparison of SERS spectra of EVs probed by NSL from mesenchymal and prostate (PC3) cell lines.	81
Figure 5.1 - Exosomes trapped within “nanowire-on-micropillar” structures and subsequently separated from cellular debris and proteins. Inlay shows (a) Nanowires; (b) Micropillars; (c) “Nanowire-on-micropillar” structures. Reproduced with permission. ¹²	92

List of Abbreviations, Symbols and Nomenclature

ν_n	Frequency of timing ' n '
V_n	Vibrational level ' n '
λ	Wavelength
λ_{\max}	LSPR excitation wavelength maximum
ν	Asymmetric or symmetric stretch
δ	In-plane/out-of-plane stretch
ω	Frequency
Ω	Ohm
4-MPBA	4-mercaptophenylboronic acid
AFM	Atomic force microscopy
CCD	Charge-coupled device
CE	Chemical enhancement
CM	Conditioned media
DMSO	Dimethyl siloxane
E	Enhancement factor
EBL	Electron beam lithography
e-beam	Electron beam
EDTA	Ethylenediaminetetraacetic acid
EF	Enhancement factor
EM	Electromagnetic
EOT	Extraordinary optical transmission
EV	Extracellular vesicle

EV+	Extracellular vesicle positive (i.e. contains extracellular vesicles)
$E(w)$	Electric-field enhancement factor at incident frequency
$E(w')$	Shifted electric-field enhancement factor
FBS	Fetal bovine serum
FC	Flow cytometry
FT-IR	Fournier transform infrared
I	Light intensity (transmitted)
I_0	Initial light intensity
IIDP	Integrated Islet Distribution Program
LSPR	Localized surface plasmon resonance
LTRS	Laser-tweezers Raman spectroscopy
MG	Malachite green
MS	Mass spectrometry
MSC	Mesenchymal stem cell
MSC-CM	Mesenchymal stem cell conditioned media
MVB	Multivesicular body
N.A.	Numerical aperture
NHA	Nanohole array
NIDDK	National Institute of Diabetes and Digestive and Kidney Diseases
NSL	Nanosphere lithography
NTA	Nanoparticle tracking analysis
Panc	Pancreatic
Panc-MSC	Pancreatic mesenchymal stem cell
PC 3	Prostate cancer cell line
PBS	Phosphate-buffered saline

PCA	Principle component analysis
PFA	Paraformaldehyde
PMMA	Poly (methyl-methacrylate)
PS	Polystyrene
RBC	Red blood cell
RPMI	Roswell Park memorial institute medium
SEIRA	Surface-enhanced infrared absorption
SEM	Scanning electron microscopy
SERS	Surface-enhanced Raman spectroscopy
SP	Surface-plasmon
SPP	Surface-plasmon polariton
SPR	Surface-plasmon resonance
TEM	Transmission electron microscopy
TERS	Tip-enhanced Raman spectroscopy
UC	Ultracentrifugation
UV-Vis	Ultraviolet-visible
WB	Western blotting

Chapter 1

1 General Introduction

The development of nanomaterials and their integration using micro- and nanoscale fabrication has driven a rapid increase in development of point-of-care technologies in recent decades.¹⁻⁴ These applications have yielded a variety of sensing devices with extreme sensitivity, and have been applied to study a variety of biological, physical and chemical phenomena with sensing capabilities down to the single molecule level.⁵ This thesis seeks to develop and characterize a sensing platform to trap and detect nanoscale biological materials known as extracellular vesicles. Exosomes and microvesicles, two categories of extracellular vesicles range in size between 100 nm to 1 micron and are the subjects of very active field of research due to their chemical stability and relation to disease detection and diagnostics. We propose the use of an advanced spectroscopic method with high sensitivity and specificity, known as surface-enhanced Raman spectroscopy to detect and characterize individual extracellular vesicles.

1.1 Overview

Raman spectroscopy has emerged as a powerful optical technique for studying biological materials such as cells,⁶ proteins⁷ and nucleic acids.^{8,9} Upon irradiation with an intense light source, matter will scatter light either elastically (exhibiting no change of energy), known as Rayleigh scattering, or inelastically known as Raman scattering. Raman scattering involves a change of energy either towards higher energies (anti-Stokes Raman scattering) or smaller energies (Stokes scattering).¹⁰ The energy changes associated with the Raman scattering contain information pertaining to the vibrational

modes of molecules. Inelastic scattering was first reported in the literature in 1928 by C.V Raman upon questioning the characteristic blue color of water.¹¹ This discovery led to the birth of a new field, and subsequently to a Nobel Prize awarded to C. V. Raman in 1930. Although Raman spectroscopy became a new tool in the scientist's toolkit following its initial discovery, developments within the field were limited for many years due to the relative weakness of Raman scattering without availability of intense monochromatic light sources or highly sensitive detectors. The development of lasers, charge coupled devices (CCD), and the combination of Raman measurements with optical microscopy have all led to further development of modern Raman instrumentation that provides spectra with exquisite sensitivity and spatial resolution. The applications range across many fields such as study of semiconductor materials,^{12, 13} physical materials¹⁴ and biological samples.⁹

Further to the general principle of Raman spectroscopy, in 1974, Fleischmann *et al.* observed a Raman signal one million times stronger than hypothesized when obtaining the Raman spectra of pyridine molecules adsorbed to a roughened metal electrode surface.¹⁵ This discovery led to the concept of surface-enhanced Raman spectroscopy (SERS). Following Fleischmann's serendipitous discovery, the physical principles responsible for the SERS enhancement became a field of great interest. In 1977, Creighton¹⁶ and Van Duyne¹⁷ proposed the electromagnetic and chemical enhancement mechanisms for the SERS enhancement that is observed only in conductive surfaces such as rough metals or other nanostructured conductive materials. Since then, scientists have probed information on chemical identity,¹⁸ composition,¹⁸ structure,¹⁹ purity²⁰ and

symmetry²¹ using SERS, which has now become a well used methodology for research across a variety of scientific subdisciplines.

With SERS, Raman scattering is typically enhanced by a factor of $10^2 - 10^9$ enabling the detection of the analytes positioned near a metallic nanostructured surface with weak laser intensity and/or short acquisition time.²² The large enhancement enabled by SERS is sufficient to allow for single molecule detection making it a valuable technique for biomedical applications.²³ The enhancement factor allowed by SERS depends on the shape of the nanostructure, its resonances, and the electric field enhancement near the surface of the structure.²⁴ For example, a nanoporous copper-titanium film exhibited excellent SERS enhancement up to 10^7 when functionalized with Rhodamine 6G, a common Raman reporter dye.²²

With the development of nanoscale science and nanofabrication technology, a variety of nanostructures have been used for SERS applications. For SERS-based studies, common substrates are nanoparticles on a substrate,²⁵ colloidal nanoparticles,^{26, 27} metallic films,²² and nanohole arrays encased in a metallic film.²⁸ Typical metals used for preparation of SERS substrates are silver, gold and copper.²⁸⁻³⁰ Classically, metallic nanostructured surfaces displaying surface roughness are utilized for SERS, similar to Fleischmann's experiments.³¹ Since then, a variety of top-down and bottom-up fabrication techniques have been established for substrate fabrication. Bottom-up methodology involves self-assembly of individual material building components to generate larger nanostructures, whereas top-down methodology involves removal of bulk materials from a substrate to reveal desired nanostructures. Commonly, nanosphere

lithography is considered a top-down approach whereas electron beam lithography (EBL) is commonly used as a bottom-up approach.³²

1.1.1 Applications of SERS in Biology

SERS is a powerful analytical technique for studying biological materials due to its non-destructive nature and ability to work in aqueous and dry conditions. As opposed to fluorescence measurements, Raman spectroscopy does not require staining and may therefore be used to obtain native molecular and chemical information pertaining to molecules. Molecular information pertaining to the symmetry and orientation molecules is useful for applications in polymer and materials sciences,^{33, 34} biochemistry,^{35, 36} biosensing,³⁷ and electrochemistry.^{38, 39} SERS-based biosensing has been exploited to detect diseases such as Alzheimer's disease,^{40, 41} human immunodeficiency virus,⁴² and various cancers.⁴³⁻⁴⁵ SERS has additionally been used as a tool for studying cellular adhesion.⁴⁶ pH sensing,⁴⁷ glucose sensing,^{48, 49} and detection of bacteria.^{50, 51}

1.2 Biological SERS Detection Methodologies

1.2.1 Indirect Detection methods

Detection methodologies for biological SERS applications may be grouped into direct and indirect methods. Indirect methods involve monitoring of a secondary analyte, known as a "Raman reporter", which interacts with a species of interest upon introduction. The interaction of the secondary analyte with the species of interest is monitored spectroscopically by a change in peak intensity and/or peak position, which signals a successful binding event or interaction. These changes may be monitored to reveal quantitative information on the analyte of interest. Secondary analytes commonly

used for SERS are boronic acid esters,⁵² aptamers,⁵³ and nucleic acids.⁵⁴ Additional secondary analytes include 4-mercapto benzene thiol,⁵⁵ 4-amino benzene thiol,^{56, 57} and Nile blue.⁵⁸

Boronic acid esters are also commonly used for SERS applications for saccharide detection. They form cyclic boronate esters with 1,2 and 1,3- diols, making them great candidates for detection of saccharides and sugars.⁵⁹ More recently, boronic acid esters have been used for biosensing of sugars. For example, 4-mercaptophenyl boronic acid (4-MPBA) has been used to sense fructose. Detection of fructose present in urine samples reported at millimolar concentrations based on peak intensity changes of 4-MPBA. The symmetry breaking of 4-MPBA upon fructose binding lead to a change in the relative ratio between the symmetric ring mode at and non-symmetric ring mode, signaling the successful binding of glucose.⁶⁰

4-MPBA has also been used for biosensing of glycan distribution across cancerous and non-cancerous cell lines based on its interaction with 1,2- and 1,3- diols of saccharides present in glycans.⁵² Monitoring of the relative intensity of two peaks corresponding to B-OH stretching and C-C phenyl stretching of the phenyl group of 4-MPBA were studied to determine overall glycan distribution and expression on cellular surfaces. Biosensing capabilities allowed by 4-MPBA allowed for determination of an elevated glycan distribution in cancerous cell lines when compared to the non-cancerous cell line.

Aside from commonly studied sugar and glycan detection, boronic acid esters have been used as reporters to detect biomolecules such as dopamine. For example,

quantitative detection of dopamine was reported in human cerebrospinal fluids by functionalization of gold nanoparticles with 3-MPBA.⁶¹ No SERS signal detected for the nanoparticle probes, however an intense SERS signal was gained upon introduction of dopamine, signaling a successful binding event.

1.2.2 Direct Detection Methods

Incorporation of a secondary analyte for indirect SERS monitoring of biologically relevant species has proven useful for studies across a wide variety of scientific subdisciplines. However, methods involving direct monitoring without the use of a secondary labelling agent are of great interest for clinical applications and for rapid, on-site detection. Such methods typically involve use of metallic nanoparticles or roughened metallic surfaces for SERS acquisition, and are referred to as direct monitoring methods since SERS probes are placed in direct contact with the biomolecule(s) of interest.

Use of metallic nanoparticles for direct SERS detection of biological species has proven useful for virus and disease detection. Gold nanorods have been used to directly monitor spectral differences of normal red blood cells compared to red blood cells (RBCs) infected with malaria virus at various stages of disease progression.⁶² Using chemometric analysis, peak changes were identified that corresponded to expected membrane alterations upon infection of cells with the virus. One of these membrane changes corresponded to a change in the relative ratio of amino acids to cholesterol, which after infection increased more than 4-fold compared to normal RBCs. Additional to viruses, cancer biomarkers have also been monitored using direct SERS detection methodology. Gold and silver nanoparticles were used recently to encapsulate and detect cytidine in urine, a biomarker indicative of early onset of colon cancer.⁶³ Detection levels

at millimolar concentrations were reported, thereby confirming that SERS could be used to monitor cytidine for evaluation of colon cancer risk at early stages.

Chip-based approaches have also been used for direct detection methodologies by SERS. Immobilization of bacteria onto a glass coverslip, followed by introduction of charged gold nanoparticles was used recently to differentiate and detect several types of gram-positive and gram-negative bacteria.⁶⁴ Direct contact of NPs with the membranes of bacteria allowed for direct SERS sensing of nucleic acids, membrane proteins and membrane carbohydrates for each individual strain. Reproducible SERS spectra were acquired with a good signal-to-noise ratio and with low acquisition times. SERS-active substrates have been reported for direct SERS sensing of a variety of biological materials. For example, silver-coated nanohole arrays were utilized to trap biological vesicles released from an ovarian cancer cell line.³¹ Capturing of vesicles occurred without the need for antibodies or other anchoring proteins. Vesicles trapped within the nanoholes were probed by SERS, allowing for molecular-level characterization of nanometer-sized biological species.

1.2.3 Scope of Thesis

This thesis is organized into five chapters. Chapter 1 introduces the field of SERS and outlines current work within this context for biological applications. Chapter 2 focuses on experimental details of this thesis, providing in-depth background information into the physical, chemical and biological principles underlying this work. Chapter 2 also provides important information on the clinical relevance of this work. Chapter 3 outlines nanofabrication techniques to fabricate plasmonically active platforms for SERS and examines their ability to trap and probe nanoscale materials. Chapter 4 extends this work

to application-based sciences and presents results of probing spectral signatures from biological vesicles by SERS. Chapter 5 concludes this thesis with final remarks and future suggestions.

1.3 References

1. Lifson, M. A.; Ozen, M. O.; Inci, F.; Wang, S. Q.; Inan, H.; Baday, M.; Henrich, T. J.; Demirci, U., *Adv. Drug Deliv. Rev.* **2016**, *103*, 90-104.
2. McRae, M. P.; Simmons, G.; McDevitt, J. T., *Bioanalysis* **2016**, *8* (9), 905-919.
3. Alapan, Y.; Fraiwan, A.; Kucukal, E.; Hasan, M. N.; Ung, R.; Kim, M.; Odame, I.; Little, J. A.; Gurkan, U. A., *Expert Rev. Med. Devices* **2016**, *13* (12), 1073-1093.
4. Nosrati, R.; Golichenari, B.; Nezami, A.; Taghdisi, S. M.; Karimi, B.; Ramezani, M.; Abnous, K.; Shaegh, S. A. M., *Trends Analyt. Chem.* **2017**, *97*, 428-444.
5. Martin-Yerga, D.; Perez-Junquera, A.; Gonzalez-Garcia, M. B.; Hernandez-Santos, D.; Fanjul-Bolado, P., *Chem. Comm.* **2018**, *54* (45), 5748-5751.
6. Verma, R. S.; Ahlawat, S.; Uppal, A., *Analyst* **2018**, *143* (11), 2648-2655.
7. Mahmood, T.; Nawaz, H.; Ditta, A.; Majeed, M. I.; Hanif, M. A.; Rashid, N.; Bhatti, H. N.; Nargis, H. F.; Saleem, M.; Bonnier, F., et al., *Spectrochim. Acta A Mol. Biomol. Spectrosc.* **2018**, *200*, 136-142.
8. Han, B.; Zhang, Y. L.; Zhu, L.; Chen, X. H.; Ma, Z. C.; Zhang, X. L.; Wang, J. N.; Wang, W.; Liu, Y. Q.; Chen, Q. D., et al., *Sens. Actuators B Chem.* **2018**, *270*, 500-507.
9. Xu, X. M.; Ma, X. Y.; Wang, H. T.; Wang, Z. P., *Microchim. Acta* **2018**, *185* (7), 1-8.
10. Butler, H. J.; Ashton, L.; Bird, B.; Cinque, G.; Curtis, K.; Dorney, J.; Esmonde-White, K.; Fullwood, N. J.; Gardner, B.; Martin-Hirsch, P. L., et al., *Nat. Protoc.* **2016**, *11* (4), 664-687.
11. Raman, C. V.; Krishnan, K. S., *Nature* **1928**, *121*, 501-502.
12. Ilanchezhian, P.; Kumar, G. M.; Xiao, F.; Madhankumar, A.; Siva, C.; Yuldashev, S. U.; Cho, H. D.; Kang, T. W., *Sol. Energy Mater. Sol. Cells* **2018**, *183*, 73-81.
13. Lei, S. J.; Tao, C. J.; Li, J. L.; Zhao, X.; Wang, W. Z., *Appl. Surf. Sci.* **2018**, *452*, 148-154.
14. Alekseev, P. A.; Dunaevskiy, M. S.; Cirlin, G. E.; Reznik, R. R.; Smirnov, A. N.; Kirilenko, D. A.; Davydov, V. Y.; Berkovits, V. L., *Nanotech.* **2018**, *29* (31).
15. Fleischmann, M.; Hendra, P. J.; McQuillan, A. J., *Chem. Phys. Lett.* **1974**, *26* (2), 163-166.

16. Albrecht, M. G.; Creighton, J. A., *JACS* **1977**, *99* (15), 5215-5217.
17. Jeanmaire, D. L.; Van Duyne, R. P., *J. Electroanal. Chem. Interfacial Electrochem* **1977**, *84* (1), 1-20.
18. Casadio, F.; Leona, M.; Lombardi, J. R.; Van Duyne, R., *Acc. Chem. Res.* **2010**, *43* (6), 782-791.
19. Zhu, K.; Hong, Z.; Kang, S. Z.; Qin, L. X.; Li, G. D.; Li, X. Q., *J. Phys. Chem. Solids* **2018**, *115*, 69-74.
20. Carlini, L.; Fasolato, C.; Postorino, P.; Fratoddi, I.; Venditti, I.; Testa, G.; Battocchio, C., *Colloids Surf. A* **2017**, *532*, 183-188.
21. Polubotko, A. M.; Solovyeva, E. V., *Optics and Spectrosc.* **2018**, *124* (1), 43-48.
22. Perez-Mayen, L.; Oliva, J.; Torres-Castro, A.; De la Rosa, E., *Nanoscale* **2015**, *7* (22), 10249-10258.
23. Li, J. N.; Liu, T. Z.; Zheng, H. R.; Gao, F.; Dong, J.; Zhang, Z. L.; Zhang, Z. Y., *Opt. Express* **2013**, *21* (14), 17176-17185.
24. Diao, F. Y.; Xiao, X. X.; Luo, B.; Sun, H.; Ding, F.; Ci, L. J.; Si, P. C., *Appl. Surf. Sci.* **2018**, *427*, 1271-1279.
25. Solis, D. M.; Taboada, J. M.; Obelleiro, F.; Liz-Marzan, L. M.; de Abajo, F. J. G., *ACS Photonics* **2017**, *4* (2), 329-337.
26. Danno, M.; Yoshinari, S.; Igari, S.; Honda, J.; Eguchi, T.; Inoue, W.; Yasuhara, K.; Hara, S.; Ikake, H.; Shimizu, S., et al., *Chemistry Letters* **2018**, *47* (4), 429-432.
27. Ali, A.; Hwang, E. Y.; Choo, J.; Lim, D. W., *Analyst* **2018**, *143* (11), 2604-2615.
28. Liu, Y. Q.; Li, X. J.; Wu, H. C.; Zeng, Z.; Zhang, D.; Wang, P. J.; Zhang, L. S.; Fang, Y., *Plasmonics* **2017**, *12* (6), 1861-1867.
29. Mosier-Boss, P. A., *Nanomaterials* **2017**, *7* (6), 142.
30. Rodriguez, R. D.; Sheremet, E.; Nesterov, M.; Moras, S.; Rahaman, M.; Weiss, T.; Hietschold, M.; Zahn, D. R. T., *Sens. Actuators B Chem.* **2018**, *262*, 922-927.
31. Lee, C.; Robertson, C. S.; Nguyen, A. H.; Kahraman, M.; Wachsmann-Hogiu, S., *Sci. Rep.* **2015**, *5*, 11644.
32. Hobbs, R. G.; Petkov, N.; Holmes, J. D., *Chem. Mater.* **2012**, *24* (11), 1975-1991.
33. Hua, M. Z.; Feng, S. L.; Wang, S.; Lu, X. N., *Food Chem.* **2018**, *258*, 254-259.
34. Newmai, M. B.; Verma, M.; Kumar, P. S., *Appl. Surf. Sci.* **2018**, *440*, 133-143.
35. Alessandri, I.; Vassalini, I.; Bertuzzi, M.; Bontempi, N.; Memo, M.; Gianoncelli, A., *Sci. Rep.* **2016**, *6*.
36. Qu, L. L.; Liu, Y. Y.; He, S. H.; Chen, J. Q.; Liang, Y.; Li, H. T., *Biosens. Bioelectron.* **2016**, *77*, 292-298.

37. Grochowska, K.; Siuzdak, K.; Karczewski, J.; Szkoda, M.; Sliwinski, G., *Plasmonics* **2017**, *12* (6), 1939-1946.
38. Wang, J.; Dong, J. C.; Yang, J.; Wang, Y.; Zhang, C. J.; Xu, M. M.; Mao, B. W.; Yao, J. L.; Li, J. F.; Tian, Z. Q., *Electrochem. Commun.* **2017**, *78*, 16-20.
39. Wojcik, K.; Czaja, T.; Szostak, R.; Grzeszczuk, M., *J. Solid State Electrochem.* **2017**, *21* (3), 823-832.
40. Huang, A.; Zhang, L. N.; Li, W. W.; Ma, Z. Y.; Shuo, S.; Yao, T. M., *Royal Soc. Open Sci.* **2018**, *5* (4), 1-10.
41. Karadan, P.; Aggarwal, S.; Anappara, A. A.; Narayana, C.; Barshilia, H. C., *Sens. Actuators B Chem.* **2018**, *254*, 264-271.
42. Fu, X.; Cheng, Z.; Yu, J.; Choo, P.; Chen, L.; Choo, J., *Biosens. Bioelectron.* **2016**, *78*, 530-537.
43. Bassi, B.; Dacarro, G.; Galinetto, P.; Giulotto, E.; Marchesi, N.; Pallavicini, P.; Pascale, A.; Perversi, S.; Taglietti, A., *NanoTech.* **2018**, *29* (23), 1-11.
44. Nair, R. V.; Santhakumar, H.; Jayasree, R. S., *Faraday Discuss.* **2018**, *207*, 423-435.
45. Shen, Y. T.; Liang, L. J.; Zhang, S. Q.; Huang, D. S.; Deng, R.; Zhang, J.; Qu, H. X.; Xu, S. P.; Liang, C. Y.; Xu, W. Q., *ACS Appl. Mater. Interfaces* **2018**, *10* (9), 7910-7918.
46. Sun, M. M.; Qian, H. M.; Liu, J.; Li, Y. C.; Pang, S. P.; Xu, M.; Zhang, J. T., *RSC Adv.* **2017**, *7* (12), 7073-7078.
47. Shen, Y. T.; Liang, L. J.; Zhang, S. Q.; Huang, D. S.; Zhang, J.; Xu, S. P.; Liang, C. Y.; Xu, W. Q., *Nanoscale* **2018**, *10* (4), 1622-1630.
48. Kwon, J. A.; Jin, C. M.; Shin, Y.; Kim, H. Y.; Kim, Y.; Kang, T.; Choi, I., *ACS Appl. Mater. Interfaces* **2018**, *10* (15), 13226-13235.
49. Liu, Y. J.; Xu, C. X.; Lu, J. F.; Zhu, Z.; Zhu, Q. X.; Manohari, A. G.; Shi, Z. L., *Appl. Surf. Sci.* **2018**, *427*, 830-836.
50. Pearson, B.; Mills, A.; Tucker, M.; Gao, S.; McLandsborough, L.; He, L. L., *Food Microbiol.* **2018**, *72*, 89-97.
51. Singh, P.; Gupta, R.; Choudhary, M.; Pinnaka, A. K.; Kumar, R.; Bhalla, V., *Sens. Actuators B Chem.* **2018**, *262*, 603-610.
52. Tabatabaei, M.; Wallace, G. Q.; Caetano, F. A.; Gillies, E. R.; Ferguson, S. S. G.; Lagugne-Labarthe, F., *Chem. Sci.* **2016**, *7* (1), 575-582.
53. Li, C. N.; Fan, P. D.; Liang, A. H.; Liu, Q. Y.; Jiang, Z. L., *Microchim. Acta* **2018**, *185* (3), 177.
54. Chen, Y.; Bai, X. R.; Su, L.; Du, Z. W.; Shen, A. G.; Materny, A.; Hu, J. M., *Sci. Rep.* **2016**, *6*.
55. Guerrini, L.; Arenal, R.; Mannini, B.; Chiti, F.; Pini, R.; Matteini, P.; Alvarez-Puebla, R. A., *ACS Appl. Mater. Interfaces* **2015**, *7* (18), 9420-9428.

56. Phatangare, A. B.; Dhole, S. D.; Dahiwale, S. S.; Bhoraskar, V. N., *Appl. Surf. Sci.* **2018**, *441*, 744-753.
57. Kim, N. H.; Lee, S. J.; Moskovits, M., *Nano Lett.* **2010**, *10* (10), 4181-4185.
58. Camacho, S. A.; Sobral, R. G.; Aoki, P. H. B.; Constantino, C. J. L.; Brolo, A. G., *ACS Sens.* **2018**, *3* (3), 587-594.
59. Yao, G. P.; Zhang, H. Y.; Deng, C. H.; Lu, H. J.; Zhang, X. M.; Yang, P. Y., *Rapid Commun. Mass Spectrom.* **2009**, *23* (22), 3493-3500.
60. Sun, F.; Ella-Menye, J. R.; Galvan, D. D.; Bai, T.; Hung, H. C.; Chou, Y. N.; Zhang, P.; Jiang, S. Y.; Yu, Q. M., *ACS Nano.* **2015**, *9* (3), 2668-2676.
61. Zhang, K.; Liu, Y.; Wang, Y. N.; Zhang, R.; Liu, J. G.; Wei, J.; Qian, H. F.; Qian, K.; Chen, R. P.; Liu, B. H., *ACS Appl. Mater. Interfaces* **2018**, *10* (18), 15388-15394.
62. Chen, F.; Flaherty, B. R.; Cohen, C. E.; Peterson, D. S.; Zhao, Y., *Nanomedicine* **2016**, *12* (6), 1445-1451.
63. Xiang, Y.; Yang, H.; Guo, X.; Wu, Y.; Ying, Y.; Wen, Y.; Yang, H., *Microchim. Acta* **2018**, *185* (3), 195.
64. Dina, N. E.; Colnita, A.; Leopold, N.; Haisch, C., Turner, A.; Tang, A., Eds. 2017; Vol. 27, 203-207.
65. Lee, C.; Carney, R. P.; Hazari, S.; Smith, Z. J.; Knudson, A.; Robertson, C. S.; Lam, K. S.; Wachsmann-Hogiu, S., *Nanoscale* **2015**, *7* (20), 9290-9297.

Chapter 2

2 Extracellular Vesicles (EVs)

Extracellular vesicles are secreted by nearly all cell types within the body and are present in nearly all our biofluids. They were previously believed to be junk materials released from cells but are now widely accepted to play diverse and functional roles throughout the body. This chapter introduces EVs, outlines their functions and describes some spectroscopic and biological methods that may be used to validate their presence and composition.

2.1 History of EVs

In 1946, Chargaff and West unknowingly discovered extracellular vesicles (a subgroup known as microvesicles) when they observed a precipitate factor present in platelet-free plasma.¹ In 1967, Wolf described extracellular vesicles as ‘platelet dust,’ after discovering what he believed to be lipid ‘junk’ present in a fraction of a plasma sample following ultracentrifugation.² Following their serendipitous discovery, scientists discovered that EVs were anything but dust. They have since been found to play important roles in the fields of immunology,^{3,4} cell biology,^{5,6} biochemistry,^{7,8} neuroscience,^{9,10} and ophthalmology.^{11,12} The intense interest in EVs has grown largely throughout the past decade, as shown in Figure 2.1 by the number of publications accepted to journals across scientific subdisciplines.

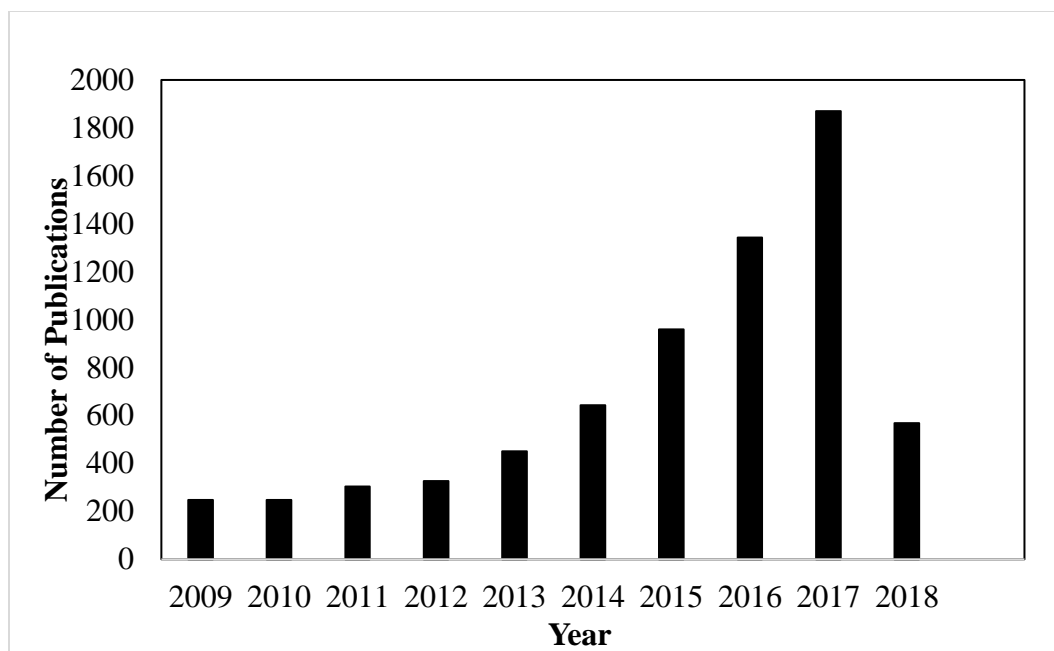


Figure 2.1 - Number of publications retrieved from webofknowledge.com mentioning 'extracellular vesicle' as of June 20, 2018

2.1.1 Classification and Composition of EVs

The umbrella term, 'extracellular vesicle' refers to three main types of vesicles: exosomes, microvesicles and apoptotic bodies. Nomenclature for classification of EVs has been under considerable debate in recent decades. Previously, EVs were solely classified based on the type of cell they were released from. For example, prostate-cell derived vesicles were classified as prostasomes,¹³ whereas neuronal vesicles were classified as synaptic vesicles.¹⁴ However, a new classification system extended classification based on origin to size, allowing for universal comparison across cell lines. Exosomes (30 nm – 100 nm) originate from the cytoplasmic region of cells and are exocytosed into the extracellular environment upon fusion of multivesicular bodies (MVBs) with the plasma membrane of cells. Microvesicles are larger versions of

exosomes (50 nm – 1000 nm) and are released by membrane blebbing from the cellular surface. Apoptotic bodies are the largest class of EV (50 - 5000 nm) and are released during cellular apoptosis. In addition, these three classifications of vesicle separate into different fractions during ultracentrifugation due to their density differences. EV classification may occur based on size, density and origin as outlined in Table 1.

Table 1 - Classification of EVs

Type of EV	Approximate Size (nm)	Density (g/mL)	Detection/ Characterization	Origin/ Location of Release	Reference
Exosome	30 – 100	1.13 – 1.19	TEM, WB, FC, MS	Exocytosis of multivesicular bodies	15, 16, 17
Microvesicle	50 – 1000	1.03 – 1.08	FC, SEM, TEM	Plasma membrane	15, 18, 19
Apoptotic Body	50 - 5000	1.16 – 1.28	FC, SEM, TEM	Plasma membrane or endoplasmic reticulum during apoptosis (cell death)	15, 20, 21

EVs have been found to play diverse and important roles in delivery of cargoes to target cells. These cargoes include functional proteins, growth factors, nucleic acids and lipids.²² Their roles include intercellular communication,²³ signal transduction,^{9, 10} T-cell stimulation,^{4, 24} cancer metastasis²⁵ and apoptosis.²⁶ Due to their release from cells into their microenvironment within the human body, EVs may be isolated from biological fluids such as tears,²⁷ urine,²⁸ blood,^{29,30} and cerebrospinal fluid.³¹ A given cohort of EVs

released from a single parent cell may vary widely in composition and location of biomarkers. Study of their composition has previously been reported by fluorescence microscopy, scanning electron microscopy (SEM), transmission electron microscopy (TEM).³² mass spectroscopy(MS),³³ flow cytometry (FC),¹⁵ western blotting (WB)^{34,35} and atomic force microscopy (AFM).³⁶

2.1.2 Methods of Isolating EVs

Ongoing studies seek to understand the modes of action as well as diverse functional roles of EVs. This information is necessary to better understand disease progression and their link to biomarker presence and distribution for a wide variety of diseases. A major challenge thus far in EV research is the lack of standardization in isolation of EVs. Advances have been noted in isolation techniques involving ultracentrifugation, differential centrifugation, microfluidics, filtration and chromatography. This section will focus mainly on isolation of EVs through ultracentrifugation and filtration.

Ultracentrifugation (UC) is considered the gold standard of EV isolation. It is the most common method used has been reported to isolate EVs of varying size, density and origin, including from bodily fluids and conditioned cell culture media. The technique requires numerous centrifugation steps to isolate EVs from other biological matter such as dead cells and proteins. UC protocol typically begins with a low-speed centrifugation step, such as 300 g for 10 minutes to remove dead cells and larger apoptotic body debris. The proceeding steps vary amongst research groups, however protocols increase speeds in subsequent steps, between 1000 g to 20,000 g to remove larger protein debris and larger vesicles.³⁷ The final centrifugation step involves a spin at 100,000 g to precipitate

EVs to the bottom of the vial, after which supernatant is removed and the EV isolate is resuspended in phosphate buffered saline, or water in some cases.³⁸ The technique has been successful at isolating exosomes and microvesicles, however apoptotic bodies have been reported less commonly in the literature, especially upon resuspension with water rather than buffer.

Though UC is a gold-standard technique for isolation of EVs, it suffers from long isolation times, often requiring 4 – 6 hours for complete. In addition, it is difficult to optimize isolation protocols due to the large variety in sample compositions from various biofluids or cell cultures. Previous literature has also reported loss of important exosomal proteins and RNAs following UC, indicating loss of important biomarkers for study of disease progression and diagnosis.^{39, 40}

Filtration techniques are often reliant on centrifugation steps to remove dead cells and debris and may minimize time compared to UC. Following initial centrifugation, filters or membranes may be used to sort EVs from remaining media or biofluids. For example, Campoy *et al.* successfully isolated vesicles from uterine cells for study of endometrial disorders by incorporating a 200-nm filter following a 10,000 *g* centrifugation for 30 minutes.⁴¹ Applying this method, the group concluded successful exosomal isolation by SEM and immunoblotting. Filtration through chromatography columns has also previously been reported following centrifugation steps.⁴² Although filtration techniques have proven successful in isolation of EVs, they are still reliant on centrifugation. In addition, pores and membranes may become clogged during isolation, meaning re-use of filters is highly discouraged.

Specificity in isolation of EVs based on biomarkers may be achieved using magnetic beads coated antibodies specific to antigen present on the surface of EVs, or antibody coated microfluidic devices.⁴¹ However, complete isolation of EVs from other biomaterials remains as a challenge since origin of samples varies widely.

2.1.3 EVs as Human Liquid Biopsies

In past years, definitive determination of disease diagnosis occurred mainly through tissue biopsies. Through surgical procedures, a suspected sample would be removed for biopsy through microscopic and analytical means. Tissue biopsies provide useful information to the clinician and patient, however the means of obtaining such samples are often time consuming, invasive, costly and risky to the patient. Additionally, tissue biopsies mainly provide site-specific information, and do not allow for differentiation of additional diseases that may be present at locations in a given body or system.

Movement towards liquid biopsies reduces many of the drawbacks of tissue biopsies. Liquid biopsies are acquired by collection of blood, urine, tears or saliva. Their modes of collection are less invasive compared to tissue extraction as they are collected by needle extraction (blood collection), or by simple collection (urine and tear collection). These methods minimize sample acquisition time, harm to the patient and provide additional insight into overall human health since they carry DNA, platelets and microparticles released from other effector areas of the body. The biofluids undergo sample preparation protocols to isolate for vesicles, DNA, platelets and other materials of interest. These biopsies allow for molecular analyses very similar to those allowed by tissue samples while providing many benefits to the patient.

Extracellular vesicles, specifically exosomes have been studied in great depth due to their small size and great stability in liquid environments. The lipid bilayer surrounding exosomes protects the internal cargo from degradation allowing for study of their internal contents.⁴³ Additionally, the internal and external biomarkers reflect those of the cell of their origin, providing a means of studying cell biology while eliminating complex cellular machinery such as a nucleus or golgi apparatus, which is exceptionally valuable for spectroscopic studies.

2.1.4 Spectroscopic Studies of EVs

Study of EVs by vibrational spectroscopy allows for study of cellular biomarkers without bulky cellular machinery. In human health studies, analysis of biomarkers present internally and externally in EVs may provide information on stage and degree of disease progression. This information has been probed using Raman,⁴⁴ SERS,^{23, 45, 46} and Fourier-transform infrared spectroscopy (FT-IR).⁴⁷

Through analysis of the spectroscopic signature of EVs derived from cancerous and non-cancerous origins, it may also be possible to generate a library spectroscopic peaks outlining the variation and common cargoes among cell lines. For example, when comparing cancerous and non-cancerous lines of EVs, some expected conserved spectroscopic peaks (listed peaks are SERS peaks) may be chain C-C stretches in lipids from the phospholipid bilayer (700 cm^{-1}), CH_2 and CH_3 deformations from proteins and lipids (1450 cm^{-1}), C=C stretches in lipids (1651 cm^{-1}), and amide II vibrations in proteins ($1480\text{-}1575\text{ cm}^{-1}$). In contrast, peaks corresponding to nucleic acids and proteins such as C-C stretching from proline and valine ($930\text{-}940\text{ cm}^{-1}$) and asymmetric phosphate stretching (1245 cm^{-1}) would be expected to vary.

2.2 Principles of Surface-Enhanced Spectroscopies

2.2.1 Plasmon Resonances in Metal

Metallic materials consist of charges (free electrons) that may be placed into motion by coupling of an oscillating electromagnetic field polarized in a defined direction. This phenomenon is defined within the field of plasmonics, which aims to control the coupling of an electromagnetic field with the free electrons in the conduction band of a metals. Plasmons are exploited widely in spectroscopy, in a subfield known as molecular plasmonics.⁴⁸ Many studies in molecular plasmonics utilize metallic nanostructures to exploit the local electromagnetic enhancement near the surface of the conductive surface or metal. Some of these fields are surface-enhanced Raman spectroscopy (SERS), tip-enhanced Raman spectroscopy, surface-enhanced fluorescence, surface enhanced infrared absorption.

2.2.2 Surface Plasmon Polaritons (SPP)

A surface plasmon polariton (SPP) is defined as a collective fluctuation in electronic density at the interface of a metal and a dielectric. The oscillation frequency of free electrons is dependent on the type of metal and the surrounding dielectric medium. Additional factors such as the size of the metallic structure, shape of metallic structure and the distance between adjacent metallic structures must also be taken into consideration. Surface plasmon waves are tightly confined to the interface between a metal and a dielectric. The intensity of a SP decays exponentially away from the surface. The decay length (i.e. the distance between maximum and minimum field) into the

dielectric medium may be estimated by $\lambda/2n$ where n is the refractive index of the dielectric.⁴⁹

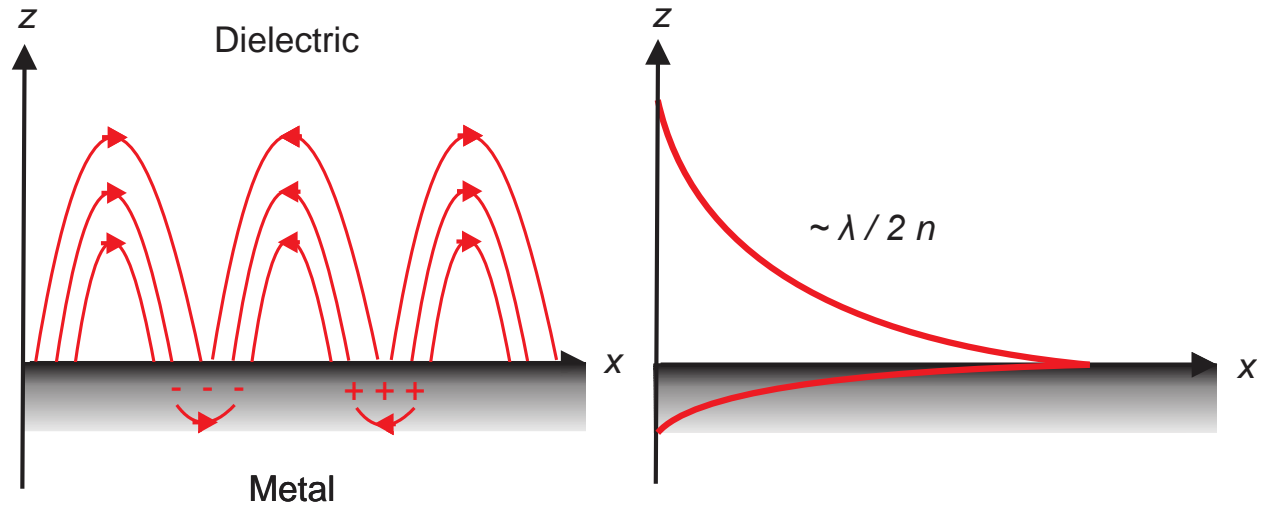


Figure 2.2 - (a) Schematic of the charge distribution and local electric field associated with surface plasmons; (b) The strength of the SP decays exponentially with increasing distance from the metal and dielectric

2.2.3 Localized Surface Plasmon Resonance

A condition known as surface plasmon resonance occurs when the frequency of incoming light exactly matches that of the frequency of oscillation of surface plasmons. In the case where a surface plasmon interacts with a nanostructure smaller than the wavelength of incident light, the surface plasmon becomes confined to the nanostructure, generating a localized surface plasmon resonance (LSPR). In LSPR, the free electrons in the metal oscillate with respect to the induced electric field causing the momentum and wavevector of the nanostructure to change.

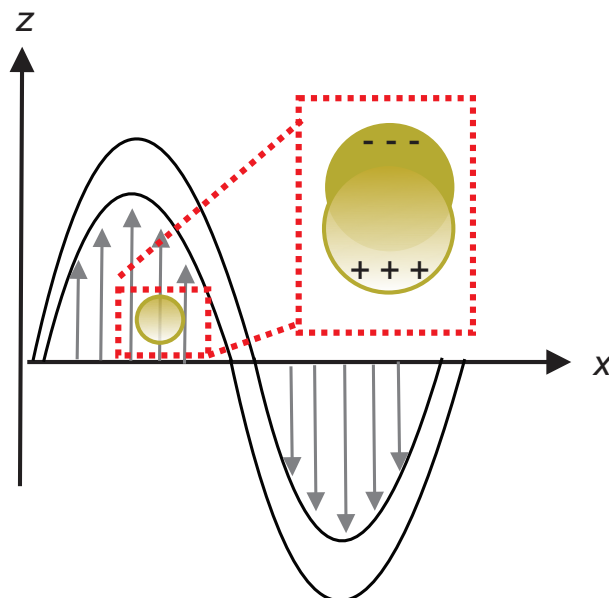


Figure 2.3 – Localized surface plasmon resonance of a metallic nanoparticle

Bulk surface plasmons are differentiated from localized plasmons when working with nanoparticles or nanostructures on the sub-wavelength size scale. LSPR modes are dependent on the metal type as well as the size and shape of the structure.⁵⁰ The localization of an incident electromagnetic field near the surface of metallic nanostructures is the basis of many surface-enhanced techniques.

2.2.4 Raman Spectroscopy

Raman spectroscopy is a spectroscopic technique used to observe vibrational modes of molecules that compose a material or a biomaterial. It is a label-free technique offering molecular information from inelastically scattered light. The interaction and scattering of light off a molecule or biomolecule of interest provides information on the molecular composition of the system and, when used in conjunction with polarized measurements, can lead to the determination of molecular orientation at surfaces. Raman spectroscopy is a powerful technique used to study biological and chemical systems, and

has also been used in the literature to analyze commonalities and differences amongst extracellular vesicles from cancerous and non-cancerous origins.^{51, 52}

When light impinges onto a molecule or particle of interest, a majority of the light is elastically scattered. This is the most common form of scattering, known as Rayleigh scattering. Rayleigh scattering occurs when scattered light is emitted at the same frequency (ν_0) as the incident light. 1 in every 10^8 photons of incident light scatters inelastically by emitting with a higher or lower frequency compared to the incident radiation. This shift of energy is known as a Raman shift. Lower energy, or higher wavelength photons are known as Stokes-shifted photons, whereas higher energy and lower wavelength photons are known as anti-Stokes shifted photons.

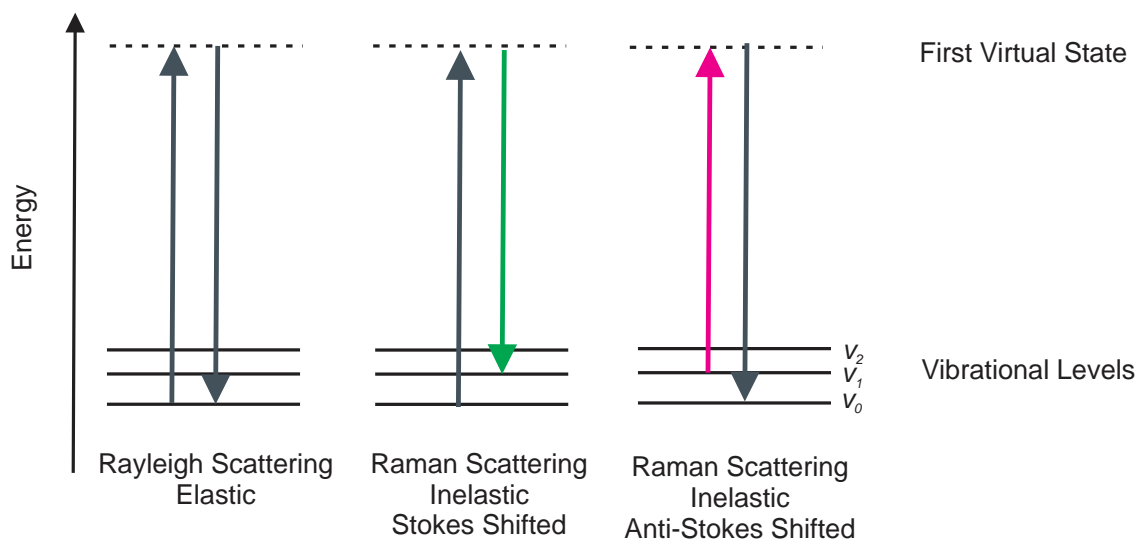


Figure 2.4 - Illustration of the various elastic and inelastic scattering paths an emitted photon may undergo following interaction with a molecule of interest

The various scattering paths a photon may take upon interaction with a molecule of interest are outlined in Figure 2.5, where ν_0 , ν_1 and ν_2 indicate various vibrational

states of a molecule. Elastic transitions with no net change in energy (such as ν_0 to ν_0 transitions) indicate Rayleigh transitions. Inelastic transitions resulting in photons of higher wavelength (ν_1 to ν_0) or lower wavelength (ν_0 to ν_2) indicate Raman-active transitions. Stokes-shifted photons occur more frequently than anti-Stokes shifted photons due to the probability distribution of molecules occupying excited and ground state vibrational modes at any temperature, modelled by the Boltzmann distribution curve.⁵³ At room temperature, most molecules exist in their ground energy state while only a small fraction exist in an excited vibrational or rotational state.

Although Raman spectroscopy is a well-adapted technique for biological and chemical studies, it has an intrinsic weak sensitivity due to the poor scattering cross section of materials. Fortunately, the Raman signal may be enhanced by using surface-enhanced Raman spectroscopy (SERS) techniques.

2.3 Surface-Enhanced Raman Spectroscopy (SERS)

2.3.1 Electromagnetic Mechanism of SERS

Two mechanisms, the chemical and electromagnetic mechanisms are responsible for the SERS enhancement. The electromagnetic mechanism of SERS is a direct result of the localized surface plasmon resonance (LSPR) of metallic nanoparticles. Upon interaction with the oscillating electromagnetic field of light, the free electrons in the conduction band of a metallic nanostructure become polarized and generate plasmons in the electron cloud of the metal.⁵⁰ At specific frequencies, the oscillation of the metallic nanostructure will be in resonance with the frequency of the incident light, generating a LSPR oscillation. Through control of the size, shape, type of metal and the local

dielectric environment of the metallic NPs, one can fine-tune the resonance condition, location and strength of the LSPR from visible to near-infrared ranges. The enhancement factor allowed by the electromagnetic mechanism may be approximately quantified using equation (1):

$$E = |E(\omega)|^2 / |E(\omega')|^2 \quad (1)$$

Where E is the enhancement factor, $E(\omega)$ is the local electric-field enhancement factor at the incident frequency, ω , and $E(\omega')$ is the Stokes-shifted enhancement factor at frequency ω' . E is often estimated by assuming $E(\omega)$ and $E(\omega')$ are the same, leading to an overall enhancement factor of $E(\omega)^4$.⁵⁴

To demonstrate the enhancement of the Raman signal by SERS, experimental Raman and SERS spectra of malachite green (MG) are shown below (Figure 2.5).

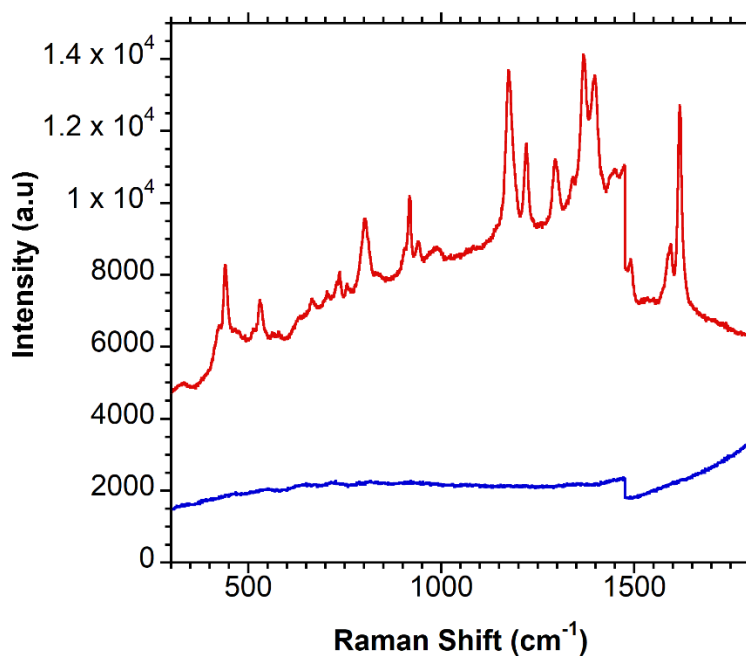


Figure 2.5 – SERS (red) and Raman (blue) spectra of malachite green

The enhancement allowed by the chemical and electromagnetic enhancement mechanisms of SERS is visibly considerable. The characteristic Raman peaks of MG were comparable to the literature. For example, the N-C bonding and C-C stretching vibrations were observed at 1617 cm^{-1} . Additionally, the bands at 1173 and 1294 cm^{-1} are assigned to aromatic C-H bending vibrations.⁵⁵ The SERS spectrum was obtained by dilution of MG powder to 1 mM in ethanol and placement onto a SERS-active substrate prepared by lithography. The Raman spectrum was obtained by placement of bulk MG powder onto a glass coverslip.

2.3.2 Chemical Enhancement Mechanism of SERS

The chemical enhancement (CE) mechanism is still an active area of study and is not yet completely understood. It is thought to occur due to formation of a bond between an adsorbed molecule and a metal. Three distinct phenomena, known as (1) charge-transfer chemical enhancement, (2) resonant Raman enhancement and the (3) non-resonant Raman enhancement mechanisms have been proposed, which work in tandem to generate the effect.⁵⁶

2.4 Preparation of Plasmonic Platforms by Nanosphere Lithography

A common method for fabricating semi-reproducible plasmonic substrates for collection of SERS spectra is by nanosphere lithography (NSL). NSL is a bench-top technique reliant on the self-assembly of nanoparticles in hexagonally arranged arrays. Following self-assembly on a substrate such as quartz, glass or silicon, metal is deposited and nanoparticles are gently removed by sonication revealing triangular nanostructures that are SERS active. These structures have previously been fabricated by members of the

Lagugn -Labarthe research group and have been reported in the literature for analyte detection⁵⁷ and mapping of cancerous biomarkers in different cell lines.⁵⁸

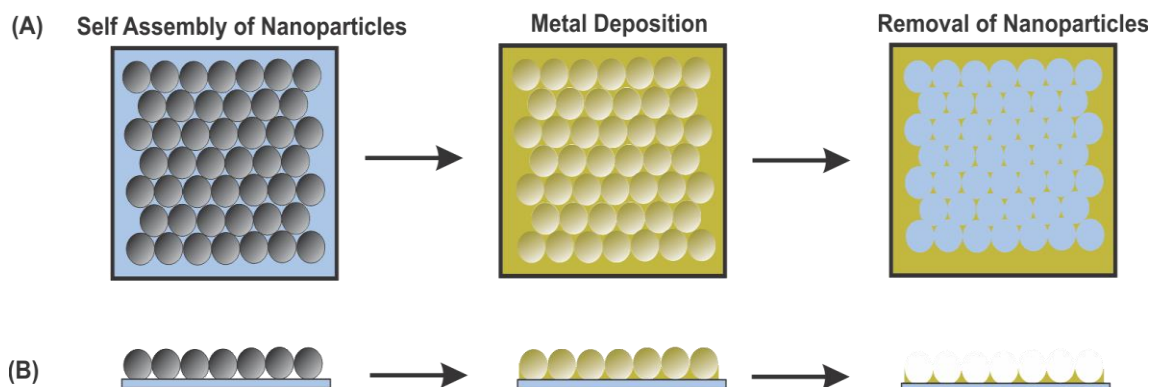


Figure 2.6 – Schematic of NSL fabrication, with top and side views

NSL offers the ability to fabricate large SERS-active domains several microns in size. In some cases, areas of coverage have also been reported as centimeters in size.⁵⁹ However, nanosphere lithography suffers from low reproducibility and homogeneity, and offers limited variations of structures that may be fabricated.¹⁹ Figure 2.7 outlines structures fabricated by NSL of 1.00 μm polystyrene microspheres by SEM. Figures 2.7 (A, B) illustrate desired nanostructures with well-defined tips at triangle apexes. The sharp apices of nanotriangles have been characterized previously to generate the maximum SERS enhancement.⁶⁰ Challenges in achieving uniformity of the nanostructures is highlighted in Figure 2.7 C). In the right-half of this image, the polystyrene distributed into a monolayer formation whereas on the left-half of this image, a bilayer of polystyrene assembled. Lift-off of the bilayer of PS revealed nanostructures that are non-uniform in size, shape and spacing.

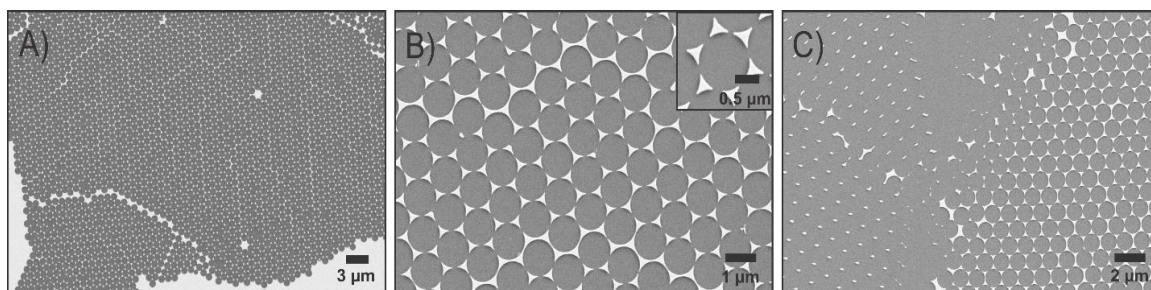


Figure 2.7 - SEM images of nanostructures prepared by NSL; A, B) Top view of nanostructures following lift-off; C) Boundary between a bilayered area and monolayered area following lift-off of nanospheres

Classic structures generated by NSL are the nanoprisms. Other nanostructures fabricated by NSL are nanopyramids,⁶¹ film-over-nanosphere,⁶² Moire patterns,⁶³ nanohole arrays,⁶³ nanocrescents⁶⁴ and nanobowls.⁶⁵

2.4.1 Preparation of Plasmonic Platforms by Electron Beam Lithography

To overcome many of the challenges of NSL, electron beam lithography (EBL) is considered a competitive technique. It offers many benefits over NSL namely precise control over the sizes and shapes of patterns for fabrication of plasmonically active substrates. It is also highly reproducible compared to NSL. EBL typically employs a scanning electron microscope, and an electron beam that is precisely scanned across a photoresist to generate a pattern. Photoresists are either ‘positive’, or ‘negative’, meaning areas exposed to the electron beam will either become *more* or *less* soluble when exposed to a developing solution. Positive resists undergo bond breaking in areas exposed to the electron beam, therefore producing a pattern that is the same as the pattern outlined by the electron beam (positive image), whereas negative resists undergo bond-making in

exposed areas, producing the reverse (negative image) as the pattern outlined by the electron beam. Following electron irradiation, exposed areas in a positive resist dissolve in developing solution (generally an organic solvent) whereas exposed areas in the negative resist are maintained. Incorporation of metals such as gold and silver may be deposited to allow for propagation of plasmons and SERS capabilities.

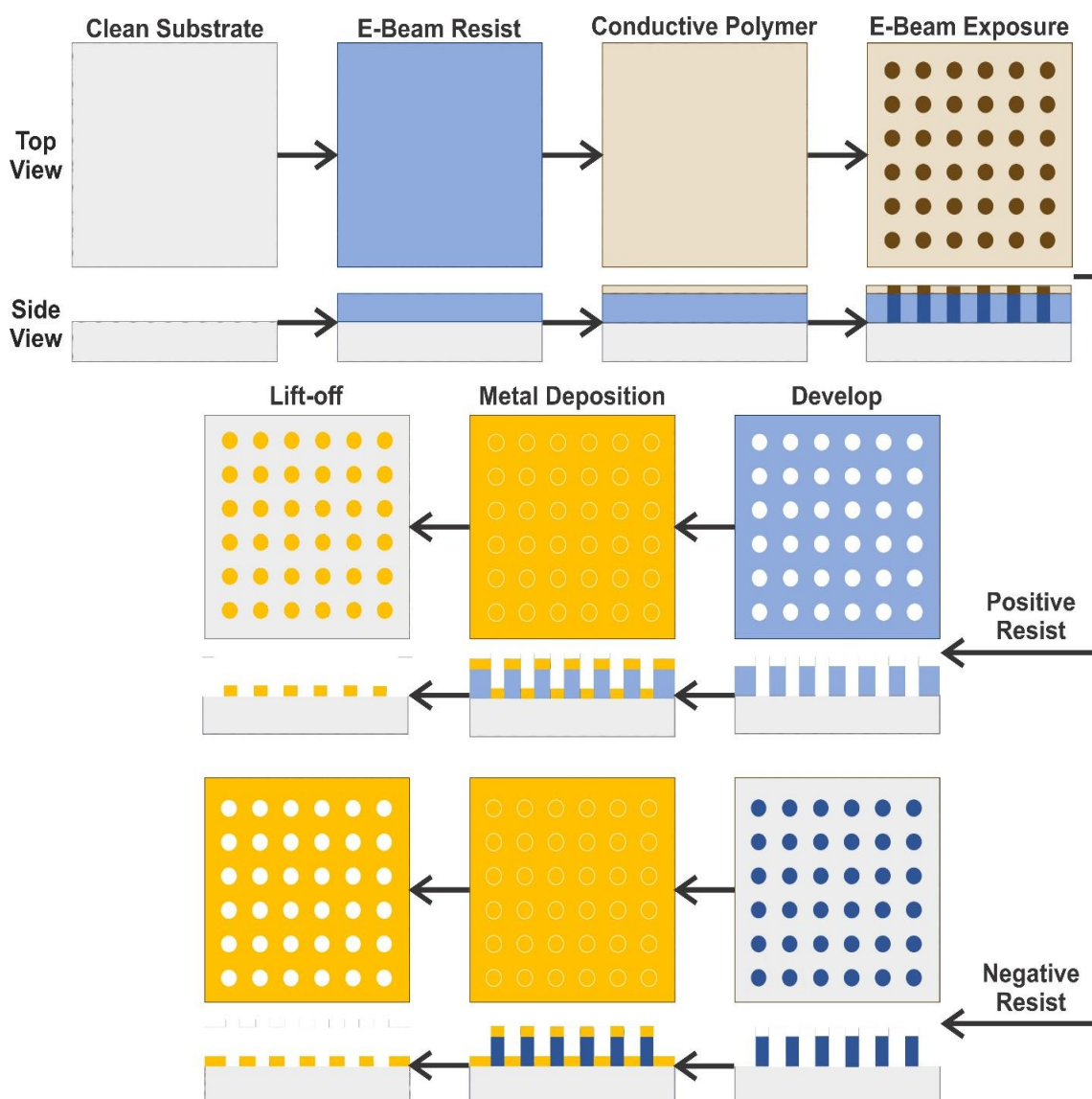


Figure 2.8 - Schematic illustration of electron beam lithography process performed on a positive and negative resist.⁶⁶

2.4.2 Characterization of Plasmonic Platforms

To characterize plasmonic platforms, the absorption spectra are typically acquired to determine the optimal wavelengths of LSPR excitation. The LSPR excitation wavelength maximum (λ_{\max}) is sensitive to a variety of factors including the dielectric constant of the metal, the refractive index as well as the structure and shape of the metallic nanostructures. Therefore, any changes in metal type, thickness, or substrate should lead to acquisition of an absorption spectra for characterization of λ_{\max} .

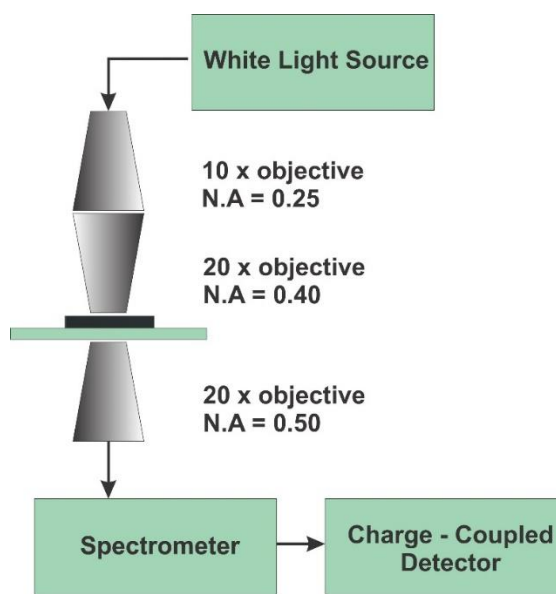


Figure 2.9 – Schematic of absorption spectra setup enabling the measurement of plasmon resonances of the nanostructured surfaces over a surface limited to a few tens of microns.

Figure 2.8 illustrates a schematic of the apparatus used to obtain an absorption spectrum. The area required to obtain an absorption spectrum is typically 40 – 100 microns in diameter. The home-built setup involves use of a white light source (halogen lamp), which is conducted through an optical fiber (100 μm diameter) to a series of

objectives to reduce the size of the probe beam yet keeping it parallel. These objectives lead the transmitted light to a spectrometer and ultimately to a charge-coupled detector. This allows for measurement of the intensity of light upon reaching the spectrometer. The light transmitted is measured as a function of incident wavelength, allowing calculation of the ratio of transmitted intensity (I) versus initial intensity (I_0) and expressed in units of absorbance ($\text{abs} = -\log(I/I_0)$).

2.5 Summary

This chapter outlines the biological makeup and clinical relevance of extracellular vesicles. In addition, the physical principles underlying lithographic techniques proposed for the characterization of EVs are highlighted. Lithographic techniques may be used to fabricate nanostructures compatible with surface-enhanced Raman spectroscopy, a technique based off the inelastic scattering of light. The low scattering cross-section of inelastically scattered light may be enhanced within plasmonic fields generated at the surface of a noble metal upon illumination with a monochromatic laser source coupled with the resonant wavelength(s) of the nanostructures. This provides the basis of surface-enhanced techniques and allows for detection of analytes down to the single-molecule level. The mechanisms responsible for this enhancement, known as the chemical and electromagnetic mechanisms are also discussed in detail.

Fabrication of metallic platforms prepared by lithography are proposed for study of biological nanomaterials known as extracellular vesicles. Two lithographic techniques, nanosphere lithography and electron beam lithography are discussed in this realm. NSL is a well-characterized technique for fabrication of large areas of nanostructures and is proposed for probing of the bulk SERS spectral signatures of EVs. Electron beam

lithography is further proposed for controlled fabrication of nanostructures and probing of individual spectral signatures of EVs. This work ultimately seeks to apply well-characterized nanofabrication techniques to study a novel biological application in a promising field.

2.6 References

1. Chargaff, E.; West, R., *J. Biol. Chem.* **1946**, *166* (1), 189-197.
2. Wolf, P., *Br. J. Haematol.* **1967**, *13* (3), 269-288.
3. He, S.; Wu, C.; Xiao, J.; Li, D.; Sun, Z.; Li, M., *Scand. J. Immunol.* **2018**, *87* (4), 1-16.
4. Calvo, V.; Izquierdo, M., *Front. Immunol.* **2018**, *9*, 684.
5. Zhong, Z. Y.; Rosenow, M.; Xiao, N.; Spetzler, D., *J. Extracell. Vesicles* **2018**, *7* (1), 1-23.
6. Sampaio, N. G.; Emery, S. J.; Garnham, A. L.; Tan, Q. Y.; Sisquella, X.; Pimentel, M. A.; Jex, A. R.; Regev-Rudzki, N.; Schofield, L.; Eriksson, E. M., *Cell Microbiol.* **2018**, *20* (5), 1-18.
7. Olaizola, P.; Lee-Law, P. Y.; Arbelaiz, A.; Lapitz, A.; Perugorria, M. J.; Bujanda, L.; Banales, J. M., *Biochim. Biophys. Acta, Mol. Basis Dis.* **2018**, *1864* (4), 1293-1307.
8. Lasser, C.; Jang, S. C.; Lotvall, J., *Mol. Aspects Med.* **2018**, *60*, 1-14.
9. Liao, K.; Niu, F.; Hu, G.; Buch, S., *J. Neuroimmune Pharmacol.* **2018**, *13*, 48.
10. Andras, I. E.; Garcia-Contreras, M.; Toborek, M., *J. Neuroimmune Pharmacol.* **2018**, *13*, S2.
11. Mead, B.; Amaral, J.; Tomarev, S., *Invest. Ophthalmol. Vis. Sci.* **2018**, *59* (2), 702-714.
12. Klingeborn, M.; Dismuke, W. M.; Rickman, C. B.; Stamer, W. D., *Prog. Retin. Eye Res.* **2017**, *59*, 158-177.
13. Aumuller, G.; Renneberg, H.; Hasilik, A., *Cell Tissue Res.* **1997**, *287* (2), 335-342.
14. Vonmollard, G. F.; Mignery, G. A.; Baumert, M.; Perin, M. S.; Hanson, T. J.; Burger, P. M.; Jahn, R.; Sudhof, T. C., *Proc. Natl. Acad. Sci. USA* **1990**, *87* (5), 1988-1992.
15. Gyorgy, B.; Szabo, T. G.; Pasztoi, M.; Pal, Z.; Misjak, P.; Aradi, B.; Laszlo, V.; Pallinger, E.; Pap, E.; Kittel, A., et al., *Cell Mol. Life Sci.* **2011**, *68* (16), 2667-2688.

16. Hessvik, N. P.; Llorente, A., *Cellular and Molecular Life Sciences* **2018**, *75* (2), 193-208.
17. Guo, P. Y.; Yu, H. T.; Wang, Y.; Xie, X. Z.; Chen, G., *Hepat. Mon.* **2017**, *17* (8), 1-10.
18. Lopez-Verrilli, M. A.; Caviedes, A.; Cabrera, A.; Sandoval, S.; Wyneken, U.; Khoury, M., *Neuroscience* **2016**, *320*, 129-139.
19. Ettelaie, C.; Collier, M. E. W.; Maraveyas, A.; Ettelaie, R., *J. Extracell. Vesicles* **2014**, *3* (1), 23592.
20. Kalra, H.; Simpson, R. J.; Ji, H.; Aikawa, E.; Altevogt, P.; Askenase, P.; Bond, V. C.; Borràs, F. E.; Breakefield, X.; Budnik, V., et al., *PLoS Biol.* **2012**, *10* (12), 1-5.
21. van der Pol, E.; Boing, A. N.; Harrison, P.; Sturk, A.; Nieuwland, R., *Pharmacol. Rev.* **2012**, *64* (3), 676-705.
22. Torro, L. M. D.; Moreira, L. R.; Osuna, A., *Front. Microbiol.* **2018**, *9*, 11.
23. Lee, C.; Carney, R. P.; Hazari, S.; Smith, Z. J.; Knudson, A.; Robertson, C. S.; Lam, K. S.; Wachsmann-Hogiu, S., *Nanoscale* **2015**, *7* (20), 9290-9297.
24. Tucher, C.; Bode, K.; Schiller, P.; Classen, L.; Birr, C.; Souto-Carneiro, M. M.; Blank, N.; Lorenz, H. M.; Schiller, M., *Frontiers in Immunology* **2018**, *9*, 534.
25. Song, W.; Yan, D.; Wei, T. S.; Liu, Q.; Zhou, X.; Liu, J., *Biomed. Pharmacother.* **2018**, *102*, 1203-1208.
26. Gregory, C. D.; Dransfield, I., *Front. Immunol.* **2018**, *9*.
27. Grigor'eva, A. E.; Tamkovich, S. N.; Eremina, A. V.; Tupikin, A. E.; Kabilov, M. R.; Chernykh, V. V.; Vlassov, V. V.; Laktionov, P. P.; Ryabchikova, E. I., *Biochem. (Mosc) Suppl. Ser. A Membr. Cell. Biol.* **2016**, *10* (2), 165-172.
28. Pisitkun, T.; Shen, R.-F.; Knepper, M. A., *Proc. Natl. Acad. Sci. USA* **2004**, *101* (36), 13368-13373.
29. Li, M.; Zeringer, E.; Barta, T.; Schageman, J.; Cheng, A.; Vlassov, A. V., *Philos. Trans. R. Soc. Lond. B. Biol. Sci.* **2014**, *369* (1652), 1-8.
30. Plawinski, L.; Angles-Cano, E., *Sang Thrombose Vaisseaux* **2013**, *25* (2), 100-110.
31. Street, J. M.; Barran, P. E.; Mackay, C. L.; Weidt, S.; Balmforth, C.; Walsh, T. S.; Chalmers, R. T.; Webb, D. J.; Dear, J. W., *J. Transl. Med.* **2012**, *10* (1), 5.
32. Cizmar, P.; Yuana, Y., Kuo, W. P.; Jia, S., Eds. Springer New York: New York, NY, 2017; 221-232.
33. Pocsfalvi, G.; Stanly, C.; Vilasi, A.; Fiume, I.; Capasso, G.; Turiák, L.; Buzas, E. I.; Vékey, K., *Mass Spectrom. Rev.* **2016**, *35* (1), 3-21.
34. Xia, Y. K.; Liu, M. M.; Wang, L. L.; Yan, A.; He, W. H.; Chen, M.; Lan, J. M.; Xu, J. X.; Guan, L. H.; Chen, J. H., *Biosens. Bioelectron.* **2017**, *92*, 8-15.

35. Val, S.; Krueger, A.; Poley, M.; Cohen, A.; Brown, K.; Panigrahi, A.; Preciado, D., *Faseb J.* **2018**, *32* (4), 1855-1867.
36. Sebaihi, N.; De Boeck, B.; Yuana, Y.; Nieuwland, R.; Petry, J., *Meas. Sci. Technol.* **2017**, *28* (3), 1-8.
37. Momen-Heravi, F.; Balaj, L.; Alian, S.; Mantel, P. Y.; Halleck, A. E.; Trachtenberg, A. J.; Soria, C. E.; Oquin, S.; Bonebreak, C. M.; Saracoglu, E., et al., *J. Biol. Chem.* **2013**, *394* (10), 1253-1262.
38. Silvas, J. A.; Popov, V. L.; Paulucci-Holthauzen, A.; Aguilar, P. V., *J. Virol.* **2016**, *90* (2), 873-886.
39. Tauro, B. J.; Greening, D. W.; Mathias, R. A.; Ji, H.; Mathivanan, S.; Scott, A. M.; Simpson, R. J., *Methods* **2012**, *56* (2), 293-304.
40. Taylor, D. D.; Zacharias, W.; Gercel-Taylor, C., Simpson, R. J.; Greening, D. W., Eds. Humana Press: Totowa, NJ, 2011; 235-246.
41. Campoy, I.; Lanau, L.; Altadill, T.; Sequeiros, T.; Cabrera, S.; Cubo-Abert, M.; Perez-Benavente, A.; Garcia, A.; Borros, S.; Santamaria, A., et al., *J. Transl. Med.* **2016**, *14*, 12.
42. Vargas, A.; Roux-Dalvai, F.; Droit, A.; Lavoie, J. P., *Am. J. Respir. Cell Mol. Biol.* **2016**, *55* (3), 450-461.
43. Cui, S.; Cheng, Z.; Qin, W.; Jiang, L., *Lung Cancer* **2018**, *116*, 46-54.
44. Krafft, C.; Wilhelm, K.; Eremin, A.; Nestel, S.; von Bubnoff, N.; Schultze-Seemann, W.; Popp, J.; Nazarenko, I., *Nanomedicine* **2017**, *13* (3), 835-841.
45. Stremersch, S.; Marro, M.; Pinchasik, B. E.; Baatsen, P.; Hendrix, A.; De Smedt, S. C.; Loza-Alvarez, P.; Skirtach, A. G.; Raemdonck, K.; Braeckmans, K., *Small* **2016**, *12* (24), 3292-3301.
46. Zong, S. F.; Wang, L.; Chen, C.; Lu, J.; Zhu, D.; Zhang, Y. Z.; Wang, Z. Y.; Cui, Y. P., *Anal. Methods* **2016**, *8* (25), 5001-5008.
47. Mihaly, J.; Deak, R.; Szigyarto, I. C.; Bota, A.; Beke-Somfai, T.; Varga, Z., *Biochim. Biophys. Acta.* **2017**, *1859* (3), 459-466.
48. Lauchner, A.; Schlather, A. E.; Manjavacas, A.; Cui, Y.; McClain, M. J.; Stec, G. J.; García de Abajo, F. J.; Nordlander, P.; Halas, N. J., *Nano. Lett.* **2015**, *15* (9), 6208-6214.
49. Torma, P.; Barnes, W. L., *Rep. Prog. Phys* **2015**, *78* (1).
50. Mayer, K. M.; Hafner, J. H., *Chem. Rev.* **2011**, *111* (6), 3828-3857.
51. Smith, Z.; Lee, C.; Rojalin, T.; Carney, R.; Hazari, S.; Knudson, A.; Lam, K.; Saari, H.; Lazaro-Ibañez, E.; Viitala, T., et al., *J. Extracell. Vesicles* **2015**, *4*.
52. Stremersch, S.; Marro, M.; Pinchasik, B. E.; Baatsen, P.; Hendrix, A.; Smedt, S. C. D.; Loza-Alvarez, P.; Skirtach, A. G.; Raemdonck, K.; Braeckmans, K., *Small* **2016**, *12* (24), 3292-3301.
53. Mishchenko, E. G., *Phys. Rev. B* **1999**, *59* (23), 14892-14895.

54. Le Ru, E. C.; Etchegoin, P. G., *Chem. Phys. Lett.* **2006**, *423* (1), 63-66.
55. Mosier-Boss, P. A., *Nanomaterials* **2017**, *7* (6), 142.
56. Fromm, D. P.; Kinkhabwala, A.; Schuck, P. J.; Moerner, W. E.; Sundaramurthy, A.; Kino, G. S., *J. Chem. Phys.* **2006**, *124* (6), 61101-61101.
57. Shanta, P. V.; Cheng, Q., *ACS Sens.* **2017**, *2* (6), 817-827.
58. Tabatabaei, M.; Wallace, G. Q.; Caetano, F. A.; Gillies, E. R.; Ferguson, S. S. G.; Lagugne-Labarthe, F., *Chem. Sci.* **2016**, *7* (1), 575-582.
59. Pisco, M.; Galeotti, F.; Quero, G.; Grisci, G.; Micco, A.; Mercaldo, L. V.; Veneri, P. D.; Cutolo, A.; Cusano, A., *Light Sci. Appl.* **2017**, *6*.
60. Galarreta, B. C.; Rugar, I.; Young, A.; Lagugné-Labarthe, F., *J. Phys. Chem. C* **2011**, *115* (31), 15318-15323.
61. Tabatabaei, M.; Sangar, A.; Kazemi-Zanjani, N.; Torchio, P.; Merlen, A.; Lagugné-Labarthe, F., *J. Phys. Chem. Lett. C* **2013**, *117* (28), 14778-14786.
62. Zhang, X.; Duyne, R. P. V., *Mater. Res. Soc. Symp. Proc.* **2011**, *876*, R8.54.
63. Chen, K.; Rajeeva, B. B.; Wu, Z.; Rukavina, M.; Dao, T. D.; Ishii, S.; Aono, M.; Nagao, T.; Zheng, Y., *ACS Nano* **2015**, *9* (6), 6031-6040.
64. Zhou, X. D.; Virasamy, S.; Knoll, W.; Liu, K. Y.; Tse, M. S.; Yen, L. W., *J. Nanosci. Nanotechnol.* **2008**, *8* (7), 3369-3378.
65. Sun, H. H.; Chen, L.; Wang, Y. X.; Hua, Z.; Liu, Y.; Zhang, Y. J.; Yang, J. H., *RSC Adv.* **2017**, *7* (69), 43671-43680.
66. Wallace, Gregory Q., Multiresonant Anisotropic Nanostructures for Plasmon-Mediated Spectroscopies. **2018**. University of Western Ontario - Electronic Thesis and Dissertation Repository. Paper 5268.

Chapter 3

3 Fabrication and Characterization of Plasmonic Platforms

This chapter explores the fabrication of plasmonic platforms by nanosphere lithography and electron beam lithography. The materials and methods used to fabricate and characterize these platforms are described in detail. The use of plasmonic platforms is presented within the scope of their desired application, to study biological vesicles.

3.1 Introduction

Advances in nanofabrication have allowed for fabrication of nanostructures with a high degree of control over the size, the shape, the geometry and the chemical properties of the materials. As such, several lithographic methods have been developed to fabricate nanostructures. These methods are typically classified into two groups, namely top-down or bottom-up fabrication.¹ Top-down approaches in nanofabrication such as electron beam lithography aim to carve large-scale materials to micro- and nano-size features using lithography or focused ion-beam methods.²⁻⁴ These approaches have proven successful in producing features less than tens of nanometers in size with high precision and resolution due to advances in photoresist technologies. In contrast, bottom-up processes such as wet chemical synthesis or nanosphere lithography rely on increasing the size of a primary building block to generate ordered nanomaterials on a larger size scale.⁵⁻⁷

Metallic nanostructures have been studied for a wide variety of applications using surface plasmon resonance (SPR),^{8,9} extraordinary optical transmission (EOT),^{10, 11} surface-enhanced infrared absorption spectroscopy (SEIRA)¹²⁻¹⁴ and surface-enhanced

Raman spectroscopy (SERS).¹⁵⁻¹⁸ One particularly interesting subclass of nanostructure previously characterized by the aforementioned technologies is nanohole arrays (NHAs). NHAs have been fabricated by a variety of methodologies. One commonly reported method of fabricating NHAs is based on self-assembly of polystyrene spheres followed by an etching process, metal deposition and subsequent lift-off of nanospheres.^{19, 20} This methodology is successful in generating areas of nanohole arrays, with nanowells corresponding to one dimension in the areas where nanospheres were originally placed.²¹ However, the self-assembly of polystyrene often leads to defective areas and allows for minimal control over the spacing and sizes of individual nanowells. Therefore, methodologies such as focused ion beam lithography,^{22, 23} interference lithography,^{19, 24} and electron beam lithography^{25, 26} are typically preferred to increase control over sizing and spacing.

A significant advantage provided by nanohole arrays arises from their ability to trap and probe materials in confined nanowells. Fabrication of nanohole arrays by interference lithography has been reported in the literature previously for detection and trapping of biological proteins.¹⁹ For example, when a protein was introduced into nanowells fabricated by laser interference lithography, optical transmission images revealed confinement of proteins to the nanowell areas.¹⁹ Channels filled with trapped protein(s) appeared darker in colour upon illumination, whereas channels free of protein would appear bright under transmissive light settings. Successful trapping of proteins was therefore achieved and validated. Laser interference lithography is a great technique for fabricating nanostructures, however it is limited by the resolution of the light source, which in this case was a UV source. Nanostructures are therefore limited by size due to

the resolution of the light source. In this case, structures may be resolved to 200 nm and larger. In cases where features less than 200 nm are desirable, an electron beam source may be employed to generate high resolution nanostructures down to ~ 50 nm in size.

Recently, plasmonic nanohole arrays have been incorporated into chip-based sensing for detection of biomaterials. For example, integration of NHAs fabricated by UV-lithography with an adjustable microfluidic cell module have been reported for direct, real-time detection of a growth factor released from live under controlled cell culture conditions.²⁷ Chip-based devices with integrated nanohole arrays hold great potential in point-of-care diagnostic testing for human health studies. The work presented throughout this chapter aims to fabricate NHAs in a reproducible manner to probe microvesicles released by cells.

3.2 Experimental

3.2.1 Materials for Nanosphere Lithography

Cover slips were obtained from VWR International (22 mm x 22 mm x 0.15 mm) and subjected to acid/base cleaning to yield a pristine surface onto which are formed NSL patterns. Coverslips were suspended in acetone (Sigma Aldrich), sonicated for 5 minutes and gently rinsed with ultrapure water. They were subsequently sonicated in a solution of Nochromix® (Godax Laboratories Inc., Maryland U.S) and sulphuric acid for 20 minutes. After rinsing with milli-Q water (18.2 MΩ.cm), they were sonicated in a 1:1:5 solution of ammonium hydroxide: hydrogen peroxide: milli-Q water for 60 minutes. NSL was adapted from a previously outlined protocol.²⁸ A 1 cm diameter O-ring was utilized with a 1:25 v/v ratio of 1 μm polystyrene microspheres to water (10% w/w polystyrene,

ThermoFisher Scientific, California, U.S.). 20 μL of the polystyrene mixture was drop casted into the O-ring and allowed to dry for 12 hours. Monolayer coverage was verified optically, and the substrates were subsequently coated with a 3-nm adhesion layer of titanium and 30 nm of gold. Lift-off of polystyrene spheres was performed in acetone (Sigma Aldrich) with mild sonication for 10 – 30 seconds.

3.2.2 Materials for Electron Beam Lithography

3.2.2.1 Polymethymetacrylate (PMMA) Nanohole Arrays

Microscope coverslips were subjected to reactive O_2 plasma for 10 minutes. A positive resist, 495-PMMA-A4 (Microchem, Westborough, MA) was spin coated onto the substrate surface at 3000 rpm corresponding to a thickness of 1800 \AA , respectively.²³ Substrates were baked for 90 seconds at 180 $^\circ\text{C}$. Aquasave[®] conductive polymer (Mitsubishi Rayon Co.) was spin coated onto the PMMA surface as a conductive layer and subsequently baked at 110 $^\circ\text{C}$ for 2 minutes. Electron-beam lithography was performed using a LEO 1530 SEM microscope with electron beam capabilities. Patterns of arrays were designed with varying sizes (0.1 - 1.0 μm , with a 0.1 μm step in between sizes) and varying shapes (circle and square) using a CAD software (NPGS), and all patches of patterns measured 50 μm x 50 μm^2 . A standard procedure using a 1:3 solution of methyl-isobutyl ketone and isopropanol allowed for development of arrays and removal of the resist that was exposed to the electron beam.

3.2.2.2 Metallic Nanohole Arrays

Microscope coverslips were subjected to reactive O_2 plasma for 10 minutes, after which a negative resist, Ma-N 2405 (Microchem, Westborough, MA) was spin coated onto the substrate at a spin speed of 3000 rpm, corresponding to a thickness of

approximately 6300 Å, and baked for 90 seconds at 90 °C. AquaSAVE conductive polymer (Sigma-Aldrich) was spin coated at 3000 rpm as a conductive layer and subsequently baked at 90 °C for 45 seconds. Electron-beam lithography was performed using a LEO 1530 SEM microscope with electron beam capabilities. Patterns of arrays were fabricated of varying sizes (0.1 - 1.0 μm, with a 0.1 μm step in between sizes) and varying shapes (circle, triangles and square) using a CADsoftware(NPGS), and all patches of patterns measured 50 μm x 50 μm². Following lithography, samples were developed in MF-319 developer (MicroChem, Westborough, MA) for 30 - 45 seconds. Samples were subjected to a 30-second O₂ plasma descum process to remove residual resist surrounding nanopillars. A 3-nm adhesion layer of titanium was then deposited followed by a 30-nm layer of gold by electron beam evaporation (Angstrom Engineering). Lift-off was allowed by exposure to remover-PG, a common photoresist remover heated to 80 °C (MicroChem, Westborough, MA) for 90 minutes to two hours, depending on the sample. Samples were subjected to a 1:3 solution of methyl isobutyl ketone and isopropanol to remove remaining remover-PG. Samples were then subjected to Nanostrip, a stabilized formulation of sulfuric acid and hydrogen peroxide compounds often used for removal of positive and negative photoresists (Cyantek, California, U.S.A) heated to 80 °C for 30 minutes and placed in water for 15 minutes to remove remaining nanostrip. Lastly, samples were subjected to O₂ plasma for 5 minutes to remove remaining resist from inside metallized nanoholes.

3.2.3 Raman and Surface-Enhanced Raman Spectroscopy

A LabRAM HR (Horiba Scientific, NJ, USA) spectrometer was utilized for Raman and SERS spectroscopy. The spectrometer was equipped with a liquid nitrogen

equipped charge-coupled detector (CCD), and the excitation source was a helium-neon laser with a wavelength of 632.8 nm. A 100 × objective (N.A 0.9) was used to collect backscattered light. Laser power was set to ~ 0.5 mW and acquisition time varied between 20 – 200 s depending on the sample. A confocal pinhole of 200 μm and grating of 600 grooves /mm were used for these measurements.

3.2.4 Fluorescence Imaging

Fluorescence imaging was performed with a Zeiss LSM 510 META Multiphoton Confocal Laser Scanning Microscope. A Zeiss 63 × (N.A. 0.75) air objective as well as a 632.8 nm He-Ne Laser were employed.

3.2.5 Functionalization of Nanohole Arrays

Samples were functionalized for 24 hours in a 10^{-3} M solution of 4-MPBA (4-mercaptophenylboronic acid) in ethanol for preliminary testing. A helium neon laser ($\lambda = 632.8$ nm) was used as the excitation source, and a 100 × (NA = 0.9) objective was used to collect back-scattered light. A mapping stage was employed to map the surface surrounding individual nanoholes measuring 0.9 μm in diameter for both square and circular shapes, and acquisition time was 5 s per pixel.

3.3 Results and Discussion

3.3.1 Characterization of Platforms Prepared by Nanosphere Lithography

Several methods were tested to prepare NSL platforms such as drop-casting, air-water interface or spin-coating. The O-ring method was selected due to its facile implementation and the desire to improve the method by manipulation of dilution ratio.²⁸

Figure 3.1 outlines the O-ring method, highlighting the placement of polystyrene solution inside a 1-cm diameter O-ring and the subsequent self-assembly of polystyrene spheres (1 μm diameter, 10% w/w, ThermoFisher Scientific, California, U.S.) following 12 hours of drying time.

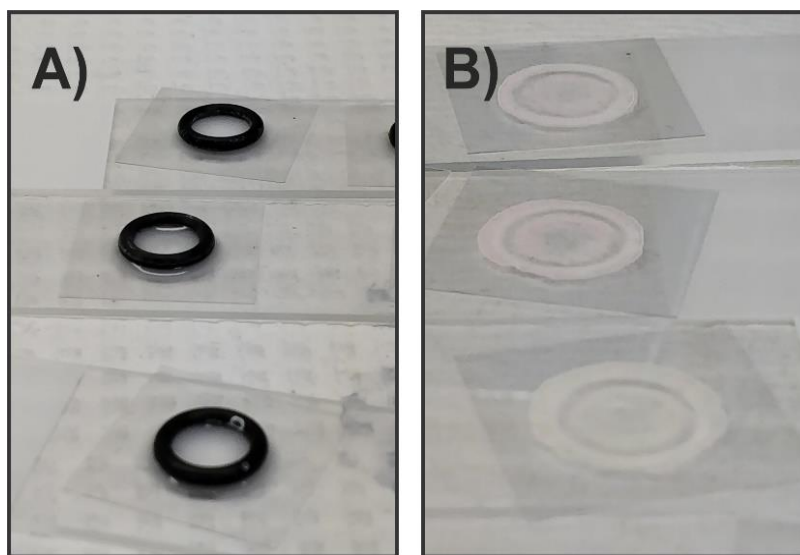


Figure 3.1 – Photographs of the O-ring method of NSL (A) prior to drying and (B) after 12 hours of drying time, prepared with 1 μm diameter polystyrene spheres.

The dilution ratio of 1 μm diameter polystyrene spheres to milli-Q water was initially varied between 1:15, 1:20, 1:25, and 1:50. The best ratio to fabricate the larger areas of spheres monolayer was determined to be 1:25 by optical assessment of monolayer packing. This ratio lead to well-packed and high-density monolayered areas of polystyrene spheres. The characterization of the resulting NSL substrates were done using by scanning electron microscopy (SEM) and UV-Vis spectroscopy.

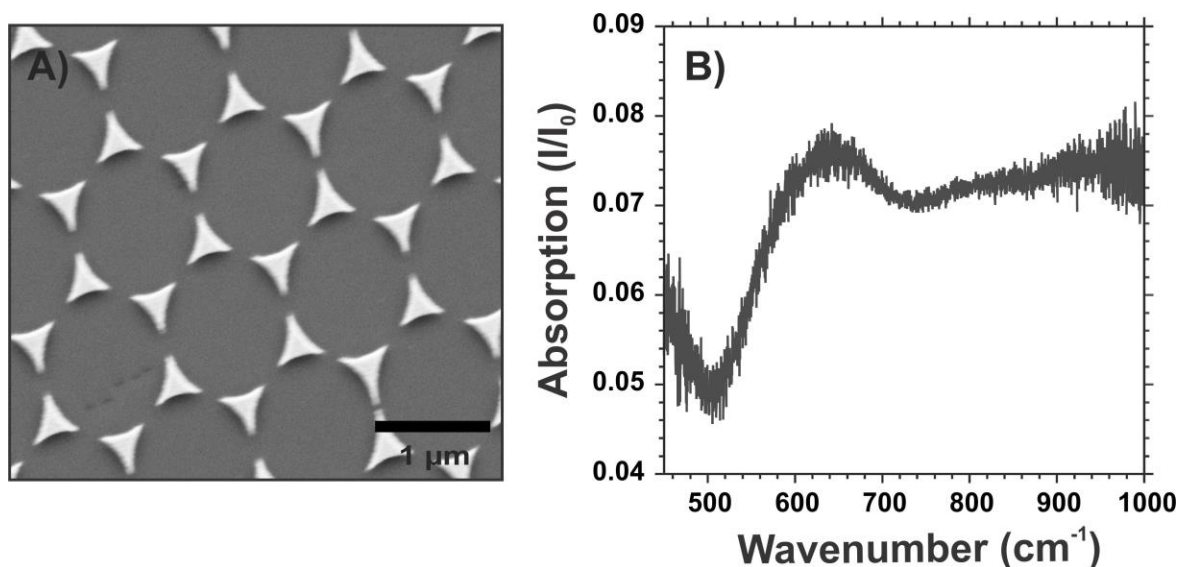


Figure 3.2 – Characterization of NSL nanostructures fabricated using 1-micron spheres by (A) SEM (B) absorption spectra.

As illustrated in Figure 3.2 A), areas of packed polystyrene spheres allow for fabrication of regular nanostructures (nanoprisms) with sharp, well defined apices. Previous research on nanoprisms prepared by NSL has demonstrated confinement of the EM field occurs at apices, accounting for most of the plasmonic enhancement for SERS-based applications.²⁹ To obtain the most intense SERS enhancement from the NSL substrate, it is important to match the wavelength of the incident laser with the plasmon wavelength of the platform. Therefore, the absorption spectra of a NSL substrate is shown in in Figure 3.2 B). From this graph, the LSPR frequency appears to lie between 630 - 650 cm^{-1} , presenting similar results to those previously reported in the literature.³⁰ Matching of the incoming laser source within this range will allow for the best SERS signal.

3.3.2 Preparation of Plasmonic Platforms by Electron Beam Lithography

To overcome many of the challenges of NSL such as the presence of defects, electron beam lithography (EBL) is a great alternative. In particular, it allows for control over shapes, sizing and spacing of nanostructures and provides excellent reproducibility.³¹ EBL employs the electron beam of a scanning electron microscope to scan the surface of a photoresist along defined sets of spatial coordinates. Photoresists vary between positive or negative types.³² Incorporation of metals such as gold and silver may be deposited following development to allow for propagation of plasmons and SERS capabilities.

In this project, nanohole arrays were fabricated with both, positive and negative resists to ultimately test the ability to trap and probe nanoscale materials. The positive resist was non-metallized and was solely fabricated for trapping of nanoscale materials, whereas the negative resist was fabricated with a different protocol and metallized, allowing for SERS acquisition of trapped nanomaterials. Circular and square nanowells were fabricated with varying size. The size ranged between 0.1 – 1 μm , with a 0.1 μm step/increase in size between adjacent patterns, with the same sizes, shapes and parameters for both resist forms. Fig. 3.3 displays dark-field images of both types of fabricated arrays, obtained with a Zeiss Axioskop2 MAT microscope.

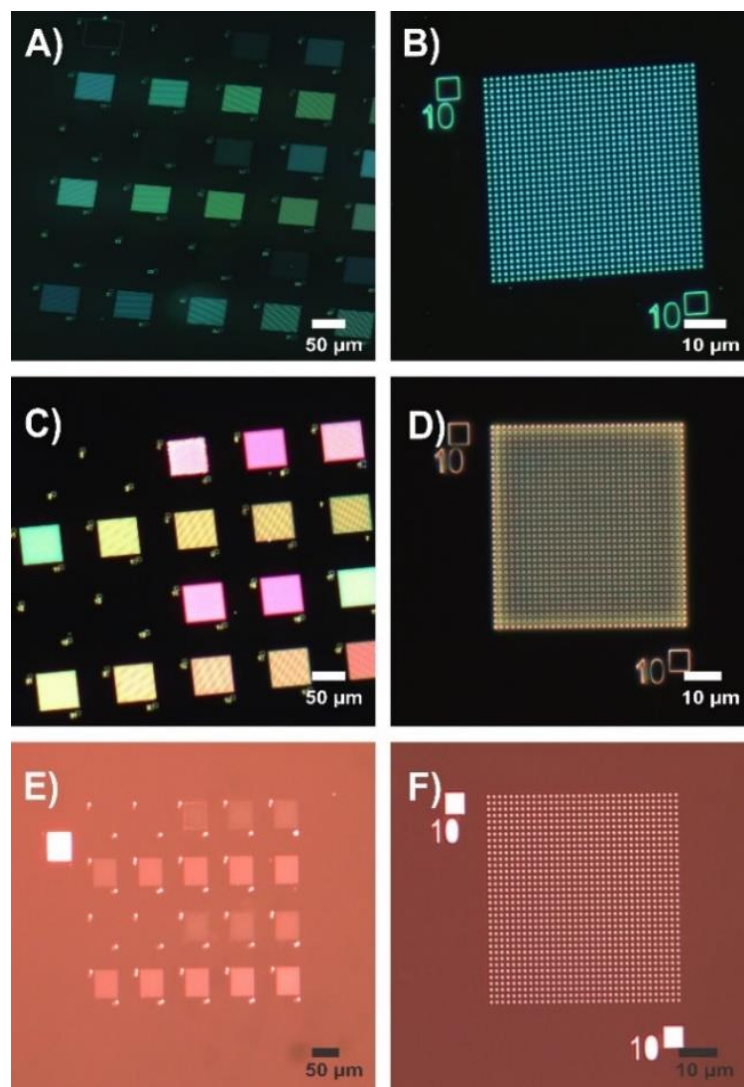


Figure 3.3 - (A) NHA fabricated with a positive resist for assessment of trapping abilities of NHAs; (B) Close-up of positive resist-fabricated 0.9 μm diameter circular nanowells; (C) NHA fabricated with negative resist, coated with 30 nm of gold prior to lift-off of nanopillars; The different colors of the individual patches indicate distinct plasmon frequencies (D) Close-up of negative resist-fabricated 0.9 μm diameter circular nanopillars; (E) NHA fabricated with negative resist, coated with 30 nm of gold following lift-off of nanopillars, revealing nanowells; (F) Close-up of negative resist-fabricated 0.9 μm diameter circular nanowells.

Nanostructures revealed shapes and sizes of desired dimensions. For example, array number 10, enlarged in Fig. 3.3 (B) displays evenly shaped and sized nanowells, of dimensions 0.9 μm . The precise control of shape and sizes, as well as their high resolution indicate some of the benefits of electron beam lithography over nanosphere lithography.

The variety of colours seen in in 3.3 C) under the same illumination conditions are indicative of varying sizes and shapes of nanostructures and are known as plasmon resonances.³³ Nanostructures of different shapes, but of the same dimensions will reflect and scatter light such that the waves of given frequencies will constructively interfere, giving rise to colour.^{34, 35} This phenomenon is known as structural colour, and varies from traditional colouring since the colour does not arise from the use of pigments. The colours visualized are dependent on four main factors, namely the size, shape, dielectric environment and illumination conditions.³⁶ In other terms, changing the size and shape of nanostructures changed the local refractive index, ultimately changing the colours associated with the samples.

Initial characterization of metallic nanohole arrays by optical imaging was helpful to ensure successful fabrication of desired nanostructures. However, scanning electron microscopy was still required for full device examination. For example, during initial fabrication steps involving nanopillars, nanostructures < 400 nm in size are difficult to observe with a $100\times$ (N.A 0.9) objective. Additionally, different sized nanostructures may require different area doses for optimal fabrication. Structures inscribed with a dose greater than the optimal/nominal dose could display cracking, breaking, and may produce structures larger than desired. In addition, deposition of metal on top of nanostructures

could potentially lead to destruction of nanostructures due to the heaviness of metal deposited, an observation best viewed under SEM conditions. Lastly, developing nanostructures in solvent following lithography can cause removal of nanostructures if the adhesion force between the nanostructure and substrate is weak. Removal of nanostructures following developing in solvent would also be difficult to observe optically for nanostructures tens of nanometers in size. SEM is therefore required to assess these factors.

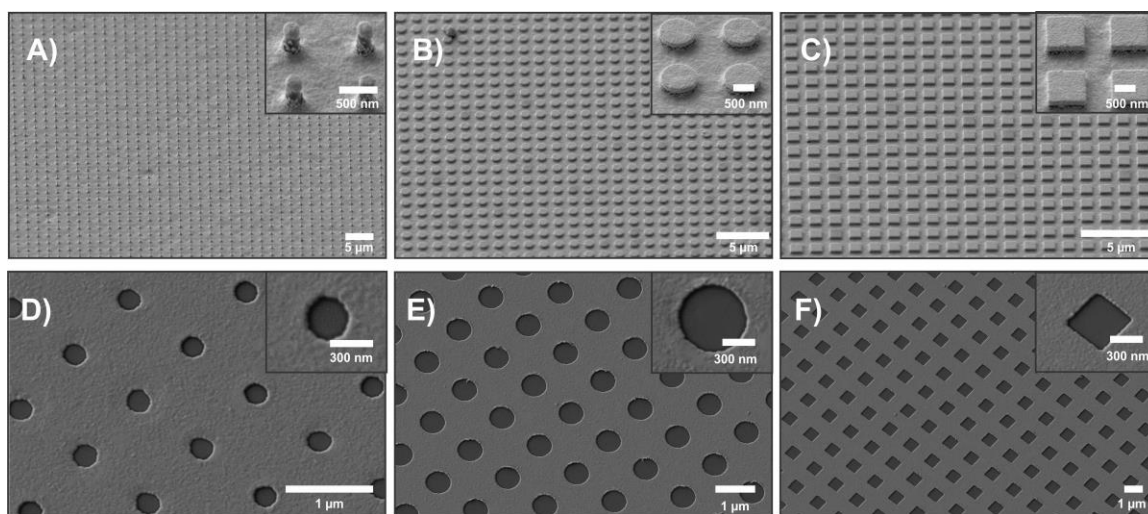


Figure 3.4 - SEM nanopillars and nanowells. (A) 200 nm circular nanopillars; (B) 900 nm circular nanopillars; (C) 900 nm square nanopillars; (D) 300 nm circular nanowell; (E) 700 nm circular nanowells; (F) 600 nm square nanowells.

Figure 3.4 displays SEM images of nanopillars and resultant nanowells following lift-off. A dose test was performed for all sizes and shapes of nanopillars to determine the optimal electron beam energy density for each nanostructure. Optimal doses for circular and square nanostructures are outlined in Table 2. Study of optimal doses for each nanostructure was important to ensure for ideal resolution and correct sizing of structures.

When a pattern becomes exposed at a lower dose than the optimal dose for best resolution, this pattern is said to be underexposed. Underexposure may lead to a structure width smaller than the desired structure width, and has also been found to increase the probability of pattern irregularities.³⁷ In contrast, exposing the nanostructure to a higher dose, or overexposing (dosage is higher than the optimum dose) may lead to a widening of the structure size. Tailoring the exposure dose for each nanostructure allowed for fabrication of structures of desired width and shape.

Table 2 - Optimal electron beam dosage for fabrication of nanostructures of desired sizes

Size (μm)	Dosage ($\mu\text{C}/\text{cm}^2$)
0.1	100
0.2	110
0.3	105
0.4	110
0.5 – 1	90

Using the nanopillars shown in Figure 3.4 (A – C), nanoholes were produced in a 30 nm gold metal film. Following lift-off of nanopillars, SEM was used to validate cleanliness of this the procedure. Important factors to assess were definition of edges of nanostructures as well as residual resist remaining in nanowells. The lift-off procedure is further illustrated in Figure 3.5, where (A) illustrates the intact nanopillar, (B) illustrates lift-off with resist remaining in nanowells and (C) shows ideal structures with full removal of resist.

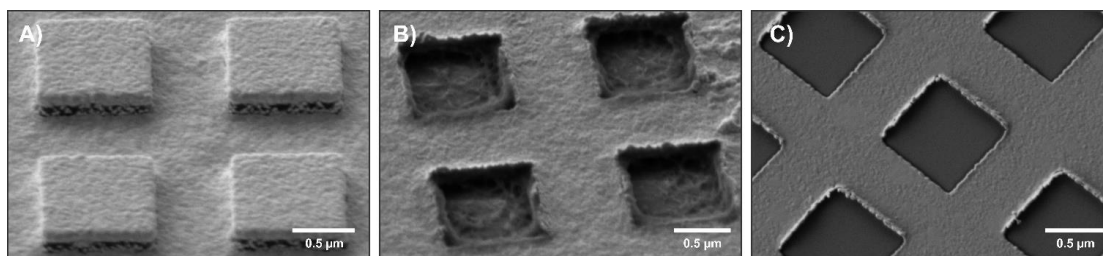


Figure 3.5 – Lift-off of nanopillars. (A) Intact nanopillar followed by (B) lift-off revealing residual resist in nanowells, which is removed fully in (C), showing exposed glass nanowells.

Any residual resist remaining in nanowells such as in Figure 3.5 B) could interfere with materials sensed in welled areas during vibrational spectroscopic acquisition. The protocol for removal of residual resist therefore incorporated nanostrip, a formulation of sulfuric acid and hydrogen peroxide to remove this material without damage to the gold metal film. Reactive plasma O₂ treatment was additionally incorporated to further remove/descum remaining resist in welled areas. This treatment revealed clean lift-off of nanopillars and well-defined nanowells, indicating successful fabrication of desired structures.

3.3.3 Plasmonic Properties of Metallic Nanohole Arrays

Further characterization of NHAs was allowed by absorption measurements. Alterations in the physical parameters of the nanohole array such as hole size, periodicity, thickness and type of metal shift resonances to different spectral locations.³⁸ Characterization of absorption wavelengths was therefore important to determine optimal wavelength(s) for SERS acquisition. Fig. 3.6 displays the absorption spectra of fabricated nanohole arrays for square and circularly shaped nanoholes of 0.4, 0.6, 0.8 and 1 μm

diameter. Spectra acquired for square wells indicate two resonances in the spectral ranges between $620 - 630 \text{ cm}^{-1}$ and $790 - 890 \text{ cm}^{-1}$. Resonances associated with the circular nanowells are seemingly less pronounced compared to the square nanowells. Two resonances are depicted at $630 - 650 \text{ cm}^{-1}$ and $820 - 850 \text{ cm}^{-1}$ for circular nanowells.

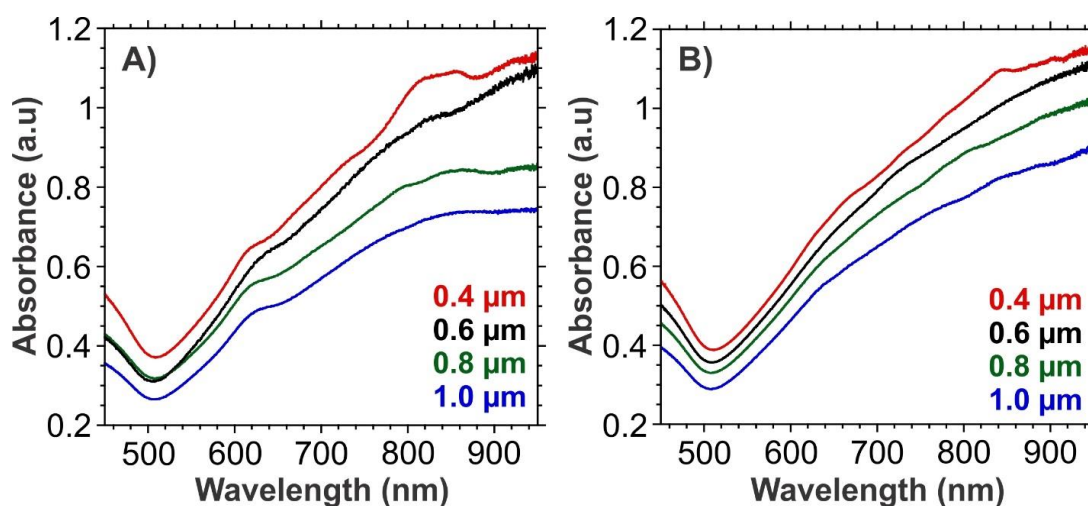


Figure 3.6 – Absorption for horizontally polarized light through (A) square and (B) circular nanowells of varying size.

To ensure the fabricated platforms were SERS active and to additionally characterize the representative location of strongest SERS enhancement of the nanowells, the surface of the NHA was functionalized for 24 hours in a 1 mM ethanolic solution of 4-mercaptophenyl boronic acid (4-MPBA). 4-MPBA is a well characterized Raman reporter known to form a self-assembled monolayer with gold, through a strong sulfur-metal bond. It additionally has applications in biosensing.^{39,40} Fig. 3.6 displays Raman maps for a $0.9 \mu\text{m}$ circle and $0.9 \mu\text{m}$ square integrated over the 1074 cm^{-1} peak correlating to the B-OH stretch⁴¹ (integration range $1055 - 1100 \text{ cm}^{-1}$). Maps indicate the

strongest enhancement lies in the central cavities of the nanoholes, a promising finding for sensing nanoscale materials in these confined regions.

Representative SERS spectra of 4-MPBA maps are displayed in Fig. 3.7 (C, F). SERS-active areas show a strong 4-MPBA signal in central regions of the nanohole array, as depicted by spots 1 and 3, whereas areas with a lower SERS enhancement (spots 2 and 4) show a negligible 4-MPBA signal. Optimal areas of sensing biological materials such as EVs would therefore lie in the central cavities of the NHAs.

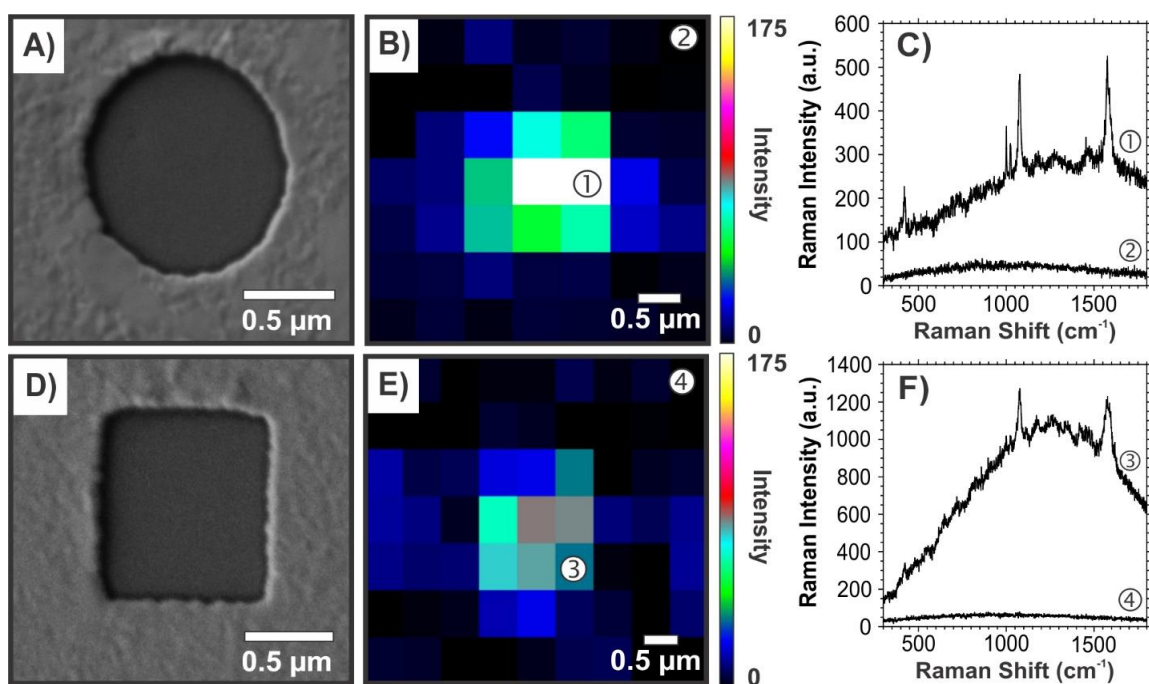


Figure 3.7 - Mapping of 4-MPBA on a nanohole array surface with f. (A) SEM image of 0.9 μm diameter circular nanohole; (B) SERS map of corresponding nanohole; (C) SERS spectra of pixels indicated in (B); (D) SEM image of 0.9 μm diameter square nanohole; (E) SERS map of corresponding nanohole; (F) SERS spectra of pixels 3 and 4 selected in (E).

As displayed in Figure 3.7, the SERS enhancement is localized within the central cavity of the circular or square nanowells. Due to the beam diameter and step size, we observe an overall enhancement over the entire surface of the nanohole cavities, whereas no distinguishable SERS response is observed on the nanofilm area (areas 2 and 4). Due to the spot-size of the objective (~ 1 micron), we are not able to achieve sufficient spatial resolution to map the edges of structures with higher resolution. Since no signal is observed from the bare gold substrate, the SERS-active regions are located at the outer edges of the nanostructures.

3.3.4 Trapping Capabilities of Nanohole Arrays

Trapping of nanomaterials (polystyrene spheres) within nanowells was characterized with non-plasmonic nanohole arrays fabricated with a positive resist. To trap polystyrene spheres in nanohole arrays, either $1.0\ \mu\text{m}$ fluorescent polystyrene spheres or $0.2\ \mu\text{m}$ non-fluorescent polystyrene spheres were drop casted onto circular and square nanoholes and allowed to settle for 30 minutes. The non-trapped polystyrene spheres were removed by application of an absorbent wipe in the corner of the droplet containing the polystyrene solution. This allowed for semi-controlled positioning of polystyrene, as cohesive forces resulted in confinement of PS spheres to the edges of the nanowells, as seen in Fig. 3.8.

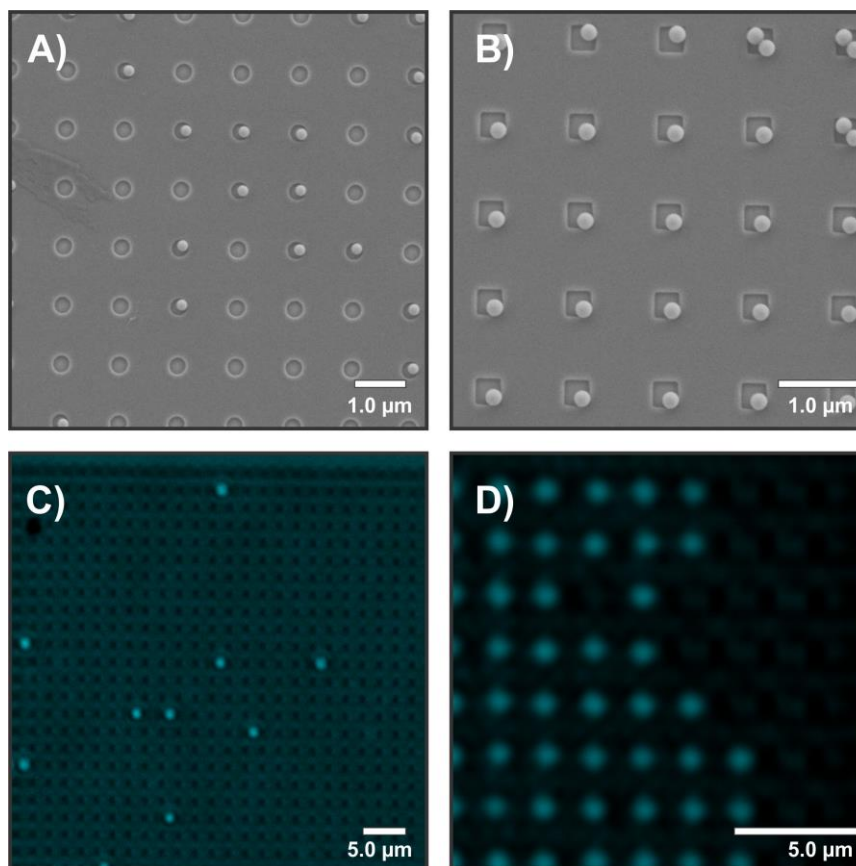


Figure 3.8 - Polystyrene spheres trapped within PMMA nanohole arrays. (A) Nanohole array of 0.3 μm circles with 0.2 μm polystyrene beads (B) nanohole array of 0.4 μm squares with 0.2 μm polystyrene beads (C) 1.0 μm fluorescent polystyrene beads trapped in 1 μm circular wells. (D) 1.0 μm fluorescent polystyrene beads trapped in 0.9 μm square wells.

In cases where nanowells were larger than the diameter of polystyrene spheres, more than one sphere could become trapped within an individual well, as seen in Fig. 3.8 B). This is an undesirable finding for vibrational spectral acquisition due to the inability to isolate overlapping spectral peaks. However, when the size of the well has similar dimension than of the sphere, trapping was noted as more precise (Figure 3.8 A). Therefore, when possible, characterization of the size range of the trapped materials is

helpful. In the case of polystyrene, the aspect ratio and exact dimensions of the beads are known allowing for semi-precise control over the dimensions of wells to best allow for successful, non-aggregated trapping.

The location of trapping of polystyrene spheres is a point of great interest. The direction of placement of the absorbent paper in the final step of the trapping protocol indicates the direction of trapping of polystyrene spheres, as the spheres are pulled in the direction of the capillary force. Spatial control when trapping materials smaller than the size of the wells is highly desired for spectroscopic analyses, as control over the location of materials may allow for automation of optical measurements since each nanomaterial may be referenced by a set of spatial (x,y) coordinates.

The ability to steer trapped objects to a desired location within nanowells also highlights another important benefit of using electron beam lithography to fabricate plasmonic materials versus nanosphere lithography. The use of a resist, matched with control over the acceleration energy of electrons used to fabricate EBL patterns allows for control of depth of wells for trapping. In contrast, nanosphere lithography does not allow for controlled spatial positioning in the same manner as EBL, as the large quantity of defects and inability to fabricate deeper wells via a resist makes it difficult to trap objects reproducibly in controlled locations.

To further analyze the trapping abilities of nanohole arrays, the same methodology as described for trapping of PS microspheres within the non-plasmonic NHAs was used with a plasmonic nanohole array fabricated with a negative resist. Once polystyrene spheres settled into nanowell cavities, it was possible to probe the SERS

spectra from each individual PS sphere from both above and below/through the nanohole array. Probing of SERS spectra above the nanohole array was successful, however sensing of PS spheres from below the NHA was of specific interest to confirm that PS microspheres were in-fact sitting within individual nanowell cavities. This experiment is shown in Figure 3.9.

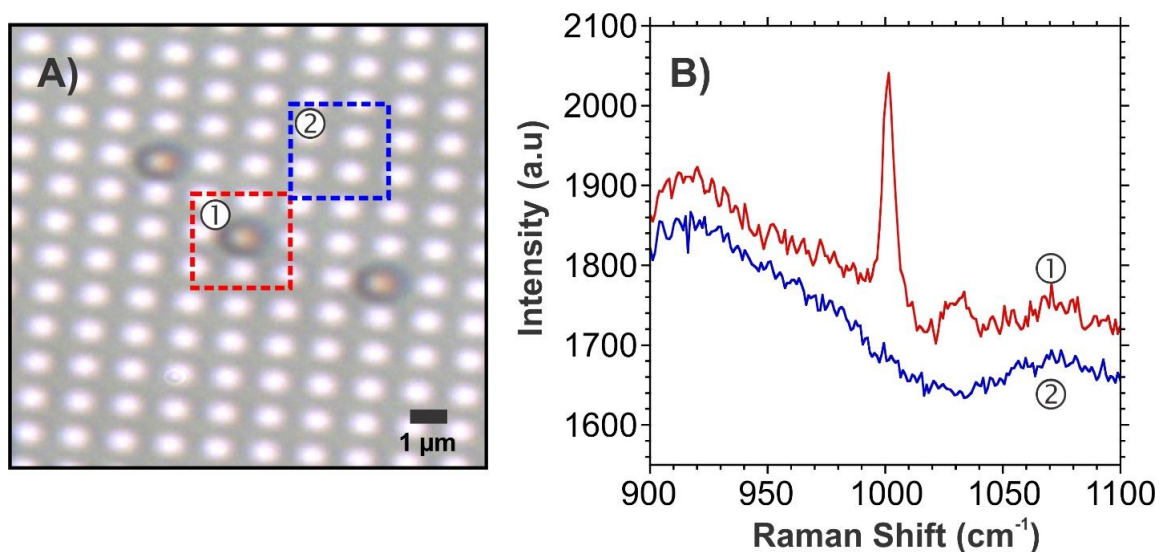


Figure 3.9 - Sensing of polystyrene spheres through a nanohole array. The sample was mounted face-up, facing away from the laser beam source. (A) Areas of interest for SERS spectral acquisition. Area 1 highlights a trapped polystyrene sphere 1 μm in diameter trapped within a nanowell, whereas area 2 corresponds to a background area with no trapped material. Corresponding spectra to (A) are displayed in (B), where area 1 displays a peak characteristic of polystyrene and area 2 lacks this spectral peak.

Figure 3.9 B) displays a SERS spectrum obtained from a nanohole array with PS trapped in nanowells, facing away from the excitation laser. The peak located at 1000 cm^{-1} corresponds to the aromatic breathing mode of the benzene ring and was chosen as a

reference peak due to its strong intensity.⁴² Sensing of materials through the nanohole array in confined nanowells was indicative of successful capturing of materials within desired areas. This finding is also promising for extending use of this nanodevice to a broader set of applications such as trapping of extracellular vesicles, proteins, nucleic acids, or growth factors. Incorporation of this nanodevice into point-of-care technologies is also promising based on these findings.

3.4 Conclusions

In this chapter, two methods are introduced to fabricate plasmonic nanostructured substrates for surface-enhanced Raman spectroscopy. Nanosphere lithography was successfully performed and characterized with absorption measurements, revealing structures with well-defined LSPR positions. Electron beam lithography was also completed to allow for better control with positioning of nanostructures. Two separate protocols of EBL were successfully demonstrated, one on a positive resist for trapping of nanoscale materials, and one on a negative resist for acquisition of SERS spectra. The hot spots of nanohole arrays were mapped with a well-known Raman reporter (4-MPBA), which successfully demonstrated that hotspots lie within central cavities of wells, highlighting ideal sensing areas for materials. Sensing was further tested with polystyrene spheres. Trapping of nanoscale polystyrene spheres displayed controlled positioning of materials within desired welled areas, which may allow for future automation of spectral acquisitions to well-defined sets of spatial coordinates. The SERS spectrum of a trapped polystyrene sphere was also successfully acquired from below a nanowell and referenced to the background, indicating successful localization of material within confined areas.

3.5 References

1. Biswas, A.; Bayer, I. S.; Biris, A. S.; Wang, T.; Dervishi, E.; Faupel, F., *Adv. Colloid Interface Sci.* **2012**, *170* (1-2), 2-27.
2. Yamada, Y.; Ito, K.; Miura, A.; Iizuka, H.; Wakayama, H., *Nanotechnology* **2017**, *28* (20), 1-11.
3. Fischer, A. J.; Anderson, P. D.; Koleske, D. D.; Subramania, G., *ACS Photonics* **2017**, *4* (9), 2165-2170.
4. Nuzaihan, M. N. M.; Hashim, U.; Arshad, M. K. M.; Ruslinda, A. R.; Rahman, S. F. A.; Fathil, M. F. M.; Ismail, M. H., *PLoS One* **2016**, *11* (3), 1-21.
5. Sun, Z. Y.; Tzaguy, A.; Hazut, O.; Lauhon, L. J.; Yerushalmi, R.; Seidman, D. N., *Nano. Lett.* **2017**, *17* (12), 7478-7486.
6. Brassat, K.; Kool, D.; Burger, J.; Lindner, J. K. N., *Nanoscale* **2018**, *10* (21), 10005-10017.
7. Colson, P.; Henrist, C.; Cloots, R., *J. Nanomater.* **2013**.
8. Wang, S.; Dong, Y. Y.; Liang, X. G., *Biosens. Bioelectron.* **2018**, *109*, 1-7.
9. Lee, H.; Jeon, T. Y.; Lee, S. Y.; Lee, S. Y.; Kim, S. H., *Adv. Funct. Mater.* **2018**, *28* (18), 1-10.
10. Lei, C. X.; Chen, L. Y.; Tang, Z. X.; Li, D. Y.; Cheng, Z. Z.; Tang, S. L.; Du, Y. W., *Opt. Lett.* **2016**, *41* (4), 729-732.
11. Oh, Y.; Kim, K.; Hwang, S.; Ahn, H.; Oh, J. W.; Choi, J. R., *Appl. Spectrosc. Rev.* **2016**, *51* (7-9), 656-668.
12. Nagao, T.; Chen, K.; Dao, T. D.; Ishi, S.; Chang, R. P. H.; Hoang, C. V.; Oyama, M.; Maeda, M., *Bunseki Kagaku* **2018**, *67* (2), 81-94.
13. Yang, X. X.; Sun, Z. P.; Low, T.; Hu, H.; Guo, X. D.; de Abajo, F. J. G.; Avouris, P.; Dai, Q., *Adv. Mater.* **2018**, *30* (20), 1-23.
14. Chong, X. Y.; Zhang, Y. J.; Li, E. W.; Kim, K. J.; Ohodnicki, P. R.; Chang, C. H.; Wang, A. X., *ACS Sens.* **2018**, *3* (1), 230-238.
15. Caridad, J. M.; Winters, S.; McCloskey, D.; Duesberg, G. S.; Donegan, J. F.; Krstic, V., *Nanotechnology* **2018**, *29* (32), 1-6.
16. Kahraman, M.; Ozbay, A.; Yuksel, H.; Solmaz, R.; Demir, B.; Caglayan, H., *Plasmonics* **2018**, *13* (3), 785-795.
17. Shang, Y. X.; Shi, J.; Liu, H.; Liu, X. F.; Wang, Z. G.; Ding, B. Q., *Nanoscale* **2018**, *10* (20), 9455-9459.
18. Xu, Y.; Yan, X. F.; Fang, W. Z.; Daniele, S.; Zhang, J. L.; Wang, L. Z., *Microporous Mesoporous Mater.* **2018**, *263*, 113-119.
19. Wang, Y.; Kar, A.; Paterson, A.; Kourentzi, K.; Le, H.; Ruchhoeft, P.; Willson, R.; Bao, J., *ACS Photonics* **2014**, *1* (3), 241-245.

20. Wang, J. J.; Duan, G. T.; Li, Y.; Liu, G. Q.; Cai, W. P., *ACS Appl. Mater. Interfaces* **2014**, *6* (12), 9207-9213.
21. Zheng, P.; Cushing, S. K.; Suri, S.; Wu, N., *Phys. Chem. Chem. Phys.* **2015**, *17* (33), 21211-21219.
22. Fukuda, Y.; Saotome, Y.; Nishiyama, N.; Saidoh, N.; Makabe, E.; Inoue, A., *Jpn. J. Appl. Phys* **2012**, *51* (8), 1-5.
23. De Leebeeck, A.; Kumar, L. K. S.; de Lange, V.; Sinton, D.; Gordon, R.; Brolo, A. G., *Anal. Chem.* **2007**, *79* (11), 4094-4100.
24. Seo, J. H.; Park, J. H.; Kim, S. I.; Park, B. J.; Ma, Z. Q.; Choi, J.; Ju, B. K., *J. Nanosci. Nanotechnol.* **2014**, *14* (2), 1521-1532.
25. Escobedo, C., *Lab Chip* **2013**, *13* (13), 2445-2463.
26. Yu, Q. M.; Golden, G., *Langmuir* **2007**, *23* (17), 8659-8662.
27. Li, X.; Soler, M.; Ozdemir, C. I.; Belushkin, A.; Yesilkoy, F.; Altug, H., *Lab Chip* **2017**, *17* (13), 2208-2217.
28. Wallace, G. Q.; Tabatabaei, M.; Hou, R. J.; Coady, M. J.; Norton, P. R.; Simpson, T. S.; Rosendahl, S. M.; Merlen, A.; Lagugne-Labarthe, F., *ACS Photonics* **2016**, *3* (9), 1723-1732.
29. Rang, M.; Jones, A. C.; Zhou, F.; Li, Z. Y.; Wiley, B. J.; Xia, Y. N.; Raschke, M. B., *Nano. Lett.* **2008**, *8* (10), 3357-3363.
30. Garreau, A.; Tabatabaei, M.; Hou, R.; Wallace, G. Q.; Norton, P. R.; Lagugne-Labarthe, F., *J. Phys. Chem. Lett. C* **2016**, *120* (36), 20267-20276.
31. Takano, Y.; Taniguchi, J., *Microelectron. Eng.* **2018**, *193*, 41-46.
32. Gangnaik, A. S.; Georgiev, Y. M.; Holmes, J. D., *Chem. Mater.* **2017**, *29* (5), 1898-1917.
33. Hu, M.; Chen, J. Y.; Li, Z. Y.; Au, L.; Hartland, G. V.; Li, X. D.; Marquez, M.; Xia, Y. N., *Chem. Soc. Rev.* **2006**, *35* (11), 1084-1094.
34. Siddique, R. H.; Mertens, J.; Holscher, H.; Vignolini, S., *Light Sci. Appl.* **2017**, *6*, 1-8.
35. Gu, Y. H.; Zhang, L.; Yang, J. K. W.; Yeo, S. P.; Qiu, C. W., *Nanoscale* **2015**, *7* (15), 6409-6419.
36. Kelly, K. L.; Coronado, E.; Zhao, L. L.; Schatz, G. C., *J. Phys. Chem. B* **2003**, *107* (3), 668-677.
37. Grigorescu, A. E.; Hagen, C. W., *Nanotechnology* **2009**, *20* (29), 1-31.
38. Najiminaini, M.; Vasefi, F.; Kaminska, B.; Carson, J. J. L., *Opt. Express* **2011**, *19* (27), 26186-26197.
39. Sun, D.; Qi, G. H.; Xu, S. P.; Xu, W. Q., *RSC Adv.* **2016**, *6* (59), 53800-53803.
40. Yuan, Q. Q.; He, J. L.; Niu, Y. Z.; Chen, J.; Zhao, Y. L.; Zhang, Y. C.; Yu, C., *Biosens Bioelectron.* **2018**, *102*, 321-327.

41. Tabatabaei, M.; Wallace, G. Q.; Caetano, F. A.; Gillies, E. R.; Ferguson, S. S. G.; Lagugne-Labarthe, F., *Chem. Sci.* **2016**, *7* (1), 575-582.
42. Ingram, W. M.; Han, C.; Zhang, Q.; Zhao, Y., *J. Phys. Chem. C* **2015**, *119* (49), 27639-27648.

Chapter 4

4 Surface-Enhanced Raman Spectroscopy of Extracellular Vesicles

4.1 Introduction

As cells grow and divide, extracellular vesicles are actively released. The umbrella term extracellular vesicle (EV) encompasses three main subgroups of vesicles that are classified by their size: (i) exosomes, (ii) microvesicles, and (iii) apoptotic bodies.¹ The different classifications of vesicles originate from distinct regions of cells and through different cellular processes. Depending on the origin of the EV, the biochemical composition of the membrane and internal cargoes may vary. As EVs are formed, biomolecules including DNA, mRNA, lipids, and proteins from the parent cell are introduced into the cytosolic core.² Examining both the external and internal components of the extracellular vesicle may be used as a means of determining the source and modes of action of specific EVs within the body.

The study of EVs has intensified in recent years due to their potential diagnostic and prognostic applications. EVs have been found to play important roles in disease progression and have been related to neurodegenerative diseases such as Alzheimer's^{3, 4} and Parkinson's diseases^{5, 6}, as well as prostate^{1, 7-9}, lung¹⁰ and breast cancers^{11, 12}. One diagnostic approach to examine biomarkers incorporated in EVs is by western blotting^{13, 14}. This approach is particularly useful for comparing EVs originating from healthy and diseased cells, as different biomarkers may become overexpressed or expressed to a greater degree in diseased states. For example, the expressions of exosome biomarkers present in breast cancer patients are significantly higher when compared to healthy

controls or benign breast tumor patients. There is potential to use these biomarkers for detection and diagnosis of breast cancer.¹³

Isolation of EVs from human biofluids, such as tears,¹⁵ urine,¹⁶ blood,^{7, 11, 16} and cerebrospinal fluid³ present many challenges for researchers. Their isolation from other biological components such as free-floating proteins and cell debris highlights the fundamental importance of being able to capture and probe the EVs at low quantities. It is necessary to note that although there is a correlation amongst a parent cell and the EVs it releases, the presence and distribution of biomarkers may vary depending on the type, mode, and location of the vesicle released. Therefore, a given parent cell releases EVs with varying biomarker expressions.¹⁷ As such, techniques capable of identifying the variability and presence of biomarkers at the single EV level in short periods of time are of great interest.

Recently, several novel methods have been reported indicating noteworthy progress towards detection and characterization of individual EVs. For example, Hu *et al.* incorporated surface plasmon resonance (SPR) sensing into antibody-specific microarrays to detect and sense individual exosomes.¹⁸ Microarrays were functionalized with antibodies complementary to membrane surface proteins of exosomes, allowing for immobilization of individual of exosomes upon interaction. Changes in the local refractive index at the surface of the nanodevice signaled successful binding events for enumeration. This method was successful at counting individual exosomes, however it required labelling with antibodies. As a result, any exosomes lacking the antigen on their membrane surface, or expressing a low quantity of antigens on their surface may not been eliminated from final counts. Alternatively, nanoparticle tracking analysis (NTA) has

been presented in recent years as a technique to quantify individual exosomes in real-time. Song *et al.* utilized NTA to quantify exosomes collected from human sweat samples.¹⁹ NTA employs a laser beam to measure and single particle size and concentration of particles in solution. This technique was successful at quantifying exosome counts, however was not capable of providing molecular or proteomic information without incorporation of additional techniques such as western blotting. In addition to SPR sensing and NTA, Raman spectroscopy and surface-enhanced Raman spectroscopy (SERS) have emerged as promising techniques for quantification of individual EVs.

Raman spectroscopy is a well-established technique for characterizing biological materials. It provides molecular information in a non-destructive and label-free manner, making it a highly useful technique for studying biological materials in their natural environments. It has been applied to a variety of biological studies including cancer studies,^{20,21} neurodegenerative diseases,^{22,23} immunology^{24,25} and microbiology^{26,27}. It has previously been utilized as a tool to study extracellular vesicles by laser tweezers Raman spectroscopy (LTRS), which utilizes a tightly focused laser beam to trap particles at the lasers focal point. Smith *et al.* used LTRS to trap and discern the similarities and differences amongst individual exosomes isolated from eight different cell lines.²⁸ Since LTRS is a label-free technique, no prior knowledge of surface proteins was required. They reported spectral variability in the relative expressions of phospholipids to cholesterol amongst exosomes released when comparing cancerous to non-cancerous cell lines. They were also successful in trapping and probing molecular information from individual exosome. Braeckmans *et al.* attempted to characterize the diversity of

individual exosomes isolated from different cell lines based on a nanoparticle approach.²⁹ Deposition of a gold nanoparticle shell allowed for SERS sensing of exosomes. The study was successful at identifying and characterizing individual exosomes, however their isolation protocol introduced intense SERS peaks from background reagents, which limited the information gained by the study.

Detection of individual extracellular vesicles from human biofluids or cell culture supernatant is often a challenge due to lack in characterization methodology and lack of standardization in isolation protocol. Of the many methods proposed for isolation, some of the most common methods are differential/gradient ultracentrifugation and low-speed centrifugation by commercial isolation reagent kits.³⁰ Ultracentrifugation techniques are known to be time-consuming and tedious, but have yielded good purification results. Commercial isolation reagent kits lack specificity in isolation. These kits act by precipitating vesicles with polyethylene glycol or similar polymers, which ultimately results in contamination of isolates with the polymeric agents.^{17, 29} This largely limits vibrational spectroscopy results, as peaks from isolation reagent kits may predominate over the natural/intrinsic spectral response of the biological materials.

In this chapter, a new approach to detect the chemical content and presence of bulk EV samples with surface-enhanced Raman spectroscopy (SERS) is presented. We additionally extend this work to detection and trapping of individual EVs using nanohole arrays (NHAs). EVs from a pancreatic mesenchymal stromal cell line were isolated to analyze the similarities and differences amongst EVs. Protocols used for EV isolation aimed to minimize spectral contamination from backgrounds to ultimately extract

molecular information directly from EVs by use of centrifugation and filtration methodologies.

4.2 Experimental

4.2.1 Cell Culturing of Pancreatic Mesenchymal Stem Cell Line

Ricordi-chamber isolated human islets were obtained through the Integrated Islet Distribution Program (IIDP) funded by the National Institute of Diabetes and Digestive and Kidney Diseases (NIDDK). 200 islet equivalents were cultured in RPMI 1640 + 10% FBS (Thermo Fisher) for up to 7 days. Between days 5-7, cells with a mesenchymal stem cell (MSC) phenotype¹ were trypsinized and segregated from adherent islet preps using a 40 μ m cell strainer (Corning). Single cell suspensions were subsequently seeded on tissue culture plastic at 4,000 cells/cm² in Amniomax-C100TM (Gibco Life Technologies) supplemented with AmniomaxTM E100 Supplement (Gibco Life Technologies) to support MSC colony formation. Primary human pancreatic cells were deemed to be tissue-specific MSC (Panc-MSC), according guidelines established by the International Society of Cellular Therapies. Panc-MSC were passaged when flasks reached 80-90% confluency and utilized for experimentation at passage 4. Cells were enumerated using Countess II FL (Life Technologies) prior to subsequent experimentation.

4.2.2 Isolation of EVs from Mesenchymal Cell Line

Conditioned media (CM) was generated by culturing Panc-MSC to ~80% confluency, rinsed twice with pre-warmed PBS, and cultured for 24 hours in serum-free Aminomax C100. To remove contaminating dead cells or debris, MSC-CM was centrifuged at 600g for 7 minutes. Cell-free MSC-CM was centrifuged in Amicon Ultra-15 100kDa centrifuge filter units (Millipore) for 20 minutes at 2800g. This concentrated

fraction is enriched with extracellular vesicles (EV+ MSC-CM) and depleted proteins <100kDa. EV+ MSC-CM was rinsed twice with deionized water to remove any residual phenol red from prepared samples.

4.2.3 Cell Culturing of Human Prostate Cancer Cell Line (PC3)

Human prostate cancer cell line, PC3 cells were obtained from ATCC (CRL 1435TM, Manassas, VA, USA) and maintained in Roswell Park Memorial Institute (RPMI)-1640 medium (Wisent, Saint-Jean-Baptiste, QC) and supplemented with 10% fetal bovine serum (FBS, Wisent, Saint-Jean-Baptiste, QC). The cultures were maintained and grown to a confluency of ~80% in an incubator at 37 °C, 5% CO₂, 100% humidity for three to four days. For fluorescent studies, human PC3 cells were labelled with zeta-green through a lentiviral transduction according to a protocol similar to Swaison *et al.*³¹

To grow additional cells, cells were split by rinsing with phosphate-buffered saline (PBS) (Wisent, Saint-Jean-Baptiste, QC) followed by treatment with trypsin-EDTA (Wisent, Saint-Jean-Baptiste, QC) and incubation for 2-5 minutes in 37°C, 5% CO₂, 100% humidity for detachment. Twice the quantity of RPMI, supplemented with 10% FBS was added to the trypsinized cells for neutralization, after which cells suspended in trypsin and culture media were centrifuged at 250 g for two minutes to pellet cells. Supernatant was collected for exosome extraction, and the cellular pellet was re-suspended in cell culture media in new flasks with RPMI for further cell growth and EV isolation. Flasks were incubated under the same conditions as mentioned above until cells reached a confluency of ~ 80%.

4.2.4 Isolation of EVs from Human Prostate Cancer Cell Line (PC3)

Following cell culturing and media isolation as described in section 2.1, collected media containing released EVs was centrifuged at 250 *g* for 5 minutes. Pellets of remaining cells were discarded and supernatant was poured into an Amicon EMD 100 kDa Millipore filter (Millipore Sigma), centrifuged at 3200 *g* for 20 - 30 minutes, while shaking every five minutes to reduce the concentration gradient between the filter and filtrate. Timing of centrifugation varied between 20 – 30 minutes depending on the volume and concentration of EVs being sorted through the Millipore filter. EVs were collected and placed into Eppendorf tubes, and stored at – 20 °C for up to 1 month, or at – 80 °C for long-term storage.

4.2.5 EV Preservation for SEM Imaging

For scanning electron micrograph (SEM) purposes, preservation of EVs to retain their natural spherical shape without bursting upon drying was carried out according to protocol by Wu *et al.*³² EVs isolated from media were fixed in 4 % paraformaldehyde (PFA) (v/v) for 10 minutes. After which, the process of preservation was completed by adding 20% dimethyl siloxane (DMSO) (v/v) to the sample. The sample was aliquoted into vials and stored at – 20 °C for up to one month prior to use.

4.2.6 Substrate Fabrication and Trapping of EVs within Nanohole Arrays

Fabrication of NSL substrates and metallic nanohole arrays followed the protocols outlined in 3.2.1 and 3.2.2.2. To prepare nano-array samples, concentrated EV samples were diluted with milli-Q water. The dilution factor varied based on the concentration of EVs in the sample, and dilutions were either 1:2, 1:3, 1:4, 1:5 or 1:10 depending on the

sample. 20 μL of EV-water solution was drop-casted onto the nano-arrays fabricated by EBL (see section 2.2) and allowed to dry for 20 – 30 minutes to trap EV within nano-wells. Removal of EV-water solution from the array was performed using the cohesive properties allowed by an absorbent paper (Kimberly-Clark Inc.). The edge of the absorbent paper was placed onto the corner of the solution droplet, allowing for removal of solution via capillary action.

4.2.7 Spectroscopic Characterization

Raman spectra were obtained with a Horiba Jobin-Yvon Raman spectrometer equipped with a 600 grooves/mm grating and a 623.8 nm excitation source. An optical objective of $100\times$ (N.A 0.9) was used to collect backscattered light. The pinhole of the spectrometer was opened to 200 μm . Acquisition time was 20 seconds per spectra, and power at the sample was 0.5 mW. For SERS mapping experiments of 4-MPBA, an acquisition time of 5 seconds was used. For SERS measurements with extracellular vesicles, laser power was 0.5 mW at the sample and exposure time varied between 20 – 100 s.

4.3 Results and Discussion

4.3.1 Characteristics of EVs

The human prostate cancer cell line, PC3 was used for characterization of EVs. This cell line was chosen due to its ability to grow, proliferate and produce EVs rapidly. In addition, this cell line is straight-forward to work with, requiring standard cell-handling protocols and is a cell line of interest for this research project due to its

cancerous nature. Optical, fluorescence and scanning electron micrograph (SEM) images were obtained of growing cell cultures, as indicated in Figure 4.1.

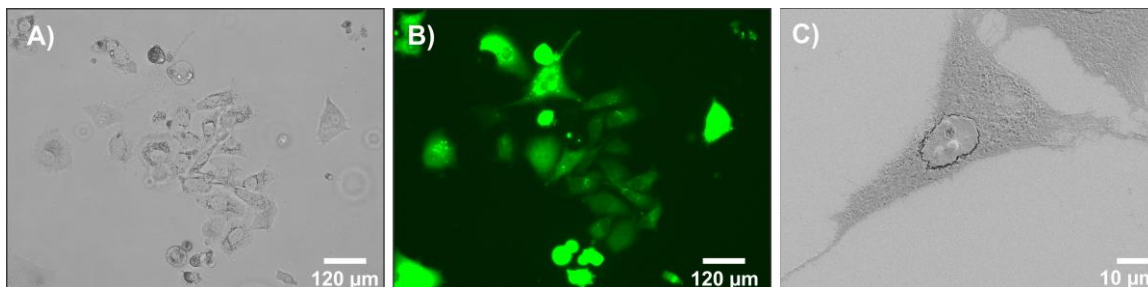


Figure 4.1 – Images of a healthy PC3 cell line used for EV isolation and characterization (A) Optical image of a growing cell culture, with its corresponding fluorescence image (B); (C) SEM of a healthy PC3 cell, displaying sharp edges and protrusions.

Optical and fluorescence images were obtained to determine confluency and health of growing cell cultures. Live-cell images were obtained with an EVOS FLoid Cell Imaging Station (Thermo Fisher Scientific). For concentrated extraction of EVs in cell culture media, the confluency of cells was measured to be $> 80\%$. Therefore, images 4.1 (A) and (B) display confluencies too low for EV isolation but show healthy cell cultures for eventual EV isolation. Cells depicted in these images would require a few additional days for growth before EVs extraction takes place. A SEM image is included in Fig. 4.1 (C) to highlight the characteristic morphology of healthy PC3 cells. Healthy PC3 cells are polygonal in shape, have sharp boundaries between adjacent cells and have characteristically long ‘arm-like’ projections radiating from their sides.³³

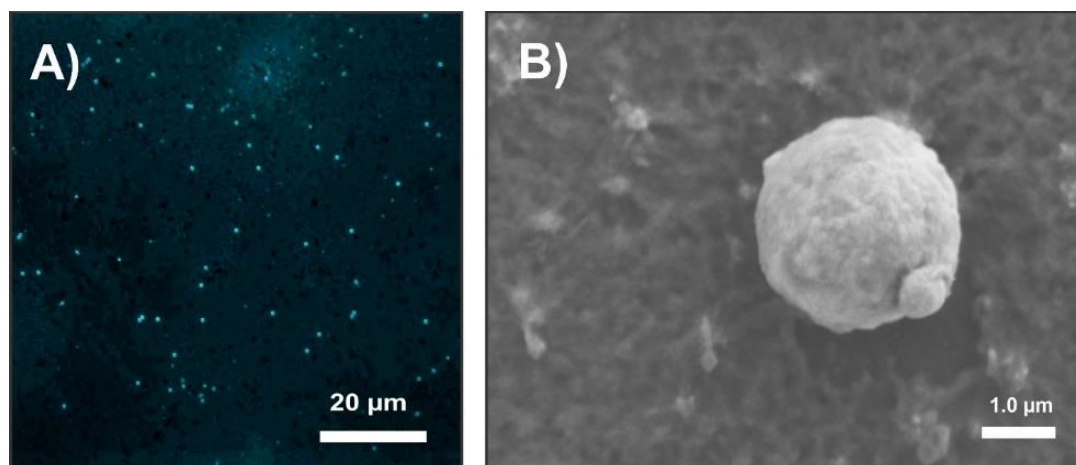


Figure 4.2 – Images of isolated EVs. (A) Fluorescent image of isolated EVs (B) preserved EVs on a silicon wafer.

Isolation of EVs was validated by fluorescence microscopy and SEM. The fluorescence image in Figure 4.2 A) displays a large quantity of isolated vesicles varying in size. There also exists a variability in fluorescence, highlighting a fundamentally important aspect of cellular release of EVs. When parent cells are stained with fluorescent dye, the dye becomes integrated into different areas of the cell in variable amounts. Depending on the location and method of release of each EV, it is expected that EVs may display differences in their fluorescence intensities based on their mode and location of release.³⁴

To visualize the spherical nature of EVs, protocol by Wu *et al.*³² was followed to preserve EVs, which involved immersing the EV solution in 4% PFA (v/v) followed by treatment with 20% DMSO (v/v). Preserved EVs show their expected, characteristic spherical shape (Figure 4.2 B). EVs outlined in this image display a dramatic size difference and are therefore thought to be a larger EV (apoptotic body) attached to a smaller EV (microvesicle). Both vesicles would be released through different cellular

mechanisms, and likely adhered to one another during fixation. It is important to note that although preservation of EVs maintains structural integrity, the PFA and DMSO used for preservation may lead to spectral changes to the natural spectroscopy of EVs, making this method ideal for imaging and trapping of EVs, but non-ideal for spectral acquisition.

4.3.2 SERS of EVs (PC3)

Following successful isolation of EVs, it was desirable to probe their spectral characteristics by SERS. Nanosphere lithography substrates were fabricated to obtain preliminary SERS spectra to determine the biochemical makeup of bulk sets of EVs.

Vesicles were drop casted onto NSL substrates and allowed to dry overnight. The sample was then mounted in an inverted configuration, facing the 633 nm He-Ne laser.

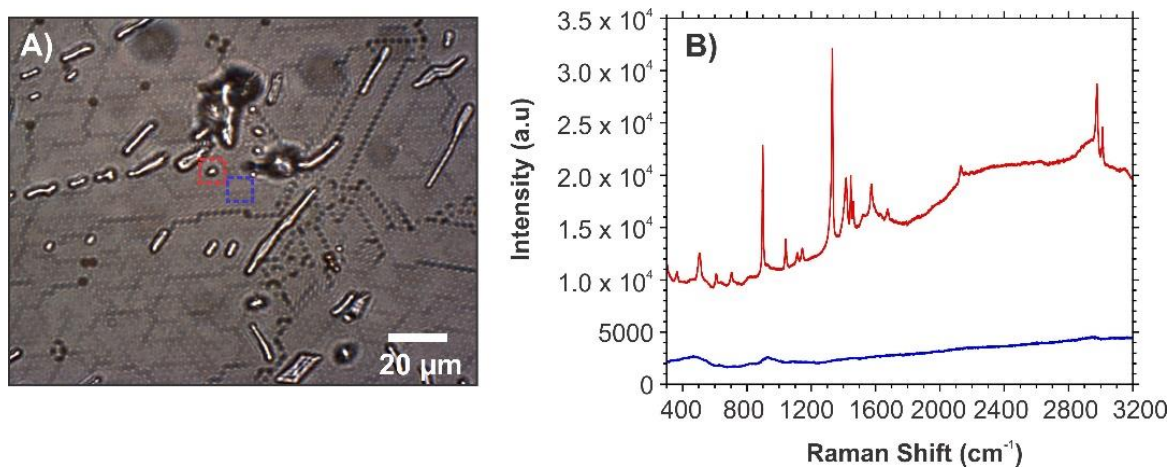


Figure 4.3 (a) NSL substrate containing dried EVs, of which a (b) SERS spectra was obtained of an EV (red) and of the background (blue).

Figure 4.3 outlines setup of the spectroscopic experiments. First, the laser was focused on the EV (highlighted in red). Following acquisition of this spectra over a 20-second period, the laser was moved to the background area beside the dried EV for

comparison (highlighted in blue). Representative spectra are shown in Figure 4.3 (B). The sharp, well defined peaks obtained from the EV were compared to those presented in the literature and displayed many commonalities with EVs previously probed with Raman and SERS (Table 3). Commonalities with previous spectroscopic experiments on EVs included peaks correlating to lipids, nucleic acids and proteins such as the $\nu(\text{C-C})$ peak at 1139 cm^{-1} , the C–O ribose nucleic acid stretch at 1109 cm^{-1} and the $\delta(\text{CH}_2/\text{CH}_3)$ protein or lipid stretch located at 1444 cm^{-1} . Differences also existed when compared to the literature. These variations are expected to exist not only amongst EVs released from different cell lines, but also within a given cohort of EVs released from the same cell line.^{35, 41, 42}

Table 3 - SERS peak assignment for PC3 EV

Raman Shift (cm⁻¹)	Presumed Origin/Assignment of Peak	Reference
1039	$\nu(\text{C-C})$ (lipid)	22, 44
1110	$\nu(\text{C-O})$ (nucleic acid)	22, 44
1142	$\nu(\text{C-C})$ (lipid)	43
1330	$\omega(\text{CH}_3\text{CH}_2)$ (nucleic acid)	22, 44
1412	$\delta(\text{CH}_2)$ (lipid)	22, 43
1444	$\delta(\text{CH}_2/\text{CH}_3)$ (protein, lipid)	22, 35, 44
1569	$\omega(\text{CH}_2/\text{CH}_3)$ tryptophan (nucleic acid)	22, 44
1667	$\nu(\text{C=O})$ Amide I (protein, cholesteryl ester)	35, 43, 45
2976	$\nu(\text{CH}_3)$ (lipid, fatty acid, cholesterol ester)	43

To confirm consistency in peaks acquired from EVs of the PC3 cell line, additional SERS spectra were acquired on NSL substrates. A high degree of similarity was noted, as seen in Figure 4.4. Note that the green trace corresponds to the spectra previously displayed in Figure 4.3 (B). Peaks outlined in Figure 4.4 showed a high degree of similarity to those previously outlined in Table 3. Additional peaks arose for lipids and carbohydrates between 2900 – 3400 cm⁻¹, noting C-H and unsaturated =CH stretches.⁴³

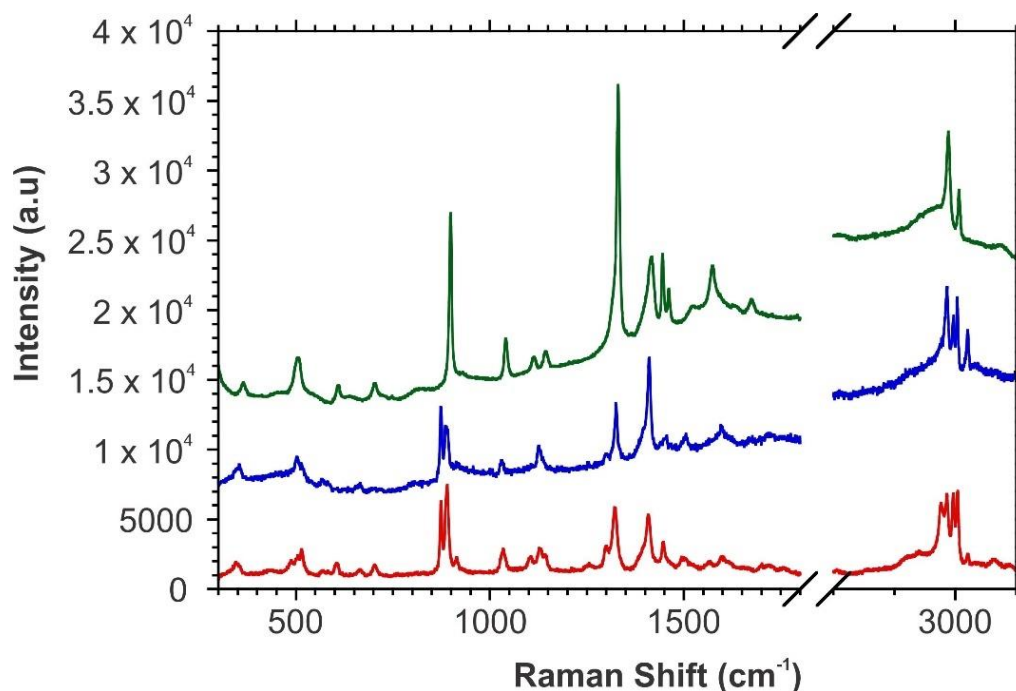


Figure 4.4 – SERS spectra obtained from PC3 derived EVs on a NSL substrate prepared by the O-ring method.

To confirm that vibrational peaks arose from EVs rather than background contamination from cell culture reagents, background spectra were acquired for all agents used during cell culture and EV isolation. These background spectra include (1) RPMI media; (2) RPMI media supplemented with 10% fetal bovine serum; (3) fetal bovine serum; (4) PBS buffer and (5) Trypsin-EDTA. Concentrated solutions of each background solution were drop-casted onto individual glass cover slips and probed by Raman spectroscopy. Representative spectra for these backgrounds, acquired over 10 second acquisition times are displayed in Figure 4.5.

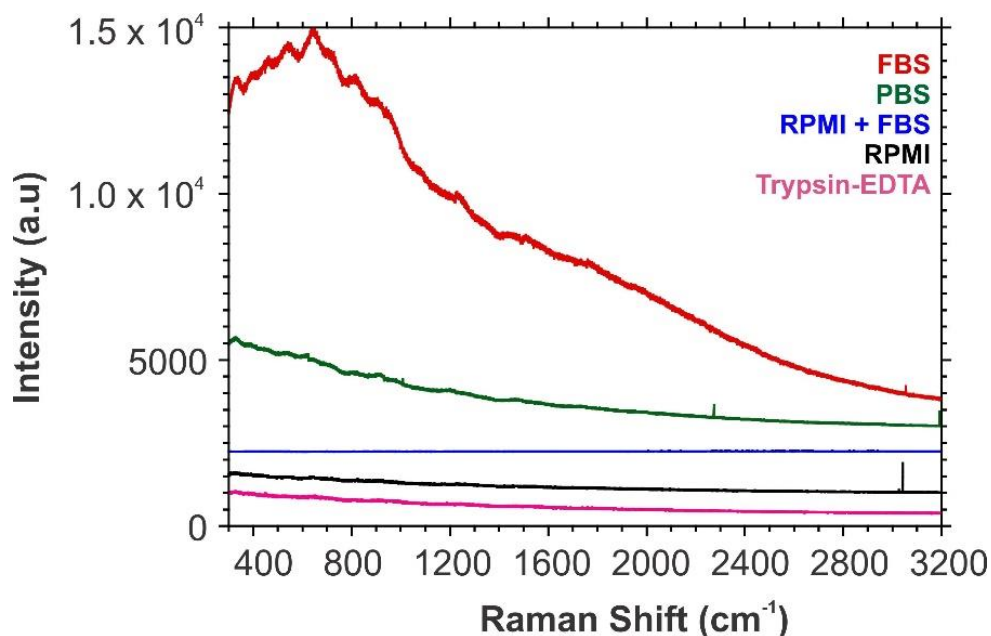


Figure 4.5 – Representative background spectra from PC3 cell line.

Background spectra did not display any sharp spectroscopic peaks and therefore do not compare to those previously acquired for EVs. SERS peaks obtained from EVs on NSL substrates may be assigned directly to the EVs, rather than from spectral contamination by background agents.

To gain a better understanding of the variability that exists amongst vesicles released from different cell lines, a mesenchymal stem cell line was cultured for EV isolation. Study of EVs released from mesenchymal stem cells have applications in regenerative medicine,⁴⁰ and in studies for organ injury repair.⁴¹ A NSL-based experiment was prepared in the same manner as previously outlined PC3 isolated EVs. Spectra were acquired for 100 s, and three representative spectra are shown in Figure 4.6.

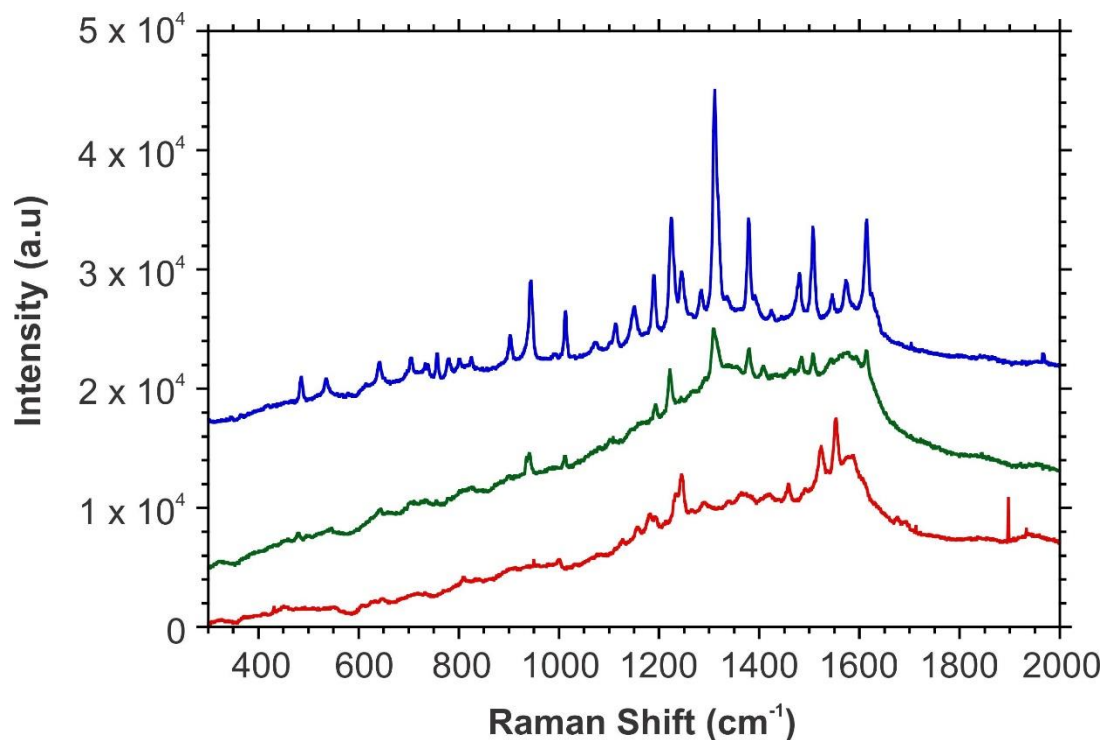


Figure 4.6 – SERS of EVs from a mesenchymal stem cell line on a NSL platform.

These spectra display similarities and differences when compared to one another.

These similarities and differences are further discussed in 4.3.3.

4.3.3 Trapping and Spectral Probing of EVs in NHAs

To visualize trapping of EVs within nanowells, a diluted solution was prepared by mixing EVs with milli-Q water in a 1:3 v/v ratio. The solution was drop-casted onto the nanohole array substrate, and an absorbent wipe was placed on the nanohole array to remove excess and non-trapped EVs. Trapping of EVs displayed similar trapping patterns compared polystyrene particles, previously characterized in 3.3.4.

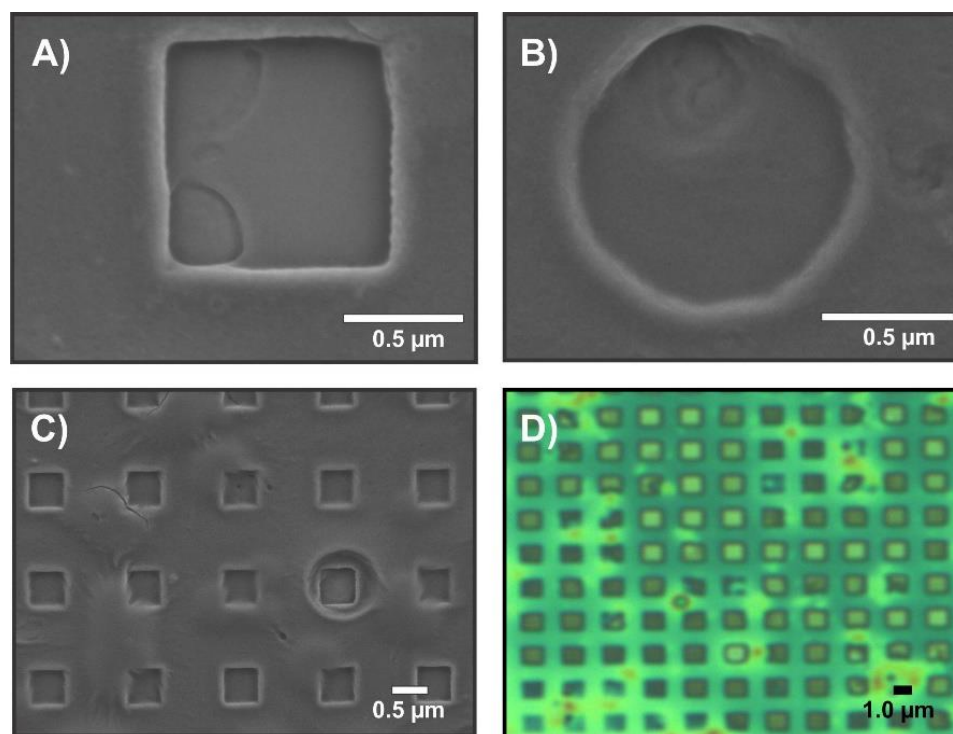


Figure 4.7 – SEM images of EVs trapped within (A) a square nanowell of 0.8 μm diameter; (B) a 1 μm diameter circular nanowell (C) a 0.5 μm square nanowell; (D) optical image of a 1 μm diameter square nanowells.

Figure 4.7 displays SEM and optical images obtained for trapping of EVs within nanowells. Within the 0.8 μm diameter square nanowell, two EVs visibly became trapped in opposite corners. The spectral readout of this nanowell would therefore likely correspond to both EVs, therefore delineation of peaks arising from one EV would not be possible. To this point, if a 100 × objective with a N.A of 0.9 was utilized for spectroscopic measurements, the laser focal diameter would measure roughly 1 μm in diameter, probing information from the entire nanowell. However, in cases where one EV becomes trapped within a given well, the spectral information of one EV would be probed. Trapping of one EV per nanowell is the desired result of this experiment,

however it is important to recognize that probed spectra may be resultant from the spectral overlap of more than EV due to the beam diameter. To allow for more precise trapping of only one EV per well, possible experimentation could be to functionalize nanowells with antibodies for capture based on membrane antigens/proteins.⁴² Dilution of antibodies and functionalization could allow for more precise control over capture. Since this work seeks to minimize spectral contamination from background reagents, capture by antibodies was not explored.

In Figure 4.7 C), an EV larger than the diameter of the nanowell became trapped, and eventually ruptured. This trend is promising for capture and probing of larger sized EVs. An optical image is also provided in Figure 4.7 D) to highlight the trapping efficiency of EVs within a given array of wells. The bright yellow colours correspond to dried cell culture media or background agents used for isolation of EVs, whereas the darker regions within well areas are thought to correspond to trapped vesicles. Trapping efficiency in this case is quite high for the 1 μm diameter square nanowells, although variability has been noted to exist when comparing samples.

Following trapping and sorting of EVs within metallic nanohole arrays, SERS spectra were acquired. SERS spectra of the mesenchymal cell line obtained within the NHA correlated strongly to those previously obtained on the NSL substrate. Background spectra of cell culture media is shown in Figure 4.8, and three representative spectra are shown in Figure 4.9.

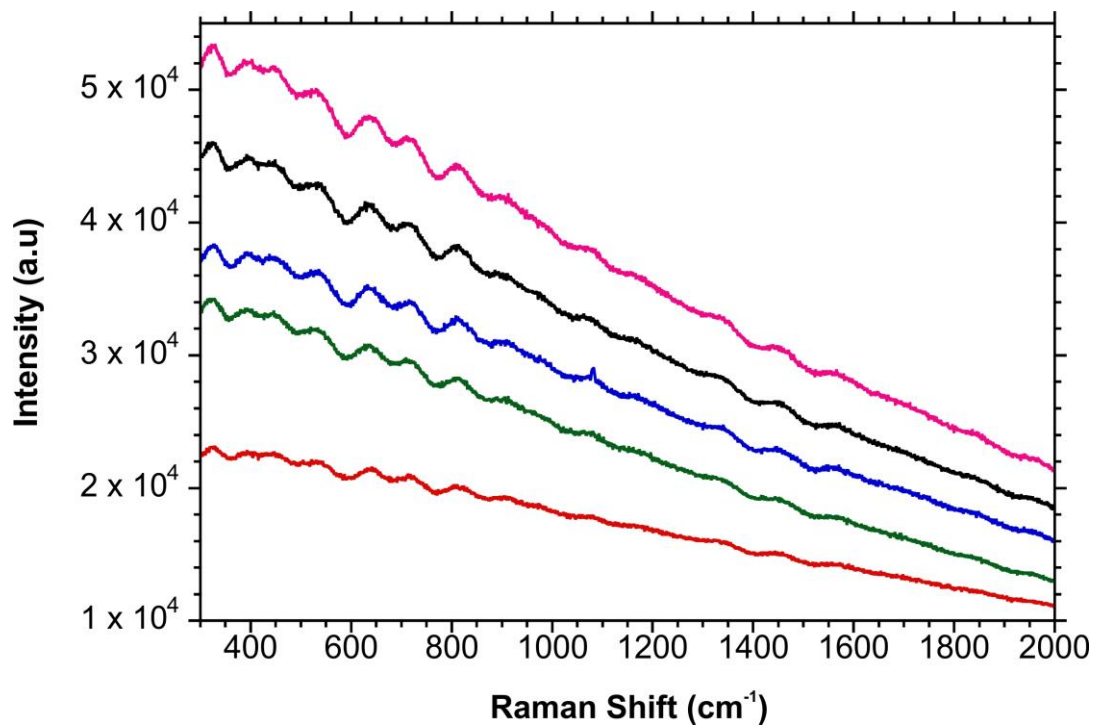


Figure 4.8 - Background Raman spectra of cell culture media for mesenchymal stem cell line.

Background spectra display no defined Raman peaks that would interfere with the intrinsic SERS response of EVs. Acquisition times ranged between 10 – 100 s for the spectra displayed.

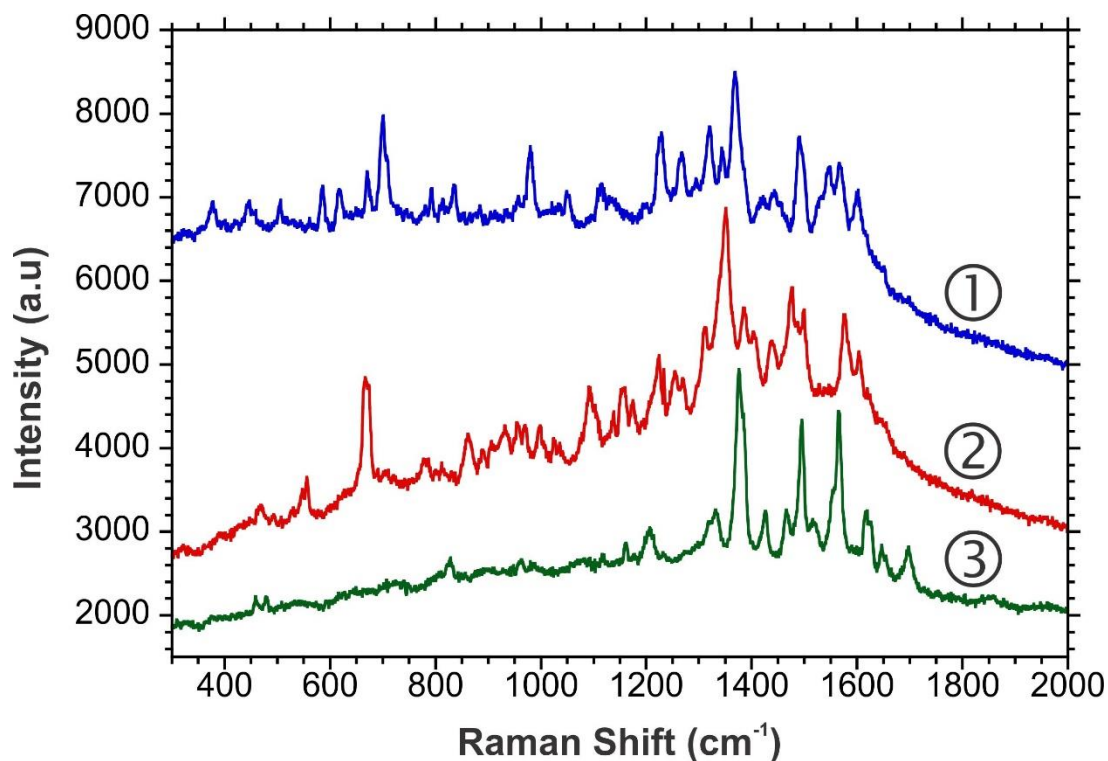


Figure 4.9 - SERS of EVs trapped in a nanohole array within (1) 0.7 μm diameter circular well; (2) 0.9 μm diameter square well; (3) 0.8 μm diameter square. Spectra are shifted for clarity.

The Raman spectra selected are representative of the data set acquired, and were selected due to their similar intensities, thereby eliminating any need for data processing software for enhancement signal to noise ratios. The spectra displayed common vibrational peaks. The intensities of predominant peaks varied, which we hypothesize is due to the intrinsic differences amongst the EV population, even when released from the same cell line. The peaks arising at 669, 1320 and 1602 cm^{-1} come from nucleic acids and amino acids.^{29, 37, 43} The peak located at 1386 cm^{-1} present in spectra 1 and 2 corresponds to a δCH_3 vibration, most likely associated with the membrane of the vesicles. Depending on location of entrapment within the nanowell, it is possible that this membrane vibration

was not detectable for the vesicle probed in spectra 3. The strong peaks between 1490 and 1497 cm^{-1} , present in all three spectra correlate to δ C-N/ ν (N-H), likely from an amide II stretch in proteins.³⁷ The peaks present between 1566 and 1576 cm^{-1} correlate to the nucleic acids or proteins such as tryptophan, guanine and phenylalanine, respectively.^{29, 37} These results provide information regarding variability at the single vesicle level, information that may be used to further clarify the roles of EV subtypes in reference to their chemical makeup and ultimate biological function(s).

Table 4 - SERS peak assignment for mesenchymal EVs

Raman Shift (cm^{-1})	Presumed Origin/Assignment of Peak	Reference
669	ν (C-S) cytosine (nucleic acid)	37
700	ν (C-S) methionine (protein)/ ν (C-C) cholesterol ester (lipid)	38, 37
1320	ω (CH_3CH_2) (nucleic acid)	29, 37
1344	δ (CH) deformations (lipid or nucleic acid)	44
1379	δCH_3 (lipid)	29
1386	δCH_3 (lipid)	29, 37
1494	δ C-N/ ν (N-H) (protein)	37
1566	ν (C-C) tryptophan (nucleic acid)	29, 44
1576	δ (C=C) phenylalanine (protein)/ guanine (nucleic acid)	44, 29
1602	ν (C=C) phenylalanine (protein)	43

The intensity differences amongst spectra in Fig. 4.9 are believed to be resultant from a variety of factors. These factors include the presence and non-presence of biomolecules such as proteins and nucleic acids as well as the distribution of these biomolecules. Additionally, upon entrapment and bursting of extracellular vesicles in air conditions, some contents may burst on the edges or sides of the nanowells.³⁸ Bursting of the EVs on the edges of plasmonic nanowells is expected to yield a greater enhancement compared to the glass area in the center of the wells. We would therefore expect to see a variation in response due to these factors.

The height differences between peaks shared amongst the spectra are hypothesized to be indicative of the varying cargoes present on the surface and within the EVs. For example, the peak present in spectra 1 and 2 at 669 cm^{-1} is indicative of a different quantity of nucleic acids present in each vesicle. Previous literature has reported that nucleic acids may be present on the external surface or within the central cavities of EVs.⁴⁵ The increased strength of this peak in spectra 2 compared to spectra 3 may be indicative of the presence of DNA/RNA on the surface of the EV in spectra 2. This likely would yield a more intense signal, as the DNA would be located closer to the metallic nanohole array generating the greatest electromagnetic enhancement by SERS. However, it is also possible that these nucleic acids may have been released upon drying and bursting of the EVs within the nanowells.³⁸ These findings suggest that for one given class of EV, there exists a diversity in the biochemical composition and distribution of biological cargoes.

4.3.4 Extracellular Vesicle Differentiation and Similarity

When the spectral characteristics of the PC3-derived EVs are compared to the mesenchymal stem cell produced EVs, similarities are noted for nucleic acid, protein and lipid stretches. Figure 4.9 highlights commonalities and differences amongst these vesicles.

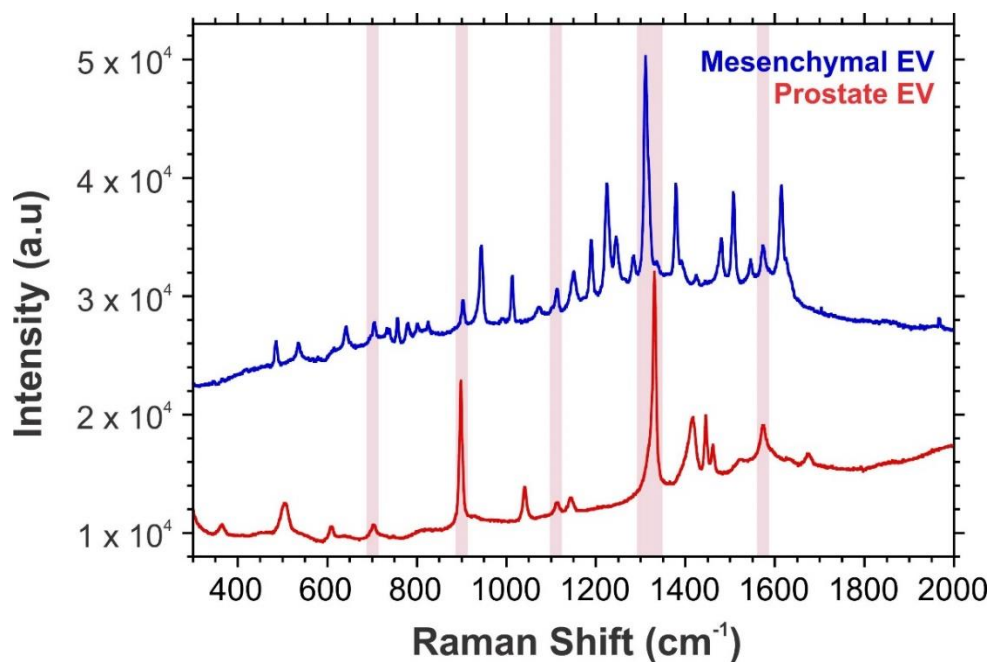


Figure 4.10 - Comparison of SERS spectra of EVs probed by NSL from mesenchymal and prostate (PC3) cell lines.

A high degree of similarity is noted when comparing SERS spectra from EVs of varying origin. Analysis of common peaks arising from individual EVs derived from different cell lines suggests conserved biological functions. Since membrane components are composed of lipids a high degree of overlap for peaks arising from membranous lipids is expected. In addition, since EVs are released through the cytosolic center of

cells, proteins and nucleic acids packaged into their core are expected to be universally present. Peaks common amongst both EV lines are assigned in Table 5.

Smith *et al.* noted similar findings, suggesting conserved biological function amongst EVs released from seven different cell lines.²⁸ Using statistical analysis (principle component analysis), cholesterol content, surface protein expression and the relative expression of phospholipids to cholesterol were highly conserved. Statistical analysis by principle component analysis would be of great interest for discerning the most common peaks shared amongst the two EV lines studied in this work. PCA could also be used to generate a library or barcoding system to definitively differentiate and compare EVs, which has previously been suggested in the literature.^{46, 47} Barcoding of EVs by SERS could provide potential benefits in disease diagnosis, as understanding the variability shared amongst one EV line and between different EV lines may potentially allow for definitive detection of biomarkers present in diseases and cancers. To perform statistical analysis, large sets of data would be required. Multiplexing by on-chip sensing would assist greatly in acquisition of large data sets. Automation of spectroscopic measurements of fabricated NHAs by defining each nanowell to a set of spatial coordinates may potentially allow for this type of analysis in future work.

Table 5 - Peak assignment for peaks shared amongst PC3 and mesenchymal EVs

Raman Shift (cm⁻¹)	Presumed Origin/Assignment of Peak	Reference
695 - 705	$\nu(\text{C-S})$ (methionine, protein) / $\nu(\text{C-C})$ Cholesterol ester (lipid)	38, 37
895 – 900	$\rho(\text{CH}_2)$ (protein)	29
1110 - 1115	$\nu(\text{C - O})$ (ribose, nucleic acid)	29
1310 – 1330	$\nu(\text{C- N})$ (protein)/ $\tau(\text{CH}_3\text{CH}_2)$ (lipid)	29
1570 - 1575	$\nu(\text{C-C})$ Tryptophan (nucleic acid)	29, 44

4.4 Conclusion

Throughout this chapter, isolation of EVs was successfully verified by fluorescence and scanning electron microscopy. Fixation of the membranes of EVs revealed intact, spherical membranes and displayed a variation in size verifying successful isolation of exosomes, microvesicles and apoptotic bodies. Trapping of EVs was subsequently characterized by fabrication of nanohole arrays, which revealed capture of EVs in corner regions of square and circular nanowells. Nanohole arrays with plasmonic capabilities were also fabricated for compatibility with surface-enhanced Raman spectroscopy.

Sorting and probing by SERS of individual extracellular vesicles was allowed by fabrication of metallic nanohole arrays. SERS results presented good agreement to those presented in the literature, showing presence of expected lipid, protein and nucleic acid peaks. Raman spectra of background reagents further concluded that peaks were from intrinsic EV signatures. This approach therefore eliminates the need for background subtraction from isolation reagent kits, as direct isolation of EVs occurred by combination of filtration and centrifugation.

Amongst EVs isolated from the same cell line, similarities and differences were noted, suggesting some EVs contain higher quantities of biomolecules compared to others. Comparison of EVs isolated from two different cell cultures also showed similarities and differences. Similarities included nucleic acid content as well as lipid and protein content, suggesting conserved biological functions. We therefore demonstrated that nanowell-based SERS substrates may be used to capture and probe nanomaterials for molecular-level characterization. This nanodevice holds high potential in point-of-care diagnostics for cancer or disease detection.

4.5 References

1. Brett, S. I.; Kim, Y.; Biggs, C. N.; Chin, J. L.; Leong, H. S., *Prostate Cancer P. D.* **2015**, *18* (3), 213-220.
2. Ofir-Birin, Y.; Abou Karam, P.; Rudik, A.; Giladi, T.; Porat, Z.; Regev-Rudzki, N., *Front. Immunol.* **2018**, *9*, 1011.
3. Street, J. M.; Barran, P. E.; Mackay, C. L.; Weidt, S.; Balmforth, C.; Walsh, T. S.; Chalmers, R. T.; Webb, D. J.; Dear, J. W., *J. Transl. Med.* **2012**, *10* (1), 5.
4. Xiao, T.; Zhang, W.; Jiao, B.; Pan, C.-Z.; Liu, X.; Shen, L., *Transl. Neurodegener.* **2017**, *6*, 3.
5. Shi, M.; Liu, C.; Cook, T. J.; Bullock, K. M.; Zhao, Y.; Gingham, C.; Li, Y.; Aro, P.; Dator, R.; He, C., et al., *Acta Neuropathol.* **2014**, *128* (5), 639-650.
6. Wu, X.; Zheng, T.; Zhang, B., *Neurosci. Bull.* **2017**, *33* (3), 331-338.

7. Krafft, C.; Wilhelm, K.; Eremin, A.; Nestel, S.; von Bubnoff, N.; Schultze-Seemann, W.; Popp, J.; Nazarenko, I., *Nanomedicine* **2017**, *13* (3), 835-841.
8. Pan, J.; Ding, M.; Xu, K.; Yang, C.; Mao, L.-J., *Oncotarget* **2017**, *8* (57), 97693-97700.
9. Biggs, C. N.; Siddiqui, K. M.; Al-Zahrani, A. A.; Pardhan, S.; Brett, S. I.; Guo, Q. Q.; Yang, J.; Wolf, P.; Power, N. E.; Durfee, P. N., et al., *Oncotarget* **2016**, *7* (8), 8839-8849.
10. Cui, S.; Cheng, Z.; Qin, W.; Jiang, L., *Lung Cancer* **2018**, *116*, 46-54.
11. Zhong, Z. Y.; Rosenow, M.; Xiao, N.; Spetzler, D., *J. Extracell. Vesicles* **2018**, *7* (1), 1458574.
12. Jia, Y.; Chen, Y.; Wang, Q.; Jayasinghe, U.; Luo, X.; Wei, Q.; Wang, J.; Xiong, H.; Chen, C.; Xu, B., et al., *Oncotarget* **2017**, *8* (25), 41717-41733.
13. Wang, M.; Ji, S.; Shao, G.; Zhang, J.; Zhao, K.; Wang, Z.; Wu, A., *Clin. Transl. Oncol.* **2018**, *20* (7), 906-911.
14. Conde-Vancells, J.; Rodriguez-Suarez, E.; Gonzalez, E.; Berisa, A.; Gil, D.; Embade, N.; Valle, M.; Luka, Z.; Elortza, F.; Wagner, C., et al., *Proteomics Clin. Appl.* **2010**, *4* (4), 416-425.
15. Grigor'eva, A. E.; Tamkovich, S. N.; Eremina, A. V.; Tupikin, A. E.; Kabilov, M. R.; Chernykh, V. V.; Vlassov, V. V.; Laktionov, P. P.; Ryabchikova, E. I., *Biochem. (Mosc) Suppl. Ser. A Membr. Cell. Biol.* **2016**, *10* (2), 165-172.
16. Pisitkun, T.; Shen, R.-F.; Knepper, M. A., *Proc. Natl. Acad. Sci. U.S.A* **2004**, *101* (36), 13368-13373.
17. Smith, Z.; Lee, C.; Rojalin, T.; Carney, R.; Hazari, S.; Knudson, A.; Lam, K.; Saari, H.; Lazaro-Ibañez, E.; Viitala, T., et al., *J. Extracell. Vesicles* **2015**, *4*, 28533.
18. Zhu, L.; Wang, K.; Cui, J.; Liu, H.; Bu, X. L.; Ma, H. L.; Wang, W. Z.; Gong, H.; Lausted, C.; Hood, L., et al., *Anal. Chem.* **2014**, *86* (17), 8857-8864.
19. Ning, X. F.; Zhang, H. R.; Wang, C.; Song, X. Q., *Med. Sci. Monit.* **2018**, *24*, 2350-2359.
20. Falamas, A.; Dehelean, C. A.; Pinzaru, S. C., *Vib. Spectrosc.* **2018**, *95*, 44-50.
21. Abramczyk, H.; Imiela, A., *Spectrochim. Acta A Mol. Biomol. Spectrosc.* **2018**, *188*, 8-19.
22. Devitt, G.; Howard, K.; Mudher, A.; Mahajan, S., *ACS Chem. Neurosci.* **2018**, *9* (3), 404-420.
23. Mattana, S.; Caponi, S.; Tamagnini, F.; Fioretto, D.; Palombo, F., *J. Innov. Opt. Health Sci.* **2017**, *10* (6).
24. Brown, K. L.; Palyvoda, O. Y.; Auner, G. W.; Gruber, S. A., *J. Immunol. Methods* **2014**, *415*, 31-35.

25. Yakes, B. J.; Lipert, R. J.; Bannantine, J. P.; Porter, M. D., *Clin. Vaccine Immunol.* **2008**, *15* (2), 235-242.
26. Wang, S. W.; Setlow, B.; Setlow, P.; Li, Y. Q., *J. Antimicrob. Chemother.* **2016**, *71* (6), 1540-1546.
27. Kusic, D.; Rosch, P.; Popp, J., *Syst. Appl. Microbiol.* **2016**, *39* (2), 132-140.
28. Smith, Z.; Lee, C.; Rojalin, T.; Carney, R.; Hazari, S.; Knudson, A.; Lam, K.; Saari, H.; Lazaro-Ibañez, E.; Viitala, T., et al., *J. Extracell. Vesicles* **2015**, *4*, 1-15.
29. Stremersch, S.; Marro, M.; Pinchasik, B. E.; Baatsen, P.; Hendrix, A.; De Smedt, S. C.; Loza-Alvarez, P.; Skirtach, A. G.; Raemdonck, K.; Braeckmans, K., *Small* **2016**, *12* (24), 3292-3301.
30. Li, P.; Kaslan, M.; Lee, S. H.; Yao, J.; Gao, Z. Q., *Theranostics* **2017**, *7* (3), 789-804.
31. Swainson, L.; Mongellaz, C.; Adjali, O.; Vicente, R.; Taylor, N., Ewbank, J.; Vivier, E., Eds. Humana Press: Totowa, NJ, 2008; 301-320.
32. Wu, Y.; Deng, W.; Klinke, D. J., *Analyst* **2015**, *140* (19), 6631-6642.
33. Cui, Y.; Yamada, S., *PLoS One* **2013**, *8* (1), 1-11.
34. Usman, W. M.; Pham, T. C.; Kwok, Y. Y.; Vu, L. T.; Ma, V.; Peng, B.; Chan, Y. S.; Wei, L.; Chin, S. M.; Azad, A., et al., *Nat. Commun.* **2018**, *9* (1), 2359.
35. Tatischeff, I.; Larquet, E.; Falcón-Pérez, J. M.; Turpin, P.-Y.; Kruglik, S. G., *J. Extracell. Vesicles* **2012**, *1*.
36. Gualerzi, A.; Niada, S.; Giannasi, C.; Picciolini, S.; Morasso, C.; Vanna, R.; Rossella, V.; Masserini, M.; Bedoni, M.; Ciceri, F., et al., *Sci. Rep.* **2017**, *7*, 9820.
37. Talari, A. C. S.; Movasaghi, Z.; Rehman, S.; Rehman, I. U., *Appl. Spectrosc. Rev.* **2015**, *50* (1), 46-111.
38. Lee, C.; Carney, R. P.; Hazari, S.; Smith, Z. J.; Knudson, A.; Robertson, C. S.; Lam, K. S.; Wachsmann-Hogiu, S., *Nanoscale* **2015**, *7* (20), 9290-9297.
39. Krafft, C.; Neudert, L.; Simat, T.; Salzer, R., *Spectrochim. Acta A Mol. Biomol. Spectrosc.* **2005**, *61* (7), 1529-1535.
40. Shafei, A. E.; Ali, M. A.; Ghanem, H. G.; Shehata, A. I.; Abdelgawad, A. A.; Handal, H. R.; ElSayed, A. S.; Ashaal, A. E.; Ali, M. M.; El-Shal, A. S., *J. Cell. Biochem.* **2018**, *119* (7), 5274-5286.
41. Yamashita, T.; Takahashi, Y.; Takakura, Y., *Biol. Pharm. Bull.* **2018**, *41* (6), 835-842.
42. Jackman Joshua, A.; Linarydy, E.; Yoo, D.; Seo, J.; Ng Wei, B.; Klemme Daniel, J.; Wittenberg Nathan, J.; Oh, S.-H.; Cho, N.-J., *Small* **2015**, *12* (9), 1159-1166.
43. Huang, Z. W.; McWilliams, A.; Lui, H.; McLean, D. I.; Lam, S.; Zeng, H. S., *Int. J. Cancer* **2003**, *107* (6), 1047-1052.

44. Notingher, I.; Verrier, S.; Haque, S.; Polak, J. M.; Hench, L. L., *Biopolymers* **2003**, 72 (4), 230-240.
45. Nemeth, A.; Orgovan, N.; Sodar, B. W.; Osteikoetxea, X.; Paloczi, K.; Szabo-Taylor, K. E.; Vukman, K. V.; Kittel, A.; Turiak, L.; Wiener, Z., et al., *Sci. Rep.* **2017**, 7, 16.
46. Beach, A.; Zhang, H.-G.; Ratajczak, M. Z.; Kakar, S. S., *J. Ovarian Res.* **2014**, 7, 1-11.
47. Nazimek, K.; Bryniarski, K.; Askenase, P. W., *Int. Arch. Allergy Immunol.* **2016**, 171 (1), 1-26.

Chapter 5

5 Conclusions and Outlook

5.1 Conclusions

Nanofabrication techniques such as nanosphere lithography and electron beam lithography are promising methods of fabricating metallic nanostructures in a reproducible manner. Although the applications of metallic nanostructures vary widely across scientific subdisciplines, they have been used extensively for spectroscopic analyses due to their plasmonic capabilities.¹⁻⁵ Incorporation of nanostructures into chip-based sensors holds extreme potential in development of point-of-care technologies for disease detection and diagnosis. Recently, chip-based sensors involving nanofabrication techniques have developed devices with extreme sensitivities to study a variety of biological, physical and chemical phenomena.⁶⁻⁸

Throughout this thesis, nanosphere lithography and electron beam lithography were presented as lithographic techniques to probe molecular information from biological vesicles. Chapter 1 highlighted current work within the fields of nanofabrication, extracellular vesicles and point-of-care sensor development. Chapter 2 presented the main biological, chemical and physical information underlying extracellular vesicles and nanofabrication. Specific interest was also placed on direct and indirect sensing of biomaterials for disease diagnosis and detection.

Fabrication and characterization of nanostructures and substrates were characterized throughout Chapter 3, wherein the LSPR positions of NSL and EBL structures were obtained by absorption measurements to allow for matching of LSPR

positions with the incident light source. The O-ring method of NSL was offered as a means of fabricating reproducible and semi-controlled regions of nanoprisms.⁹ EBL was further performed on a positive-tone resist to assess the trapping capabilities of nanowell cavities with polystyrene spheres of a known aspect ratio. These samples were characterized by SEM, fluorescence and optical imaging. Results indicated successful fabrication of nanostructures by NSL and EBL, and successful confinement of PS spheres within nanowell areas in nanohole arrays was noted.

The ability to efficiency trap and probe EVs in metallic NHAs was presented in Chapter 4. Electron beam lithography was performed on a negative-tone resist, allowing for fabrication of glass nanowells surrounded in metal. Functionalization of the NHA with a well-known Raman reporter highlighted ideal sensing areas for SERS. Spatial resolution was limited during mapping due to the $100\times$ (0.9 N.A.) objective, which confined the laser beam to a $1\ \mu\text{m} \times 1\ \mu\text{m}^2$ area on the NHA substrate. However, mapping was successful in proving hot-spots lied within central glass nanowell cavities. This was tested by detection of polystyrene spheres from below a metallic nanohole array. SERS acquisition revealed expected spectra for polystyrene, demonstrating successful confinement of nanomaterials to desired sensing areas.

Successful trapping of PS nanospheres and subsequent SERS acquisition lead to probing of spectral signatures of EVs in Chapter 4. The structural characteristics of EVs were first characterized by fluorescence and SEM, revealing isolated vesicles with intact lipid membranes. NSL substrates were subsequently used to characterize the average SERS response of a bulk EV sample (unsorted). The components of bulk EV samples revealed contents with nucleic acids, lipids and proteins and displayed high similarity to

the EV samples characterized previously in the literature.^{1, 10, 11} Metallic NHAs were then used to sort and trap individual EVs and for acquisition of SERS spectra. Trapping within nanowells was successful. SEM imaging revealed the ability of the NHA to capture more than one EV per nanowell, which may be circumvented future work by use of antibodies specific to EV membranes.

Probing of SERS spectra from EVs trapped within wells of a metallic NHA revealed spectral characteristics similar to those acquired on NSL substrates. There existed a diversity amongst EVs isolated from the same cell line, suggesting different roles and release mechanisms for individual vesicles. Intensity differences amongst the EV population from an individual cell line signaled increases in the quantity of specific biomaterial components. The SERS spectra of EVs released from two cell lines, a prostate cancer cell line and a mesenchymal stem cell line were also compared. The presence of nucleic acids, as well as lipid and protein contents suggested conserved biological functions, a finding previously reported in the literature.¹⁰ Conserved biological functions such as lipid membranes for protection and encapsulation of materials are essential for formation of EVs and were therefore expected to display themselves in SERS spectra from both EV lines.

This thesis demonstrated successful fabrication of a nanohole-array based sensor capable of probing molecular information from nanoscale biological materials. This nanodevice holds high potential in point-of-care diagnostics for cancer or disease detection.

5.2 Outlook

Throughout this thesis, a nanoscale device was fabricated for trapping, sorting and probing of nanoscale biological materials known as extracellular vesicles. The nanodevice allowed for molecular-level characterization of biological vesicles isolated from cultured cell lines by SERS. Future work may seek to combine nanohole arrays with microfluidic technologies. If microfluidic channels are fabricated to sort and isolate vesicles from other biological debris, flow through of EVs onto nanohole arrays could allow for direct and rapid detection of EVs from human liquid biopsies. This would extend the device to a point-of-care screening tool, whereby clinicians could better assess and diagnose patients with less-invasive screening tools.

In line with incorporation of NHAs into a microfluidic device, previous literature by Wang *et al.* highlights a method of isolating EVs from biological samples by incorporation of microfluidics and nanofabrication.¹² This group fabricated a nanodevice containing ciliated micropillar structured forming a nanowire-on-micropillar trap for selective capture of exosome-like vesicles (40 – 100 nm in diameter). Flow of EVs through the device selectively trapped exosomes within nanowires, while proteins and cell debris flowed through the device for removal (Figure 5.1). Exosomes were recovered by flooding the device with phosphate-buffered saline (PBS), a buffer solution commonly used during cell culture/EV isolation. In the future, a device incorporating nanowire-on-micropillar traps for initial isolation of EVs from complex biological samples, followed with recovery of EVs in PBS and subsequent flow through of EVs onto a nanohole array could allow for SERS-based detection of EVs from complex biological samples.

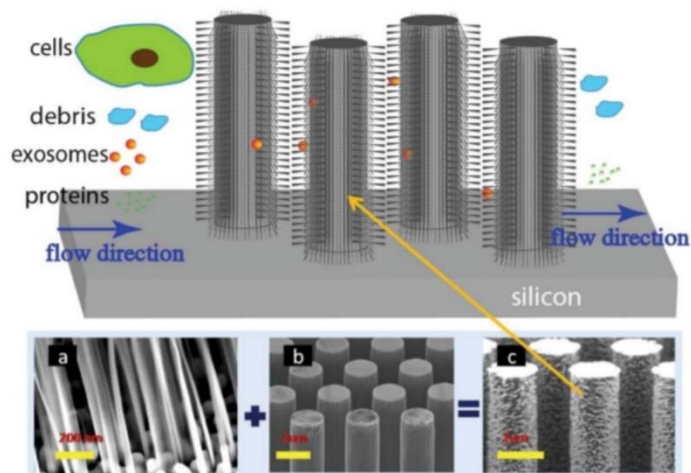


Figure 5.1 - Exosomes trapped within “nanowire-on-micropillar” structures and subsequently separated from cellular debris and proteins. Inlay shows (a) Nanowires; (b) Micropillars; (c) “Nanowire-on-micropillar” structures. Reproduced with permission.¹²


In this thesis, electron beam lithography (EBL) was presented as a means of fabricating metallic nanohole arrays in a reproducible manner. Although EBL presents many advantages over other lithographic techniques due to its high resolution and reproducibility, fabrication of metallic nanohole arrays requires significant amounts of time and requires advanced nanofabrication skills. Other methods of fabrication may be explored in the future to minimize these limitations. In recent years, stencil lithography has emerged as a great method for fabrication of nanohole arrays.¹³ Stencil lithography is a resistless, scalable and high-throughput technique allowing for fabrication of nanostructures over large surface-areas with a reusable mask. Nanostencil lithography has also been presented on non-conventional lithographic substrates such as flexible polymers^{14, 15} and PDMS-based microfluidic devices.¹³ Fabrication costs can largely be

minimized by reuse of nanostencil masks. In addition, the mask may be fabricated to cover the entire surface area of the substrate and requires less advanced training due to non-use of resists and an electron beam source.


5.3 References

1. Stremersch, S.; Marro, M.; Pinchasik, B. E.; Baatsen, P.; Hendrix, A.; De Smedt, S. C.; Loza-Alvarez, P.; Skirtach, A. G.; Raemdonck, K.; Braeckmans, K., *Small* **2016**, *12* (24), 3292-3301.
2. Repetto, D.; Giordano, M. C.; Foti, A.; Gucciardi, P. G.; Mennucci, C.; de Mongeot, F. B., *Appl. Surf. Sci.* **2018**, *446*, 83-91.
3. Shang, Y. X.; Shi, J.; Liu, H.; Liu, X. F.; Wang, Z. G.; Ding, B. Q., *Nanoscale* **2018**, *10* (20), 9455-9459.
4. Subr, M.; Kuzminova, A.; Kylian, O.; Prochazka, M., *Spectrochim. Acta A Mol. Biomol. Spectrosc.* **2018**, *197*, 202-207.
5. Xu, Y.; Yan, X. F.; Fang, W. Z.; Daniele, S.; Zhang, J. L.; Wang, L. Z., *Microporous Mesoporous Mater.* **2018**, *263*, 113-119.
6. Akil-Jradi, S.; Jradi, S.; Plain, J.; Adam, P. M.; Bijeon, J. L.; Royer, P.; Bachelot, R., *RSC Adv.* **2012**, *2* (20), 7837-7842.
7. Gjergjizi, B.; Cogun, F.; Yildirim, E.; Eryilmaz, M.; Selbes, Y.; Saglam, N.; Tamer, U., *Sens. Actuators B Chem.* **2018**, *269*, 314-321.
8. Li, Y.; Chen, Q.; Xu, X. F.; Jin, Y. P.; Wang, Y.; Zhang, L. Y.; Yang, W. J.; He, L. D.; Feng, X. Y.; Chen, Y. Q., *Sens. Actuators B Chem.* **2018**, *266*, 115-123.
9. Wallace, G. Q.; Tabatabaei, M.; Hou, R. J.; Coady, M. J.; Norton, P. R.; Simpson, T. S.; Rosendahl, S. M.; Merlen, A.; Lagugne-Labarhet, F., *ACS Photonics* **2016**, *3* (9), 1723-1732.
10. Smith, Z.; Lee, C.; Rojalin, T.; Carney, R.; Hazari, S.; Knudson, A.; Lam, K.; Saari, H.; Lazaro-Ibanez, E.; Viitala, T., et al., *J. Extracell. Vesicles* **2015**, *4*, 1-15.
11. Lee, C.; Carney, R. P.; Hazari, S.; Smith, Z. J.; Knudson, A.; Robertson, C. S.; Lam, K. S.; Wachsmann-Hogiu, S., *Nanoscale* **2015**, *7* (20), 9290-9297.
12. Wang, Z. X.; Wu, H. J.; Fine, D.; Schmulen, J.; Hu, Y.; Godin, B.; Zhang, J. X. J.; Liu, X. W., *Lab Chip* **2013**, *13* (15), 2879-2882.
13. Du, K.; Ding, J. J.; Liu, Y. Y.; Wathuthanthri, I.; Choi, C. H., *Micromachines* **2017**, *8* (4), 131-155.
14. Cvetkovic, N. V.; Sidler, K.; Savu, V.; Brugger, J.; Tsamados, D.; Ionescu, A. M., *Microelectron. Eng.* **2012**, *100*, 47-50.
15. Vazquez-Mena, O.; Sannomiya, T.; Tosun, M.; Villanueva, L. G.; Savu, V.; Voros, J.; Brugger, J., *ACS Nano* **2012**, *6* (6), 5474-5481.


Appendix A - Copyright



Copyright Clearance Center



[Home](#)
[Account Info](#)
[Help](#)



Title: Ciliated micropillars for the microfluidic-based isolation of nanoscale lipid vesicles

Author: Zongxing Wang, Hung-jen Wu, Daniel Fine, Jeffrey Schmulen, Ye Hu, Biana Godin, John X. J. Zhang, Xuewu Liu

Publication: Lab on a Chip

Publisher: Royal Society of Chemistry

Date: May 9, 2013

Copyright © 2013, Royal Society of Chemistry

Logged in as:
Lauren Kaufman

LOGOUT

Order Completed

Thank you for your order.

This Agreement between Mrs. Lauren Kaufman ("You") and Royal Society of Chemistry ("Royal Society of Chemistry") consists of your license details and the terms and conditions provided by Royal Society of Chemistry and Copyright Clearance Center.

Your confirmation email will contain your order number for future reference.

[printable details](#)

License Number	4385390782485
License date	Jul 10, 2018
Licensed Content Publisher	Royal Society of Chemistry
Licensed Content Publication	Lab on a Chip
Licensed Content Title	Ciliated micropillars for the microfluidic-based isolation of nanoscale lipid vesicles
Licensed Content Author	Zongxing Wang, Hung-jen Wu, Daniel Fine, Jeffrey Schmulen, Ye Hu, Biana Godin, John X. J. Zhang, Xuewu Liu
Licensed Content Date	May 9, 2013
Licensed Content Volume	13
Licensed Content Issue	15
Type of Use	Thesis/Dissertation
Requestor type	academic/educational
Portion	figures/tables/images
Number of figures/tables/images	1
Distribution quantity	100
Format	print and electronic
Will you be translating?	no
Order reference number	
Title of the thesis/dissertation	Probing Extracellular Vesicles using Surface-Enhanced Raman Spectroscopy
Expected completion date	Aug 2018
Estimated size	110
Requestor Location	Mrs. Lauren Kaufman 1151 Richmond Street London, ON N6A 5B7 Canada Attn: Mrs. Lauren Kaufman
Billing Type	Invoice
Billing address	Mrs. Lauren Kaufman 1151 Richmond Street London, ON N6A 5B7 Canada Attn: Mrs. Lauren Kaufman
Total	0.00 CAD



Thank you for your order!

Dear Mrs. Lauren Kaufman,

Thank you for placing your order through Copyright Clearance Center's RightsLink® service.

Order Summary

Licensee: Mrs. Lauren Kaufman
Order Date: Jul 10, 2018
Order Number: 4385390782485
Publication: Lab on a Chip
Title: Ciliated micropillars for the microfluidic-based isolation of nanoscale lipid vesicles
Type of Use: Thesis/Dissertation
Order Total: 0.00 CAD

View or print complete [details](#) of your order and the publisher's terms and conditions.

Sincerely,

Copyright Clearance Center

Tel: +1-855-239-3415 / +1-978-646-2777
customer@copyright.com
<https://myaccount.copyright.com>



RightsLink®

Curriculum Vitae

Name: Lauren Kaufman

Post-secondary Education and Degrees: University of Toronto Mississauga
Mississauga, Ontario, Canada
2010 – 2015 (HBSc. Biology and Chemistry, Double Major)

The University of Western Ontario
London, Ontario, Canada
2016 – 2018 (M.Sc. Candidate, Chemistry)

The University of Toronto
Toronto, Ontario, Canada
2018 – 2021 (Ph.D. Candidate, Medical Biophysics)

Conference Poster Presentations: NanoOntario (November 2016)
Optical Properties of Heterometallic Nanostructures Prepared by Nanosphere Lithography
Kaufman, L.; Garreau, A.; Wallace, G. Q.; Lagugne-Labarthet, F.

Fallona Interdisciplinary Showcase (January 2017)
Optical Properties of Heterometallic Nanostructures Prepared by Nanosphere Lithography
Kaufman, L.; Garreau, A.; Wallace, G. Q.; Lagugne-Labarthet, F.

Canadian Society for Chemistry (June 2017)
Probing Prostate Cancer Derived Exosomes through Surface-Enhanced Raman Spectroscopy
Kaufman, L.; Lagugne-Labarthet, F.; Dayarathna, T.; Leong, H.S.

NanoOntario (November 2017)
Probing Prostate Cancer Derived Exosomes through Surface-Enhanced Raman Spectroscopy
Kaufman, L.; Lagugne-Labarthet, F.; Dayarathna, T.; Leong, H.S.

Authorships: Trapping and SERS Identification of Extracellular Vesicles
Kaufman, L.; Cooper, T.; Wallace, G.Q.; Poon, A.C.; Dayarathna, T.L.; Hawke, D.C.; Betts, D.; Leong, H.S.; Hess, D.; Lagugne-Labarthet, F.
(Prepared, for submission to Biomaterials)

Analytical Considerations in Nanoscale Flow Cytometry of Extracellular Vesicles to Achieve Data Linearity

Gomes, J., Lucien, F., Kim, Y., Williams, K.C., Liao, T., Boysen, J., Chinnery, K., Neil, K., Kaufman, L.H., McIntyre, C.W., Laguné-Labarthe, F., Leong H. S.
(*Accepted*, September 2018, Journal of Thrombosis and Haemostasis)

Recipient Cells Briefly Inherit Functional Protein but not Genetic Cargo from Extracellular Vesicles
Poon A.C., Dayarathna, T.K., Kim, Y., Padda, R.S, Cooper, T.T, Kaufman, L.H., Berish, R.B., Hamilton, A.M., Laguné-Labarthe, F., Pasternak, S., Ronald, J.A, Leong, H.S.
(*In preparation*, for submission to Current Biology)

**Related Work
Experience**

Teaching Assistant
The University of Western Ontario
2016 – 2018